




Universitetet  
i Stavanger

Faculty of Science and Technology

## MASTER'S THESIS

Study programme/Specialisation: <b>Petroleum Engineering/ Reservoir Technology</b>	Spring Semester 2019  Open access
Author: <b>Erlend Andreassen</b>	 (signature of author)
Supervisor(s):  <b>Skule Strand Tina Puntervold Iván Darío Piñerez Torrijos</b>	
Title of master's thesis: <b>Production of Smart Water by Acid Flooding in Chalk: Temperature Limitation at Slightly Water-Wet Conditions</b>	
Credits: <b>30</b>	
Keywords: Enhanced Oil Recovery Smart Water Sulfuric Acid Spontaneous Imbibition Wettability Alteration	Number of pages: 78  + supplemental material: 17  Stavanger, 14th of June 2019

Faculty of Science and Engineering  
Department of Energy and Resources



MASTER'S THESIS

---

**Production of Smart Water by  
Acid Flooding in Chalk**

Temperature Limitation  
at Slightly Water-Wet Conditions

---

By:  
ERLEND ANDREASSEN



FACULTY OF SCIENCE AND ENGINEERING  
DEPARTMENT OF ENERGY RESOURCES

June 14, 2019



# *Abstract*

Seawater has proven to be an excellent injection fluid in chalk due to its ability to alter the wettability towards more water-wet conditions at high temperatures. This chemically induced wettability alteration improves the overall oil displacement by spontaneous imbibition of the seawater into the chalk matrix. Research has verified that the interactions between potential determining ions (PDIs)  $\text{Ca}^{2+}$ ,  $\text{Mg}^{2+}$  and  $\text{SO}_4^{2-}$  at the chalk surface can desorb acidic compounds from the oil. As a result, the degree of water-wetness increases. Additionally, by removing non-active salt, NaCl, from the seawater, the activity of the PDIs increases.

Smart Water is, by definition, an EOR-fluid with an optimized ionic composition able to improve oil recovery by wettability alteration. In carbonate reservoirs, seawater is considered a Smart Water. It is experimentally verified that seawater enriched in  $\text{Ca}^{2+}$  and  $\text{SO}_4^{2-}$  and depleted in  $\text{Na}^+$  and  $\text{Cl}^-$  has a significant effect on oil recovery in chalk.

In this thesis, the potential of producing an effective Smart Water by flooding sulfuric acid ( $\text{H}_2\text{SO}_4$ ) through chalk is investigated.  $\text{H}_2\text{SO}_4$  is a relatively cheap chemical if it can be used instead of other more expensive water treatments. The idea was that the  $\text{H}_2\text{SO}_4$ -solution would provide a controlled amount of  $\text{SO}_4^{2-}$  and dissolve parts of the chalk; providing the solution with an equal amount of  $\text{Ca}^{2+}$ .  $\text{H}_2\text{SO}_4$ -solutions of different concentrations were flooded through Stevns Klint (SK) outcrop chalk at 70 and 130°C. The effluent was analyzed to track the dissolution of chalk and precipitation of anhydrite ( $\text{CaSO}_4$ ). Based on these tests, a model Smart Water was made with sufficient amounts of  $\text{SO}_4^{2-}$  and  $\text{Ca}^{2+}$ . Oil recovery tests by spontaneous and forced imbibition were used to evaluate the wettability alteration potential of the Smart Water at 70°C. The total oil recovery was compared with similar cores imbibed with formation water (FW) and seawater (SW). A model crude oil with acid number (AN) of 0.50 mgKOH/g was used to establish initial mixed-wet conditions in the cores.

The  $\text{H}_2\text{SO}_4$ -flooding tests were successful in producing a Smart Water with desired amounts of  $\text{SO}_4^{2-}$  and  $\text{Ca}^{2+}$  by dissolving some calcium carbonate ( $\text{CaCO}_3$ ) from the chalk core. No precipitation of  $\text{CaSO}_4$  was detected in any of the tests. The model Smart Water used in the oil recovery tests was 13 mM gypsum dissolved in DI water, which was meant to represent the solution obtained by injecting 13 mM  $\text{H}_2\text{SO}_4$  through chalk.

Three SK chalk cores went through the same restoration process: the cores were cleaned and 10% initial FW saturation was established. Then, the cores were saturated with and exposed to the same amount of crude oil before being aged for two weeks at 70°C. The spontaneous imbibition results, and subsequent calculated wetting indices, proved that

neither SW nor Smart Water were able to induce any significant wettability alteration at 70°C. A parallel experiment testing the Smart Water at 90°C observed a change in wettability and an increase in oil recovery compared to SW (Lindanger, 2019). At higher temperatures, the PDIs become dehydrated and more reactive towards the chalk surface and, in turn, improves the wettability alteration.

The Smart Water did not have an improved EOR effect over SW or FW at 70°C. The temperature was most likely too low, which reduced the reactivity of the PDIs. However, by increasing the temperature, the Smart Water was able to induce wettability alteration toward more water-wet conditions and displayed a favorable EOR effect.

# *Acknowledgements*

First I'd like to thank associate professors Skule Strand and Tina Puntervold for their guidance and supervision throughout this thesis. I appreciate them for devoting their time to help and discuss my thesis; improving both my theoretical understanding of the work and writing proficiency. I am grateful to have been a part of their Smart Water EOR Group. It has been a great learning experience.

A special thanks to Dr. Iván Darío Piñerez Torrijos for his extensive assistance and involvement during the laboratory work and for always being available to answer questions regarding equipment, procedures and everything else. His work ethic and enthusiasm for the work is truly admirable.

Further, I would like to extend my appreciation to my lab partners Markus Lindanger, Agnes Kahlbom Wathne, Amalie Harestad and Katarina Radenkovic Janjic. Thanks for contributing to a fun work environment filled with great discussions, jokes, and banging '70s music.

I also acknowledge the National IOR Centre for funding and collaboration.

Finally, I would like to thank my family, girlfriend, fellow students and friends for their support and encouragement during this final semester.

Erlend Andreassen

# Contents

<b>Abstract</b>	<b>i</b>
<b>Acknowledgements</b>	<b>iii</b>
<b>Table of Contents</b>	<b>iv</b>
<b>List of Figures</b>	<b>vii</b>
<b>List of Tables</b>	<b>ix</b>
<b>Abbreviations</b>	<b>xi</b>
<b>Symbols</b>	<b>xii</b>
<b>1 Introduction</b>	<b>1</b>
1.1 Objectives . . . . .	2
<b>2 Theory</b>	<b>4</b>
2.1 Oil Recovery Mechanisms . . . . .	4
2.2 Displacement Forces . . . . .	7
2.2.1 Displacement Efficiencies . . . . .	7
2.2.2 Fluid Flow through Porous Media . . . . .	8
2.2.3 Gravity Forces . . . . .	10
2.2.4 Viscous Forces . . . . .	10
2.2.5 Capillary Forces . . . . .	11
2.3 Wettability . . . . .	12
2.4 Wettability Measurement . . . . .	13
2.4.1 Contact Angle Measurements . . . . .	13
2.4.2 Amott Test . . . . .	14
2.4.3 Spontaneous Imbibition . . . . .	16
2.5 Water Chemistry . . . . .	17
2.5.1 Properties of Water . . . . .	17
2.5.2 Acid and Base Chemistry . . . . .	18
2.5.3 The Carbonate System . . . . .	20
2.5.4 Solubility . . . . .	21
<b>3 Water-Based EOR in Carbonates</b>	<b>22</b>



3.1	Carbonate Rocks . . . . .	22
3.2	Waterflooding . . . . .	24
3.2.1	EOR by Seawater Injection . . . . .	24
3.2.2	Wettability Alteration in Chalk . . . . .	25
3.3	Smart Water . . . . .	26
3.3.1	Low-Salinity EOR . . . . .	29
3.4	Production of Smart Water in Carbonates . . . . .	29
3.4.1	Nanofiltration Membranes . . . . .	29
<b>4</b>	<b>Experimental Work</b>	<b>31</b>
4.1	Materials . . . . .	31
4.1.1	Core Material . . . . .	31
4.1.2	Oils . . . . .	32
4.1.3	Brines . . . . .	33
4.2	Analyses . . . . .	34
4.2.1	pH Measurements . . . . .	34
4.2.2	Density Measurements . . . . .	34
4.2.3	Viscosity Determination . . . . .	34
4.2.4	Acid and Base Number Determination . . . . .	35
4.2.5	Ion Chromatography (IC) . . . . .	35
4.2.6	Interfacial Tension (IFT) Measurements . . . . .	35
4.2.7	Scanning Electron Microscopy (SEM) Analysis . . . . .	35
4.3	Methods . . . . .	37
4.3.1	Porosity Calculation . . . . .	37
4.3.2	Permeability Determination . . . . .	37
4.3.3	Core Flooding Setup . . . . .	38
4.3.4	Core Cleaning . . . . .	38
4.3.5	Chalk Core Restoration . . . . .	38
4.3.5.1	Establishing Initial Water Saturation . . . . .	39
4.3.5.2	Oil Saturation and Flooding . . . . .	39
4.3.5.3	Ageing . . . . .	39
4.3.6	Oil Recovery by Spontaneous Imbibition . . . . .	40
4.3.7	Additional Oil Recovery by Forced Imbibition . . . . .	40
4.4	Production of Smart Water by Acid Flooding . . . . .	42
4.4.1	Bulk Solution Tests of $H_2SO_4$ - $CaCO_3$ Mixtures . . . . .	42
4.4.2	Core Flooding with Sulfuric Acid . . . . .	43
<b>5</b>	<b>Results and Discussion</b>	<b>44</b>
5.1	Sulfuric Acid Flooding - A Sensitivity Analysis . . . . .	45
5.1.1	Dissolution of $CaCO_3$ during $H_2SO_4$ Flooding at $70^\circ C$ . . . . .	46
5.1.2	Dissolution of $CaCO_3$ during $H_2SO_4$ Flooding at $130^\circ C$ . . . . .	48
5.1.3	pH Measurements during $H_2SO_4$ Flooding . . . . .	49
5.1.4	Designing the Smart Water Brine . . . . .	50
5.2	SEM and EDS Analysis of Reference Core SK1 . . . . .	52
5.3	Evaluation of Smart Water at $70^\circ C$ . . . . .	54
5.3.1	Water-wet Reference Core for SI . . . . .	55
5.3.2	Spontaneous Imbibition at $70^\circ C$ . . . . .	56

---

5.3.3	Comparison of the Results from the Spontaneous Imbibition Tests	58
5.3.4	Temperature Effects: A Brief Comparison with Smart Water at 90°C	60
5.4	Additional Oil Recovery by Forced Imbibition at 70°C . . . . .	62
5.4.1	Discussion of Results from Forced Imbibition . . . . .	65
<b>6</b>	<b>Conclusion</b>	<b>66</b>
6.1	Concluding Remarks . . . . .	66
6.2	Future Work . . . . .	67
	<b>Bibliography</b>	<b>68</b>
	<b>Appendix A Chemicals</b>	<b>73</b>
A.1	Acid Number Solutions . . . . .	73
A.2	Base Number Solutions . . . . .	74
	<b>Appendix B Experimental Data</b>	<b>75</b>
B.1	Permeability Calculation Example . . . . .	75
B.2	Viscosity of Oil A . . . . .	76
	<b>Appendix C H<sub>2</sub>SO<sub>4</sub> Flooding Data</b>	<b>77</b>
C.1	IC Results from H <sub>2</sub> SO <sub>4</sub> Flooding . . . . .	77
C.2	pH Measurements from H <sub>2</sub> SO <sub>4</sub> Flooding . . . . .	80
	<b>Appendix D Imbibition Data</b>	<b>81</b>
D.1	Results from Spontaneous Imbibition Tests . . . . .	81
D.2	Results from Forced Imbibition Tests . . . . .	84

# List of Figures

2.1	The distribution of oil and water in water-wet and oil-wet systems . . . . .	13
2.2	Wetting preference expressed by contact angle . . . . .	14
2.3	The capillary pressure curves for Amott and Amott-Harvey methods. . . . .	15
2.4	Sketch of the water molecule. . . . .	17
2.5	An illustration of the carbonate system. . . . .	20
2.6	Bjerrum Plot . . . . .	21
3.1	SEM image of Stevns Klint outcrop chalk core. . . . .	23
3.2	Estimated production trend for Ekofisk. . . . .	25
3.3	SI of water into oil saturated chalk cores with varying AN . . . . .	25
3.4	Suggested chemical reaction for the wettability modification by seawater injection . . . . .	26
3.5	Total oil recovery from oil saturated chalk cores by spontaneous imbibition at 100 and 130°C. Different imbibing brines with varying $\text{SO}_4^{2-}$ conc. were used . . . . .	27
3.6	Spontaneous imbibition of chalk cores saturated with oil at 90°C. Four different imbibing brines were compared: formation water (VB), seawater (SW), and two smart waters SW0Na and SW0Na4S . . . . .	28
3.7	Spontaneous imbibition of chalk cores saturated with oil at 70°C. Three different imbibing brines were compared: seawater (SW) and two smart waters SW0Na and SW0Na4S . . . . .	28
3.8	Successive flooding with FW and 100x diluted FW into reservoir limestone core at rate 1 PV/day and 90°C. Oil: AN=0.7 mgKOH/g. $S_{wi}$ =10%. . . . .	29
3.9	Principle of nanofiltration membrane. . . . .	30
3.10	Ion rejection for NANO-SW NF membrane with increasing pressure. . . . .	30
4.1	The viscosity of different mineral oils with increasing amounts of Marcol 85. . . . .	32
4.2	Illustration of a general core flooding setup. . . . .	38
4.3	Illustration of spontaneous imbibition setup for high temperature tests. . . . .	40
5.1	Dissolution of $\text{CaCO}_3$ at 70°C during injection of different $\text{H}_2\text{SO}_4$ solutions at 12 PV/day. . . . .	46
5.2	Dissolution of $\text{CaCO}_3$ at 130°C during injection of different $\text{H}_2\text{SO}_4$ solutions at 12 PV/day. . . . .	48
5.3	pH measurements of the effluent from the different $\text{H}_2\text{SO}_4$ floodings at 70 and 130°C. . . . .	49
5.4	Linear regression used to find the optimal concentration of $\text{SO}_4^{2-}$ at 90°C. . . . .	51
5.5	Picture of the inlet of core SK1, still in the rubber sleeve, after being subjected several PV of sulfuric acid and high temperatures. . . . .	52

---

5.6	SEM images of SK1 at a) the inlet and b) the outlet. . . . .	52
5.7	Spontaneous imbibition of DI water into a strongly water-wet core, SKWW, saturated with Mineral Oil. SI was performed at ambient temperature. . .	55
5.8	Spontaneous imbibition of formation water into oil saturated SK outcrop chalk core SK2 at 70°C. Oil A: AN=0.50 mgKOH/g. . . . .	56
5.9	Spontaneous imbibition of seawater into oil saturated SK outcrop chalk core SK3 at 70°C. Oil A: AN=0.50 mgKOH/g. . . . .	56
5.10	Spontaneous imbibition of Smart Water into oil saturated SK outcrop chalk core SK4 at 70°C. Oil A: AN=0.50 mgKOH/g. . . . .	56
5.11	Comparison of SI test for SK2, SK3, SK4 and SKWW. . . . .	58
5.12	Spontaneous imbibition into oil saturated SK outcrop chalk cores at 70°C and 90°C. Different imbining brines with different ionic compositions were used: FW, SW and Smart Water. . . . .	60
5.13	Forced imbibition with FW followed by Smart Water at 70°C . . . . .	62
5.14	Forced imbibition with SW followed by Smart Water at 70°C . . . . .	62
5.15	Forced imbibition with Smart Water at 70°C . . . . .	64
5.16	Forced imbibition at 1 PV/day at 70°C with three fluids: FW, SW and Smart Water. . . . .	65
B.1	Example of permeability calculation for one core. This example displays the permeability of SK1 before and after H <sub>2</sub> SO <sub>4</sub> -flooding. . . . .	75
B.2	The measurements used to determine the viscosity of Oil A. . . . .	76

# List of Tables

2.1	Classification of EOR methods . . . . .	6
2.2	Water-based EOR methods which induce wettability alteration. . . . .	6
4.1	Stevens Klint outcrop chalk core properties. . . . .	31
4.2	Measured oil properties. . . . .	32
4.3	Compositions of the brines in mM used in the oil recovery experiments. . . . .	33
4.4	IFT values between interacting oils and brines. Measurements taken at ambient temperature (23°C) and pressure (1 atm). . . . .	34
4.5	The results from the IC analysis of the equilibrated H <sub>2</sub> SO <sub>4</sub> -CaCO <sub>3</sub> solutions. The values in bold are samples where CaSO <sub>4</sub> precipitated. . . . .	42
4.6	Prepared sulfuric acid solutions. . . . .	43
5.1	Calculated pH averages of the H <sub>2</sub> SO <sub>4</sub> solutions after reaching equilibrium in the core. . . . .	49
5.2	Elemental composition of SK1 after acid flooding. The data is acquired from EDS analyses of three samples throughout the chalk core. . . . .	53
5.3	SI data from SKWW by imbibition of DI water at 23°C. . . . .	55
5.4	Results from spontaneous imbibition of different fluids into chalk cores. Cores SK2, SK3 and SK4 was saturated with Oil A and SKWW with mineral oil. . . . .	59
5.5	Results from spontaneous imbibition of different fluids into chalk cores at 70°C and 90°C. . . . .	61
5.6	Results from forced imbibition tests at 70°C. . . . .	65
A.1	Chemicals used for acid number measurements . . . . .	73
A.2	Chemicals used for base number measurements . . . . .	74
C.1	IC results from flooding 9.7 mM H <sub>2</sub> SO <sub>4</sub> through chalk at 70°C . . . . .	77
C.2	IC results from flooding 13.3 mM H <sub>2</sub> SO <sub>4</sub> through chalk at 70°C . . . . .	78
C.3	IC results from flooding 16.7 mM H <sub>2</sub> SO <sub>4</sub> through chalk at 70°C . . . . .	78
C.4	IC results from flooding 4.9 mM H <sub>2</sub> SO <sub>4</sub> through chalk at 130°C . . . . .	79
C.5	IC results from flooding 8.5 mM H <sub>2</sub> SO <sub>4</sub> through chalk at 130°C . . . . .	79
C.6	pH measurements of the effluent during the different H <sub>2</sub> SO <sub>4</sub> floodings at 70 and 130°C. . . . .	80
D.1	Spontaneous imbibition of FW at 70°C. . . . .	81
D.2	Spontaneous imbibition of SW at 70°C. . . . .	82
D.3	Spontaneous imbibition of Smart Water at 70°C. . . . .	82
D.4	Spontaneous imbibition of DI water into SKWW at 23°C. . . . .	83

---

D.5	Forced imbibition with FW followed by Smart Water at 70°C. . . . .	84
D.6	Forced imbibition with SW followed by Smart Water at 70°C. . . . .	86
D.7	Forced imbibition with Smart Water at 70°C. . . . .	88

# Abbreviations

<b>AN</b>	Acid Number
<b>ASP</b>	Alkaline-Surfactant-Polymer
<b>BN</b>	Base Number
<b>CBR</b>	Crude Oil-Brine-Rock
<b>DI</b>	De-Ionized
<b>EDS</b>	Energy-Dispersive X-Ray Spectroscop
<b>EOR</b>	Enhanced Oil Recovery
<b>FI</b>	Forced Imbibition
<b>FW</b>	Formation Water
<b>IC</b>	Ion Chromatography
<b>IFT</b>	Interfacial Tension
<b>IOR</b>	Improved Oil Recovery
<b>LSW</b>	Low-Salinity Waterflooding
<b>NF</b>	Nanofiltration
<b>OOIP</b>	Original Oil In Place
<b>PDI</b>	Potential Determining Ion
<b>PV</b>	Pore Volume
<b>SEM</b>	Scanning Electron Microscopy
<b>SI</b>	Spontaneous Imbibition
<b>SK</b>	Stevens Klint
<b>SW</b>	Seawater
<b>TDS</b>	Total Dissolved Solids
<b>USBM</b>	United States Bureau of Mines
<b>WAG</b>	Water-Alternating-Gas
<b>WF</b>	Waterflooding

# Symbols

$\Delta P$	Differential Pressure	$Pa$
$\Delta S_{of}$	Change in Oil Saturation by Forced Draining	
$\Delta S_{os}$	Change in Oil Saturation by Spontaneous Draining	
$\Delta S_{wf}$	Change in Water Saturation by Forced Imbibition	
$\Delta S_{ws}$	Change in Water Saturation by Spontaneous Imbibition	
$\theta$	Contact Angle	$^{\circ}$
$\lambda_D$	Mobility of the Displacing Fluid Phase	$m^2/Pa \cdot s$
$\lambda_d$	Mobility of the Displaced Fluid Phase	$m^2/Pa \cdot s$
$\lambda_o$	Mobility of the Oil	$m^2/Pa \cdot s$
$\lambda_w$	Mobility of the Water	$m^2/Pa \cdot s$
$\mu$	Fluid Viscosity	$Pa \cdot s$
$\mu_w$	Viscosity of Water	$Pa \cdot s$
$\mu_o$	Viscosity of Oil	$Pa \cdot s$
$\rho_{DIW}$	Density of DI Water	$kg/m^3$
$\rho_{FW}$	Density of Formation Water	$kg/m^3$
$\rho_o$	Density of Oil	$kg/m^3$
$\rho_w$	Density of Water	$kg/m^3$
$\sigma$	Interfacial Tension	$N/m$
$\sigma_{os}$	Interfacial Tension Between Oil and Solid	$Pa/m^2$
$\sigma_{ow}$	Interfacial Tension Between Oil and Water	$Pa/m^2$
$\sigma_{ws}$	Interfacial Tension Between Water and Solid	$Pa/m^2$
$\phi$	Porosity	
$A$	Cross-sectional Area	$m^2$
$D$	Diameter	$m$
$E$	Total Displacement Efficiency	



$E_D$	Microscopic Displacement Efficiency	
$E_V$	Macroscopic Displacement Efficiency	
$g$	Gravitational Acceleration Constant	$m/s^2$
$g_c$	Conversion Factor	
$h$	Height of Fluid Column	$m$
$I_{AH}$	Amott-Harvey Relative Displacement Index	
$I_o$	Amott Wettability Index to Oil	
$I_w$	Amott Wettability Index to Water	
$I_{W-SI}^*$	Modified Amott Wettability Index to Water	
$k$	Permeability	$m^2$
$K_a$	Acid Dissociation Constant	
$K_b$	Equilibrium Constant for a Base	
$k_{ro}$	Relative Permeability of Oil	$m^2$
$k_{rw}$	Relative Permeability of Water	$m^2$
$K_w$	Self-Ionization Constant	
$L$	Core Length	$m$
$M$	Mobility Ratio	
$P_c$	Capillary Pressure	$Pa$
$P_{NW}$	Pressure in the Non-wetting Phase	$Pa$
$P_o$	Pressure in the Oil Phase	$Pa$
$P_w$	Pressure in the Water Phase	$Pa$
$P_W$	Pressure in the Wetting Phase	$Pa$
$q$	Volumetric Flowrate	$m^3/s$
$S_{wi}$	Initial Water Saturation	
$S_{or}$	Residual Oil Saturation	
$SI_C$	Ultimate Recovery from SI of Assessed Core	
$SI_{WWC}$	Ultimate Recovery from SI of Water-wet Core	
$v_{avg}$	Average Fluid Velocity	$m/s$
$V_B$	Bulk Volume	$m^3$
$V_{o,p}$	Volume Produced Oil	$ml$
$V_P$	Pore Volume	$m^3$
$W_{dry}$	Dry Weight of Core	$kg$
$W_{sat}$	Saturated Weight of Core	$kg$



# Chapter 1

## Introduction

The Norwegian petroleum era began in the mid-to-late 1960s, and since then, the oil and gas industry has developed into one of the country's biggest industries and plays a vital role in the Norwegian economy. A lot has improved over the years in terms of exploration and production of a field, development and maintenance, and implementation of better technology. The outcome of the 2014 oil price crash was a heightened focus on cost efficiency and new and smarter solutions. As a result, the means of improving oil recovery from the reservoirs became significant in order to make new and old projects sustainable. This, along with a changing social climate and increased focus on environmental indicators, has led to expanded interest and investment in developing more efficient, cheaper and environmentally friendly solutions for improving oil recovery.

Carbonate reservoirs make up approximately half of the world's oil reserves. The average oil recovery from carbonates is generally less than 30%, which is relatively low compared to sandstone reservoirs. The low recovery is related to the fractured nature of the formations and the fact that almost 90% of carbonates are described as mixed-wet to oil-wet. This promotes negative capillary forces which prevents oil displacement by water. Furthermore, the rock properties of carbonates are often inhomogeneous and have low matrix permeability. Therefore, the potential for enhanced oil recovery (EOR) methods in carbonates is high (Austad et al., 2007).

Several different approaches have been explored and developed in order to improve oil production in carbonate reservoirs. A relatively new EOR method is the injection of Smart Water which improves the oil recovery by changing the wetting towards a more

water-wet state. This induces positive capillary forces which allows water to spontaneously imbibe into the matrix and displace the oil. Seawater is by definition a Smart Water in carbonates and has been implemented successfully at Ekofisk since 1985 (Austad et al., 2007). The chemical process which promotes wettability alteration depends on a range of conditions related to the initial wetting, crude oil and brine compositions, temperature, and more.

Recent research has found that the concentration of active surface ions ( $\text{Ca}^{2+}$ ,  $\text{Mg}^{2+}$  and  $\text{SO}_4^{2-}$ ) and non-active salt ( $\text{NaCl}$ ) has a large impact on the efficiency of the EOR process in chalk reservoirs (Fathi et al., 2011). The wettability alteration process in chalk can be described as a symbiotic relationship between the active ions and the adsorbed acidic components (carboxylic groups) from the oil. Oil recovery from chalk cores was improved by increasing the amount of  $\text{SO}_4^{2-}$  and reducing the salinity of the injected seawater. The effect became even more efficient as the temperature increased. Further research has looked into ways of producing a favorable Smart Water by ionic modification of seawater based on the conditions above, see Nair (2019). The present work explores a simplified approach to producing an effective Smart Water in chalk.

## 1.1 Objectives

The objective of this thesis is to investigate the potential of making an effective Smart Water by flooding sulfuric acid ( $\text{H}_2\text{SO}_4$ ) through chalk.  $\text{H}_2\text{SO}_4$  diluted in fresh water contains  $\text{SO}_4^{2-}$  ions which will adsorb onto the positive areas on the chalk surface; lowering the positive surface charge. The  $\text{SO}_4^{2-}$  act as a catalyst for the wettability alteration process in chalk.  $\text{H}_2\text{SO}_4$  is a strong acid and will also dissolve some calcium carbonate ( $\text{CaCO}_3$ ) from the rock; providing the solution with free  $\text{Ca}^{2+}$  ions. Due to the lowered surface charge,  $\text{Ca}^{2+}$  is able to co-adsorb onto the chalk surface and react with carboxylic material; triggering the wettability alteration by desorbing the acidic components on the surface. Oil recovery tests by spontaneous and forced imbibition will be used to evaluate the wettability alteration potential of the Smart Water at  $70^\circ\text{C}$ .  $\text{H}_2\text{SO}_4$  is a relatively cheap chemical and the concentration required is very low, making the Smart Water favorable from an economical and environmental standpoint.

The main objectives of this thesis work are summarized as:

- Investigate if sufficient amounts of  $\text{Ca}^{2+}$  can be dissolved by  $\text{H}_2\text{SO}_4$ -injection. A range of core flooding experiments with different concentrations of  $\text{H}_2\text{SO}_4$  will be conducted in chalk cores at different temperatures to analyze the solubility of the reacting minerals. This will improve knowledge of reaction chemistry between sulfuric acid and chalk.
- Find an optimal concentration for the  $\text{H}_2\text{SO}_4$ -based Smart Water based on the acid flooding tests. The goal will be to ensure sufficient amounts of  $\text{Ca}^{2+}$  and  $\text{SO}_4^{2-}$  to alter the wettability, while also preventing precipitation of  $\text{CaSO}_4$ .
- Investigate the Smart Water EOR potential in chalk at  $70^\circ\text{C}$  by oil recovery experiments. Spontaneous and forced imbibition tests will be conducted and the Smart Water will be compared with formation water and seawater at analogous conditions.

# Chapter 2

## Theory

Generally, EOR procedures should reduce the residual oil saturation and displace the oil towards the producers. However, the targeted oil bodies can be vast and occur under various conditions. Before implementing an EOR process in a reservoir, an assessment of the crude oil-brine-rock (CBR) interactions need to be made. There are several factors affecting the effectiveness and design of an EOR method, including the oil composition, wettability, mineralogy of the reservoir, formation type and more.

### 2.1 Oil Recovery Mechanisms

The process of oil depletion from a reservoir can be divided into the following three stages: primary recovery, secondary recovery and tertiary recovery (Green and Willhite, 1998). These stages describe the traditional oil production in chronological order and are mostly classified by the drive mechanisms that are expelling the oil.

During primary recovery the oil is displaced from the reservoir by the natural energy in place (Castor et al., 1981). The main drive mechanism is depletion of the reservoir pressure, which again can be subdivided into a number of mechanisms including gas-cap drive, natural water drive, solution-gas drive and gravity drive (Schlumberger, 2019). As no external forces are being applied, the oil production unfavorably lies around 10-30 % of the original oil in place (OOIP) in this stage.

As the reservoir pressure declines, the natural energy required to displace the oil is reduced and secondary recovery methods are needed beyond this point. At this stage, water or gas is usually injected into the reservoir to provide additional energy. This assists in maintaining the pressure in the reservoir and displacing the oil towards the producers. The secondary oil recovery is usually around 30-50 % of the OOIP (Castor et al., 1981).

The tertiary recovery stage often follows the primary and secondary stages when the previous mentioned processes become uneconomical. Tertiary methods target the remaining hydrocarbons in the reservoir and improves recovery by altering the properties of the oil, improving the total displacement efficiency and reducing the residual oil saturation. This is achieved through processes like chemical injection, miscible gas injection and thermal energy methods (Green and Willhite, 1998).

Despite the term, tertiary recovery methods do not necessarily need to follow primary and secondary schemes. Depending on economical and technical factors, and the quality of the reservoir, a traditionally tertiary method can be implemented as the second – and even first – recovery method in a chronological sense. Therefore, the terms Enhanced Oil Recovery (EOR) and tertiary recovery are often used interchangeably, although the former is more widely accepted in petroleum literature and is the term that is used throughout this thesis (Green and Willhite, 1998). EOR is not to be confused with Improved Oil Recovery (IOR), which is a broader term encompassing various procedures to increase the estimated recovery, including EOR, horizontal drilling, infill drilling and reservoir characterization (Green and Willhite, 1998).

EOR methods can be roughly subdivided into the following categories: chemical, miscible and immiscible gas, thermal and other methods (Taber et al., 1997; Thomas, 2008). The classification is related to their respective main driving mechanisms of oil displacement and is presented in Table 2.1.

Table 2.1: Classification of EOR methods. Based on Taber et al., 1997; Thomas, 2008.

Chemical methods	Alkaline flooding Surfactant flooding Polymer flooding Alkaline-Surfactant-Polymer (ASP) flooding Micellar flooding Emulsion
Miscible gas methods	Slug process N <sub>2</sub> injection Miscible CO <sub>2</sub> injection Vaporizing gas drive (VGD)
Immiscible gas methods	Inert gas injection Flue gas injection Immiscible CO <sub>2</sub> injection
Thermal methods	Steam processes Hot-water flooding In-situ combustion
Other methods	Foam flooding Microbiological methods Water-Alternating-Gas (WAG)

Wettability alteration has been proposed as a relatively new EOR method, which improves the microscopic displacement efficiency by increasing the capillary forces. Some examples are presented in Table 2.2. The aim in these methods is to change the wetting of the rock by only modifying the composition of the injected water. The water composition required to alter wettability is different for different rock formations. Smart Water is used as an umbrella-term for these water-based EOR methods (Austad, 2013).

Table 2.2: Water-based EOR methods which induce wettability alteration.

Wettability alteration	Smart Water/Designer Water (Modified) Seawater injection in carbonates Low salinity waterflooding in sandstones
------------------------	---



## 2.2 Displacement Forces

The flow of a fluid through a reservoir is dictated by the interplay of the various forces acting on the fluid. The three main forces which control the mobilization of fluid are capillary forces, viscous forces and gravity forces (Morrow, 1979). The expulsion of oil from the rock is generally the result of two processes: spontaneous and forced imbibition. In spontaneous imbibition, capillary and gravity forces are the main driving forces. As there are no pressure differences aiding the displacement, the viscous forces are negligible in this process. However, in a forced imbibition process the viscous forces act as the driving forces in displacing the oil.

### 2.2.1 Displacement Efficiencies

The efficiency of a displacement process is determined by its ability to mobilize the oil and overcome the capillary forces in the pores. The total displacement efficiency ( $E$ ) of an EOR process is a measurement of the amount of recovered oil with respect to the original oil in place. The term can be seen as the product of the macroscopic and microscopic displacement efficiencies, and is given by the following equation:

$$E = E_V \cdot E_D \quad (2.1)$$

where  $E_V$  and  $E_D$  are the macroscopic and microscopic displacement efficiencies as fractions, respectively. Therefore, the closer  $E_V$  and  $E_D$  are to one, the more effective the oil displacement process will be.

The macroscopic displacement efficiency, also referred to as volumetric sweep efficiency, can be described as the fraction of the total reservoir fluid contacted by the EOR-injectant. In another sense, the term conveys how effectively the displacing EOR-fluid pushes the displaced oil towards the producing wells. At this scale, the displacement efficiency is affected by the reservoir geology and structure, permeabilities and communications between layers, as well as gravity effects and viscosity differences between the displacing and displaced fluids. If these elements are not accounted for, it can lead to consequences like

fingering effects and gravity segregation which greatly reduces  $E_V$ . Unfavorable placements of the injection and production wells can also partake in reducing the displacement efficiencies.

The microscopic displacement efficiency is a measure of the amount of mobile oil relative to the total amount of oil in the pores. The term can be expressed by the following equation,

$$E_D = \frac{1 - S_{wi} - S_{or}}{1 - S_{wi}} \quad (2.2)$$

where  $S_{wi}$  is the initial water saturation and  $S_{or}$  is the residual oil saturation. A key aspect of improving microscopic displacement efficiency is the reduction of  $S_{or}$ , making it possible to produce a higher percentage of the OOIP. Interactions between the CBR-system and the EOR-injectant can initiate physical and/or chemical processes which alters the wettability and interfacial tension. Favorable alterations of these factors can contribute to lowering the  $S_{or}$  and improving the sweep at the microscopic scale.

### 2.2.2 Fluid Flow through Porous Media

It is important to note and understand how various fluids flow and interact with each other within the rock. Permeability is an integral property of a porous medium which describes its capacity to transport fluid through its pores. The Darcy equation (1856) is a relationship between a fluid and the media it flows through, and can be used to estimate the permeability:

$$q = -\frac{k \cdot A}{\mu} \cdot \frac{\Delta P}{L} \quad (2.3)$$

Where,

$q$	volumetric flowrate (m <sup>3</sup> /s)
$k$	permeability (m <sup>2</sup> )
$A$	cross-sectional area (m <sup>2</sup> )
$\mu$	fluid viscosity (Pa.s)
$\Delta P$	differential pressure (Pa)
$L$	core length (m)

The Darcy equation shows that the pressure drop across the medium is proportional to the velocity of fluid. Also, the left-hand term is often written as negative to compensate for the pressure gradient, which is negative in the flow direction.

When two fluids are present in a pore system, the efficiency of the total displacement is driven by the relationship between the fluid viscosities and rock wettability. This applies for instance to water flooding or immiscible gas flooding in an oil filled reservoir. A helpful concept when estimating macroscopic displacement efficiency in a two-phase system is the mobility ratio,  $M$ , between the two fluid phases:

$$M = \frac{\lambda_D}{\lambda_d} = \frac{\lambda_w}{\lambda_o} = \frac{\left(\frac{k_{rw}}{\mu_w}\right)_{S_{or}}}{\left(\frac{k_{ro}}{\mu_o}\right)_{S_{wi}}} \quad (2.4)$$

where the parameters are defined as follows:

$M$	mobility ratio
$\lambda_D$	mobility of the displacing fluid phase (m <sup>2</sup> /Pa.s)
$\lambda_d$	mobility of the displaced fluid phase (m <sup>2</sup> /Pa.s)
$\lambda_w$	mobility of the water (m <sup>2</sup> /Pa.s)
$\lambda_o$	mobility of the oil (m <sup>2</sup> /Pa.s)
$(k_{rw})_{S_{or}}$	relative permeability of water at residual oil saturation (m <sup>2</sup> )
$(k_{ro})_{S_{wi}}$	relative permeability of oil at irreducible water saturation (m <sup>2</sup> )
$\mu_w$	viscosity of water (Pa.s)
$\mu_o$	viscosity of oil (Pa.s)

### 2.2.3 Gravity Forces

Gravity forces are important in multiphase fluid systems where there can be large variations in the fluid densities. The main driving force acting on a fluid is dictated by the density of said fluid (Lake, 2010). Fluid segregation due to gravity forces can affect the efficiency of a displacement process in a negative manner, causing problems like overriding and underriding of the displaced fluid. However, this density difference can also act in favor of a flooding in case of a dipping reservoir.

The buoyancy force describing the difference in hydrostatic pressure between water and oil is given by:

$$\Delta P = (\rho_w - \rho_o) \cdot g \cdot h \quad (2.5)$$

where:

- $\Delta P$  pressure difference (Pa)
- $\rho_w$  density of water ( $\text{kg}/\text{m}^3$ )
- $\rho_o$  density of oil ( $\text{kg}/\text{m}^3$ )
- $g$  gravitational acceleration constant ( $\text{m}/\text{s}^2$ )
- $h$  height of fluid column (m)

### 2.2.4 Viscous Forces

Viscous forces are determined by the pressure gradient across a porous medium caused by the fluid flowing through it (Green and Willhite, 1998). A simplified way to estimate the viscous forces in a reservoir is to think of the rock as a cluster of parallel capillary tubes and assume laminar flow through these. The pressure drop is calculated using Poiseuille's law for laminar flow through a single pipe:

$$\Delta P = -\frac{8 \cdot \mu \cdot \Delta x \cdot v_{avg}}{r^2 \cdot g_c} \quad (2.6)$$

Here:

$\Delta P$	pressure drop across pipe (Pa)
$\mu$	fluid viscosity (Pa.s)
$\Delta x$	pipe length (m)
$v_{avg}$	average fluid velocity through the pipe (m/s)
$r$	pipe radius (m)
$g_c$	conversion factor

### 2.2.5 Capillary Forces

Capillary forces play an important role in fluid distribution and displacement in a reservoir system. Generally, by having two immiscible fluids coexist within a system, a pressure differential occurs across the interface between said fluids. This pressure difference is known as the capillary pressure ( $P_c$ ) and is a result of the capillary forces: surface tension and interfacial tension (IFT). In a porous media inhabited by two immiscible fluid phases (e.g. oil and water),  $P_c$  can be expressed as the difference between the pressure in the non-wetting phase ( $P_{NW}$ ) and the pressure in the wetting phase ( $P_W$ ):

$$P_c = P_{NW} - P_W \quad (2.7)$$

Depending on the fluid pressures and wetting state of a system, the capillary pressure may be positive or negative. In an oil-water system,  $P_c$  can be expressed by the Young-Laplace equation:

$$P_c = P_o - P_w = \frac{2\sigma \cos\theta}{r} \quad (2.8)$$

where:

$P_o$	pressure in the oil phase (Pa)
$P_w$	pressure in the water phase (Pa)
$\sigma$	interfacial tension between oil and water (N/m)
$\theta$	contact angle ( $^\circ$ )
$r$	pore radius (m)

The driving mechanisms derive from the interactions between pore dimensions and communication, wettability and fluid properties. Depending on these parameters within a reservoir, the capillary forces can act in favor or against an effective oil displacement.

In fractured reservoirs like carbonates, positive capillary forces act as the primary driving forces in spontaneous imbibition (Cuiec et al., 1994). Positive capillary forces are enforced by altering the wettability towards more a water-wet state, which is confirmed by the reduction of the contact angle ( $\theta$ ) in Equation 2.8.

### 2.3 Wettability

Wettability is commonly defined as the tendency of some fluid to adhere to or spread on a solid surface in presence of other immiscible fluids (Craig, 1971). Some instances of wettability in our daily lives are water droplets on a hydrophobic leaf or a newly waxed car. In a reservoir system, the wettability is used to determine if the rock prefer either water or oil on its surface. In this section, the wettability in a CBR system and its relation to EOR will be explained, as well as different methods used to determine wettability.

The wettability of a reservoir rock will majorly impact the fluid distribution and flow within the rock, as well as the efficiency of a displacement process (Anderson, 1986). Altering the wettability in a system has been proved to affect relative permeabilities,  $k_{rw}$  and  $k_{ro}$ , capillary pressure,  $P_c$ , and residual oil saturation,  $S_{or}$ .

Over several million years, the reservoir system forms an equilibrium with the oil, water and rock and establishes a certain wettability condition. The state of wettability can vary from area to area within the same reservoir and is sensitive factors like crude oil composition, reservoir rock type and surface minerals. Classification of wetting state is generally divided into four states: water-wet, mixed-wet, oil-wet and fractional wettability (Donaldson and Alam, 2013). All reservoirs are water-wet originally, but can change over time after migration of hydrocarbons into the reservoir. In a water-wet system, water acts as the wetting fluid which adheres to the grains and fills the smallest pores. In this case, the oil acts as non-wetting fluid and occupies the pore bodies (Figure 2.1a). For an oil-wet system, the preference the rock has is completely opposite, meaning oil adheres to the pore walls and water is found in the pore bodies (Figure 2.1b).

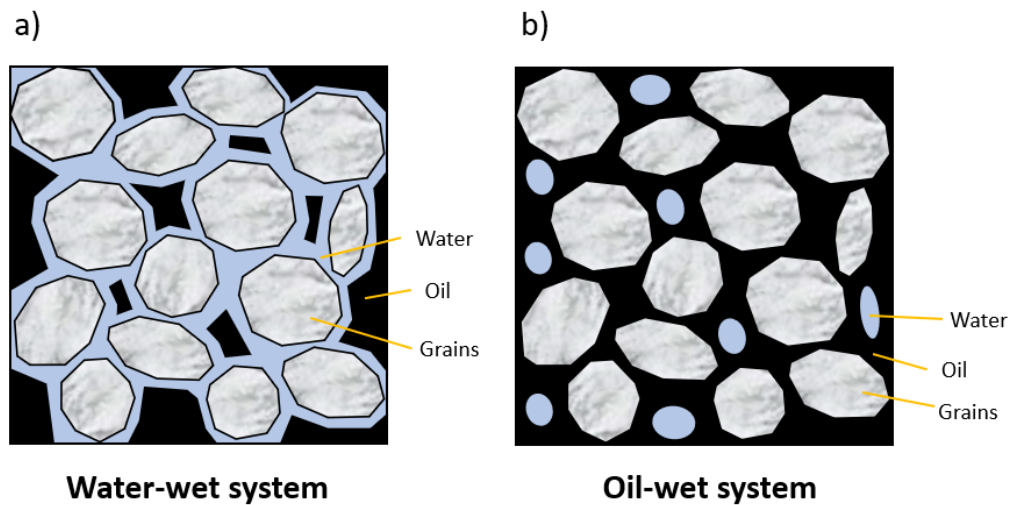


Figure 2.1: The distribution of oil and water in a) a water-wet system and b) an oil-wet system. Redrawn after Ahr (2011).

Fractional wettability is used to describe a system with heterogeneous wetting, where the wetting preference of the rock varies throughout the pore surfaces. This wetting state can exist if the rock contains randomly distributed minerals which can either have an affinity towards oil or water. This creates both oil-wet and water-wet areas on the same surface.

Mixed wettability is another term used to describe a system with heterogeneous wettability. However, the term describes a more specific wetting state in which the smaller pores are water-wet and fully saturated with water, while the larger pore throats are oil-wet (Salathiel, 1973). An example of this is a fractured reservoir where the fractures are continuously oil-wet throughout the system, but the rest of the matrix, where the pore throats are smaller, is water-wet.

## 2.4 Wettability Measurement

There are several methods used to determine the wettability, both qualitative and quantitative. Methods include contact angle measurements, the Amott test, United States Bureau of Mines (USBM) method, chromatographic wettability test and spontaneous imbibition (Anderson, 1986; Strand et al., 2006). Important parameters when using these methods are the oil and water saturation, capillary pressures and flowing conditions. In

this thesis, the wettability is determined by spontaneous imbibition and forced imbibition processes.

### 2.4.1 Contact Angle Measurements

One of the simplest method to determine the wetting state of a system is by contact angle ( $\theta$ ) measurements. In an equilibrated system consisting of two immiscible fluids and a solid, the contact angle is usually measured between the solid and the denser fluid. In a CBR system, the contact angle is therefore measured through the water phase.

A rock is considered water-wet or hydrophilic if the contact angle is below  $90^\circ$  (Figure 2.2a) and the capillary pressure across the water/oil interface is positive (Donaldson and Alam, 2013). Vice versa, the rock is considered oil-wet or hydrophobic if the contact angle is greater than  $90^\circ$  and the capillary pressure is negative (Figure 2.2c). If the contact angle is close to  $90^\circ$ . If the rock doesn't have a preference for neither oil nor water, the wettability falls under the umbrella term intermediate- or neutral-wet (Figure 2.2b).

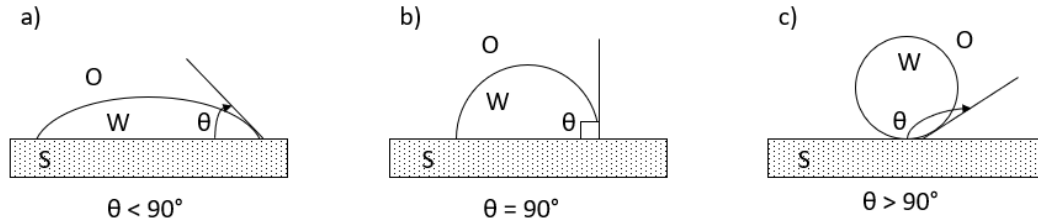


Figure 2.2: Example of wetting preference expressed by contact angle, where a) is water-wet, b) is neutral-wet and c) is oil-wet.

The shape of the droplets in the figures above is a result of the surface energies of the systems. The interfacial forces exerted by the oil-water-solid relationship may be in static equilibrium and can, together with the contact angle, be expressed by Young's equation (1855):

$$\sigma_{ow}\cos\theta = \sigma_{os} - \sigma_{ws} \quad (2.9)$$

The parameters of the equation are:



$\sigma_{ow}$	interfacial tension between oil and water (Pa/m <sup>2</sup> )
$\sigma_{os}$	interfacial tension between oil and solid (Pa/m <sup>2</sup> )
$\sigma_{ws}$	interfacial tension between water and solid (Pa/m <sup>2</sup> )
$\theta$	contact angle between 0 and 180°

### 2.4.2 Amott Test

The Amott test (Amott, 1959) is a quantitative method of determining the average wettability of a core by combining the results from spontaneous imbibition and forced imbibition. The preferred wetting fluid of the rock will spontaneously imbibe into the core and displace the non-wetting fluid. The ratio of the total oil displacement obtained from these two methods is used to reduce the effect of viscosity, relative permeability and initial saturation of the rock (Anderson, 1986).

In an Amott test, two important expressions are determined, the Amott wettability index to water and oil,  $I_w$  and  $I_o$ , respectively. The first index,  $I_w$ , is determined by first immersing the core in water and recording the maximum oil recovered by spontaneous imbibition. The increase in water saturation is noted as  $\Delta S_{ws}$ . Thereafter, the core undergoes forced imbibition, usually by waterflooding or centrifuging. If there is an additional increase in oil recovery, the resulting increase in water saturation is noted as  $\Delta S_{wf}$ . Finally,  $I_w$  is defined as:

$$I_w = \frac{\Delta S_{ws}}{\Delta S_{ws} + \Delta S_{wf}} \quad (2.10)$$

If most of the oil is expelled from the core by spontaneous imbibition,  $I_w$  will be close to 1 and the system can be characterized as water-wet. For lower values of  $I_w$ , the systems are considered less water-wet. Similarly,  $I_o$  is determined by spontaneous imbibition of oil (drainage) and forced imbibition of water by oil. The saturation changes for the two processes is noted as  $\Delta S_{os}$  and  $\Delta S_{of}$ , respectively.  $I_o$  is then defined as:

$$I_o = \frac{\Delta S_{os}}{\Delta S_{os} + \Delta S_{of}} \quad (2.11)$$

If  $I_o$  is close to -1, the system is described as strongly oil-wet. The Amott test method is a rather lengthy process, however modifications have been made to simplify it. The

Amott-Harvey method is used to characterize the wettability by a relative displacement index,  $I_{AH}$ , which is the difference between  $I_w$  and  $I_o$  (Anderson, 1986). A system is generally considered water-wet if  $+0.3 \leq I_{AH} \leq +1.0$ , mixed-wet if  $-0.3 < I_{AH} < +0.3$  and oil-wet if  $-1.0 \leq I_{AH} \leq -0.3$  (Cuiec, 1984). A complete Amott-Harvey test cycle (Figure 2.3) is divided into the following five segments:

1. Primary drainage of water by oil to establish initial water saturation
2. Spontaneous imbibition of water
3. Forced imbibition of water
4. Spontaneous imbibition (drainage) of oil
5. Forced imbibition (drainage) of oil

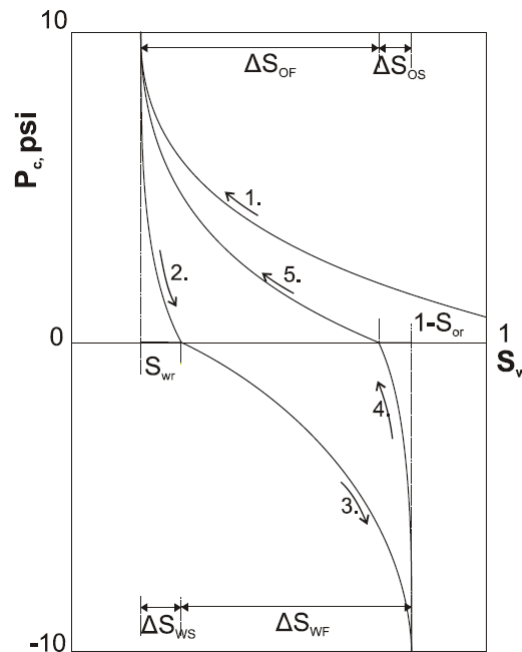


Figure 2.3: The capillary pressure curves for Amott and Amott-Harvey methods.

### 2.4.3 Spontaneous Imbibition

A qualitative way of estimating the wetting state of a core is by measuring the spontaneous imbibition of water into the core (Morrow, 1990). The rate and volume water imbibed is fast and significant for strongly water-wet cores. Both terms decrease as the wettability

of the core goes towards a mixed-wet state. If no water is imbibed, the core is most likely preferentially oil-wet.

The driving force for the rate of spontaneous imbibition is proportional to the imbibition capillary pressure. Whereas the Amott method relies mainly on the fluid saturation where imbibition capillary pressure reaches zero, the spontaneous imbibition rate relies on the magnitude of the imbibition capillary pressure. Interpretation of spontaneous imbibition data is aided by having a reference core with near-perfect wetting state, e.g. very strongly water-wet or strongly oil-wet. A simplified wetting index can be derived solely from SI tests using a strongly water-wet core as reference (Torrijos et al., 2019). The degree of water-wetness is then quantified by a modified Amott water index,  $I_{W-SI}^*$ , as shown by the following Equation 2.12:

$$I_{W-SI}^* = \frac{SI_C}{SI_{WWC}} \quad (2.12)$$

$SI_C$  is the ultimate oil recovery (% OOIP) by spontaneous imbibition from the assessed core and  $SI_{WWC}$  is the ultimate oil recovery (% OOIP) by spontaneous imbibition from the strongly water-wet core. The degree of water-wetness,  $I_{W-SI}^*$ , is close to 1 for the reference core and 0 for a neutral-wet core.

## 2.5 Water Chemistry

The chemistry of the waters encountered in reservoirs and oil recovery processes influences the initial wettability of the reservoir, the fluid distribution, as well as the effectiveness of an EOR method. Good knowledge about water chemistry is therefore important as it can optimize oil recovery and minimize issues related to reduction of injectivity and productivity.

### 2.5.1 Properties of Water

The water molecule ( $\text{H}_2\text{O}$ ) is composed of a central oxygen atom (O) and two hydrogen nuclei (H). The molecule is dipolar; due to its uneven geometry, the molecule has a slightly negative charge at the oxygen end and a slightly positive charge at the opposite hydrogen end (Figure 2.4). The dipolar nature allows for hydrogen bonding between water molecules which gives water some unique properties, e.g. high boiling temperature, large specific heat capacity, expands upon freezing, among others (Boye, 1995).

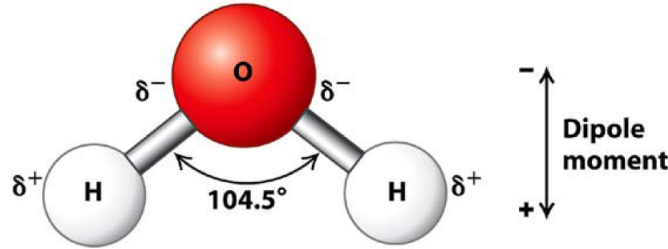


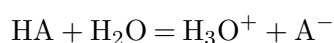
Figure 2.4: Sketch of the water molecule.  $\delta$  is the symbol for electrical charge. Illustration by Lodish (2008).

The polarity of the molecules also makes water a good solvent. Ionic or polar substances entering the water phase become surrounded by an abundance of water molecules. When minerals enter the water phase, the water molecules are able to surround ions and release them from the minerals' crystal structure until its completely dissolved. Polar substances like acids, salts and alcohol are easily solvable in water, while non-polar substances like oils and fats are not. The water molecules reduce the reactivity of the solvated ions, especially at lower temperatures. This process is called hydration and is an exothermic process. At higher temperatures, ions become less hydrated (dehydrated) which make them more reactive towards other species. Chemical reactions are normally affected by

temperature when hydrated ions are involved. Divalent ions ( $\text{Ca}^{2+}$ ,  $\text{Mg}^{2+}$ ) are more hydrated than monovalent ions ( $\text{Na}^+$ ,  $\text{Cl}^-$ ).

### 2.5.2 Acid and Base Chemistry

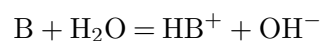
Water is an amphoteric compound, meaning it can react as both an acid and as a base. According to the Brønsted-Lowry theory (1923); an acid is a species that donate protons, while a base accepts protons. When reacting with a strong acid, the water acts as a base:



Here, the acid, HA, donates its proton to the water and forms hydronium,  $\text{H}_3\text{O}^+$ , and the conjugate base of the acid,  $\text{A}^-$ . In such reactions,  $\text{H}_3\text{O}^+$  can be used interchangeably with  $\text{H}^+$ . The strength of the acid in a solution is determined by the acid dissociation constant,  $K_a$ :

$$K_a = \frac{[\text{H}_3\text{O}^+][\text{A}^-]}{[\text{HA}]}$$

$K_a$  is an equilibrium constant and  $[\text{H}_3\text{O}^+]$ ,  $[\text{A}^-]$  and  $[\text{HA}]$  are the concentration of  $\text{H}_3\text{O}^+$ ,  $\text{A}^-$  and HA at equilibrium. A large  $K_a$  value means the acid is strong and will donate more  $\text{H}^+$  to water. Water acts as an acid when reacting with a base or a weak acid:



In this example, the base, B, receives a proton from the water and forms the conjugate acid,  $\text{HB}^+$ , and the base hydroxide,  $\text{OH}^-$ . The strength of the base in a solution is determined by the equilibrium constant for the base,  $K_b$ :

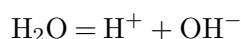
$$K_b = \frac{[\text{HB}^+][\text{OH}^-]}{[\text{B}]}$$

Larger  $K_b$  value means the base is stronger and its tendency to accept  $\text{H}^+$  increases.  $[\text{HB}^+]$ ,  $[\text{OH}^-]$  and  $[\text{B}]$  are the concentration of  $\text{HB}^+$ ,  $\text{OH}^-$  and B at equilibrium.  $K_b$  is

related to  $K_a$  for the conjugate acid. If one constant is known, the other can be calculated. For a corresponding acid-base-couple, the product of  $K_a$  and  $K_b$  is:

$$K_a \cdot K_b = K_w = [\text{H}_3\text{O}^+][\text{OH}^-]$$

The value  $K_w$  is called the ionic product of water and is the equilibrium constant for the self-ionization reaction of water:



In pure water at 25°C, the water ionization reaction gives:

$$[\text{H}_3\text{O}^+] = [\text{OH}^-] = 1.0 \cdot 10^{-7} \text{ mol/l}$$

which indicate equal amounts of both ions in the solution. These ions exist naturally in water due to the self-ionization reaction. For pure water at 25°C,  $K_w$  is then:

$$K_w = [\text{H}_3\text{O}^+][\text{OH}^-] = 1.0 \cdot 10^{-14}$$

If acid is dissolved in water, the concentration of  $\text{H}_3\text{O}^+$  increases. Then, for the ionic product of water to be constant at  $1.0 \cdot 10^{-14}$ , the concentration of  $\text{OH}^-$  has to decrease. When a solution has more  $\text{H}_3\text{O}^+$  ions than  $\text{OH}^-$  ions, the solution is considered acidic. Vice versa, a solution is considered basic, or alkaline, when it has more  $\text{OH}^-$  ions than  $\text{H}_3\text{O}^+$  ions. An easier way to determine the acidic or alkaline nature of a solution, is by using the pH-scale:

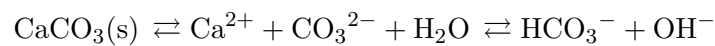
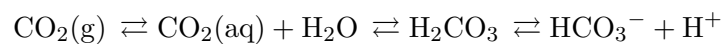
$$\text{pH} = -\log[\text{H}_3\text{O}^+]$$

A solution is considered acidic for  $\text{pH} < 7$ , neutral for  $\text{pH} = 7$  and alkaline for  $\text{pH} > 7$ . The typical pH-scale ranges from 0 for very acidic solutions to 14 for very alkaline solutions.

If a solution consists of both a weak acid and its conjugate base, or vice versa, it can be considered a buffer solution. In a buffer solution, the pH does not change very much when moderate amounts of a strong acid or base are added.

### 2.5.3 The Carbonate System

One of the most important acid-base systems in water is the oceanic carbonate system (Figure 2.5). Seawater in equilibrium with both  $\text{CO}_2$  from the atmosphere and carbonate containing rock becomes buffered to a pH of  $\sim 8.4$ . In seawater, carbon is represented by carbonate ( $\text{CO}_3^{2-}$ ), bicarbonate ( $\text{HCO}_3^-$ ), carbonic acid ( $\text{H}_2\text{CO}_3$ ) and aqueous carbon dioxide ( $\text{CO}_2$ ).



The  $\text{HCO}_3^-$  ion acts as a buffer as it can react both as an acid and a base. The buffered water can therefore resist changes to pH from additional acidic or alkaline species.

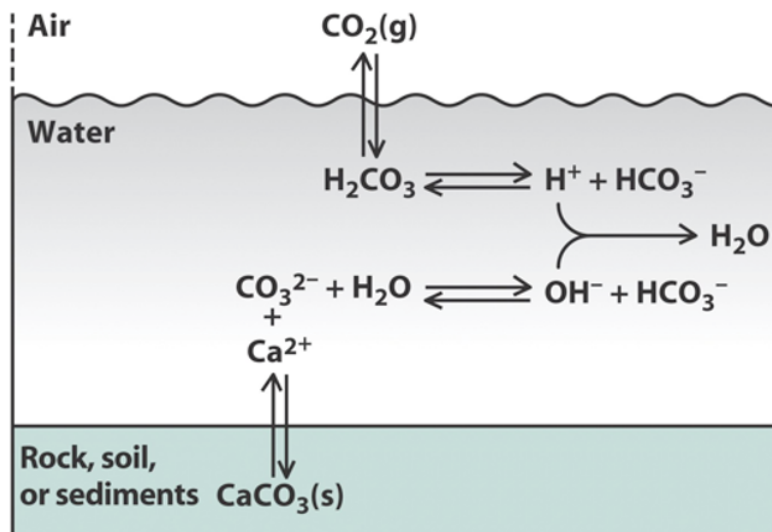


Figure 2.5: An illustration of the carbonate system. Figure by Shapley (2011).

The carbonate system can also be illustrated by a so called Bjerrum Plot (Figure 2.6), named after Danish chemist N. Bjerrum. The diagram displays the equilibrium between the three carbonate species  $\text{CO}_3^{2-}$ ,  $\text{HCO}_3^-$  and  $\text{H}_2\text{CO}_3$  (which provides the solution with  $\text{CO}_2(\text{aq})$  and  $\text{H}_2\text{O}$ ) and how it relates to the pH of the brine. E.g. as the pH decreases, the relative amount of  $\text{CO}_2(\text{aq})$  increases.

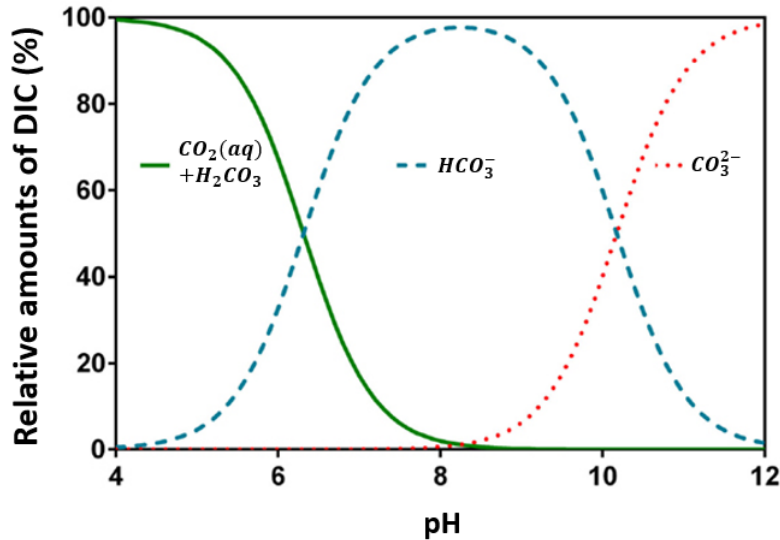


Figure 2.6: A general Bjerrum Plot. The carbonate species are presented as relative proportions of the total dissolved inorganic content (DIC). Figure based on Pedersen (2013).

#### 2.5.4 Solubility

The solubility of materials determines that some materials dissolve in water while others do not. It also determines the opposite reaction: some ions can bond together and precipitate as insoluble material. Solubility is defined as the amount of a substance in mol/l that can dissolve in a solution under a given set of conditions. There are a couple of factors that affect solubility:

- Temperature affects the equilibrium position of the precipitation, as well as the reaction rate. For most solids, solubility increases with increasing temperature. Some exceptions are  $\text{CaCO}_3$  and  $\text{CaSO}_4$ .
- Common ion effect: When a solution contains an ion that is the same as one of the ions which result from the dissolution of the solid, the solubility will be less than that when the solid dissolved in pure water. Therefore, by dissolving a solid in water, its solubility decreases as the amount of ions in the solution increases.



- Complexation: When any constituent ions of a solid precipitate in complex formation after the dissolution process, the solubility of the solid increases. The phenomena is explained by Le Châtelier's principle: When a substance is removed from either side of the reaction equation, then the equilibrium will shift towards said side. If an ion from a dissolved solid is removed or form complexes with other ions, further dissolution of the solid will take place.

## Chapter 3

# Water-Based EOR in Carbonates

### 3.1 Carbonate Rocks

Carbonate rocks and sediments are formed by accumulation and lithification of carbonate materials that are precipitated by plants, animals and other organisms. They are usually classified as biogenic rocks as they are products made from or by life forms. Due to the large amounts of calcium ( $\text{Ca}^{2+}$ ) and carbonate ( $\text{CO}_3^{2-}$ ) dissolved in seawater, these organisms can convert them directly into carbonate minerals (Grotzinger and Jordan, 2014).

There are various types of carbonate minerals that are characterized based on their composition and ionic structure. Their common factor is that they are complexes containing  $\text{CO}_3^{2-}$ . The most abundant carbonate mineral is calcium carbonate ( $\text{CaCO}_3$ ), commonly known as calcite; other minerals include aragonite ( $\text{CaCO}_3$ ), magnesite ( $\text{MgCO}_3$ ), dolomite ( $\text{CaMg}(\text{CO}_3)_2$ ), siderite ( $\text{FeCO}_3$ ), and ankerite ( $\text{CaFe}(\text{CO}_3)_2$ ) (Bjørlykke, 1989). Calcite and aragonite share the same ionic composition, however their structure is different.

Most sedimentary carbonate rocks are mainly made up of calcite and dolomite minerals. If the carbonate rock is mostly made up of calcite, it is defined as limestone. However, if the rock is dominantly dolomite, it is defined as dolostone (Grotzinger and Jordan, 2014).

Chalk is a fine-grained, biogenic limestone, composed mainly of deposits from marine algae known as coccolithophorid, as well as marine animals known as foraminifera. Coccolithophorid algae are made up of several coccolith ring structures, which in turn are made up of smaller calcite crystals. The ring structures can range from  $<1$  to  $20\ \mu\text{m}$  in diameter (INA, 2019). Figure 3.1 is a picture of chalk taken by a scanning electron microscope (SEM), magnified ten thousand times, which is clearly showing different coccolith rings and fragments.

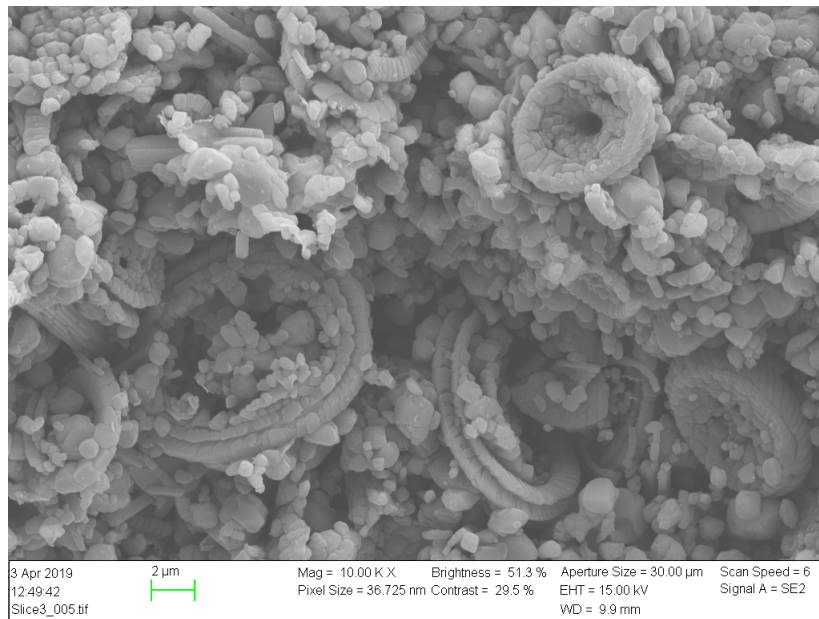


Figure 3.1: SEM image of Stevns Klint outcrop chalk core displaying coccolith rings, calcite fragments and pore space.

Chalk is normally white/light gray in color and extremely porous, permeable, soft and friable. Although, chalk is not very homogeneous and due to small calcite fragments in the rock, the permeability is usually very low.

## 3.2 Waterflooding

Waterflooding is the practice of injecting water into a reservoir and has historically served two important purposes; providing pressure support within the reservoir after primary depletion and improving displacement of oil towards the producing wells (Craig, 1971). This method has been successfully implemented in wide variety of reservoirs, both in carbonates and sandstones. Implementing a waterflooding operation comes with additional challenges such as fluid mobility control, water treatment, corrosion and scaling control, and more. The quality of a waterflooding depends the geological dimensions and rock properties, fluid compositions, and pressures and temperatures within the reservoir among others (Ahmed, 2018).

When waterflooding was first implemented, it was by re-injection of produced formation water from the reservoir. This worked great as a secondary recovery method as it increased oil production by prolonging the lifespan of the reservoirs. However, formation water has later been proven not to alter the reservoir wettability, and thus, can not be regarded as a viable EOR-injectant. Studies have shown that by altering the ionic composition of the injected waters, it can trigger a wettability alteration in the reservoir and ultimately recover more of the trapped oil reserves.

### 3.2.1 EOR by Seawater Injection

Seawater has shown to be a terrific, natural EOR-fluid in chalk reservoirs (Austad et al., 2007). Most notable and remarkable instance of enhanced oil recovery by injection of seawater is at the Ekofisk chalk field. At production start-up in 1971, the estimated oil recovery was only 17-18% of OOIP. Since then, that number has increased significantly and is predicted to hit 52% within 2028 (ConocoPhillips, 2019).

The additional oil recovery induced by seawater injection in North Sea chalk reservoirs can be attributed to two mechanisms: wettability alteration and compaction of the rock. By injecting seawater, the wettability of the chalk is improved from an oil-wet state towards an intermediate-wet to water-wet state. Thus, water is more prone to imbibe into the chalk matrix and improve the total oil sweep. The chemical reaction that takes place on the chalk surface is described in the next section. Compaction of the soft chalk formation

does also occur when seawater enters the rock matrix, which has shown to be a significant drive mechanism for oil recovery (Austad et al., 2007).

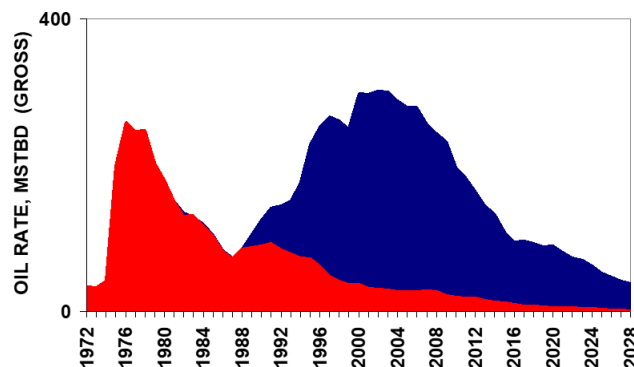


Figure 3.2: Estimated production trend for Ekofisk. The red area is the initial estimated production before seawater injection and the blue area is after. Figure by COREC (2005)

### 3.2.2 Wettability Alteration in Chalk

In fractured chalk reservoirs, oil recovery from water injection is mostly dependent on spontaneous imbibition by water into the rock matrix. The efficiency of the spontaneous imbibition process is governed by the capillary forces at play, which in turn are dictated by the wettability of the rock. A successful oil displacement depends on having positive capillary forces, which increase with increased water wetness. A majority of carbonate reservoirs are neutral to oil-wet, which means the water will have a hard time imbibing into the rock (Chilingar and Yen, 1983).

Several studies (Standnes and Austad, 2000, Strand et al., 2006, Zhang et al., 2007, Austad et al., 2007) have looked at how seawater is able to alter the wetting condition of chalk toward a more water-wet state, and how it improves the oil recovery. The wettability alteration in chalk is proposed as a result of interplay between the chalk surface, the acidic components in the oil and the potential determining ions (PDIs)  $\text{Ca}^{2+}$ ,  $\text{Mg}^{2+}$  and  $\text{SO}_4^{2-}$  in the seawater (Austad et al., 2007).

The amount of carboxylic material in crude oil is determined by the acid number (AN), which plays a significant role in the effectiveness of a wettability alteration process. The carboxylic group ( $-\text{COO}^-$ ) is negatively charged and forms strong bonds with the positively charged chalk surface. The importance of AN on the wetting condition is presented

in Figure 3.3, where water spontaneously imbibes chalk cores saturated with oils of distinctive AN (Standnes and Austad, 2000).

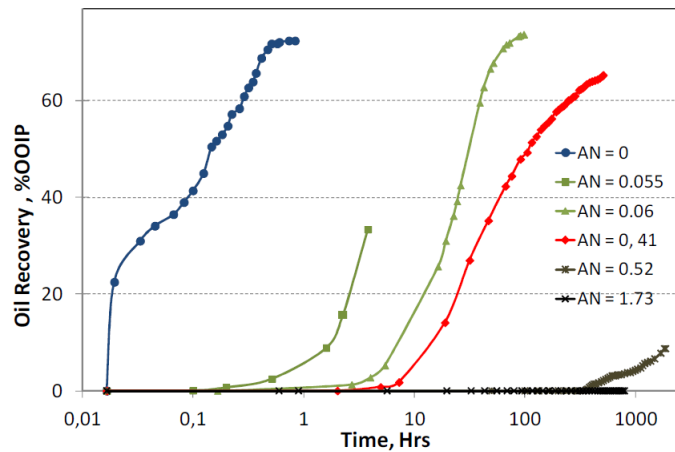


Figure 3.3: Spontaneous imbibition of water into chalk cores saturated with oil of different acid numbers. Figure by Standnes and Austad (2000).

The suggested mechanism for the wettability alteration is illustrated in Figure 3.4. Negatively charged sulfate-ions from the seawater adsorb onto the positively charged, water-wet areas on the chalk surface, lowering the overall positive surface charge. The reduced surface charge allows calcium-ions to co-adsorb near the chalk surface, which in turn will react with and release organic carboxylic components that are initially bonded to the surface (Zhang et al., 2007). The wettability alteration is triggered by disturbing the chemical equilibrium established in the system with the formation brine. Therefore, injecting a brine with a similar composition into the system will not suddenly trigger a chemical reaction. Sulfate is not present in seawater, albeit not formation brine, which is why it has an effect on the wetting condition when injected into the carbonates.

Temperature has also been proven to be a significant factor affecting this phenomenon. At higher temperatures, above 90-100°C,  $Mg^{2+}$  from the seawater was found to substitute  $Ca^{2+}$  at the chalk surface (Figure 3.4).  $Mg^{2+}$  become less hydrated with increasing temperatures and can form ion pairs with  $SO_4^{2-}$ . Thus,  $Mg^{2+}$  are able to assist in the wettability alteration process as its concentration increases near the surface. Similarly,  $SO_4^{2-}$  also become less hydrated and more reactive with higher temperatures. Therefore, the adsorption of  $SO_4^{2-}$  onto the chalk surface increases as the temperature increases (Zhang et al., 2007).

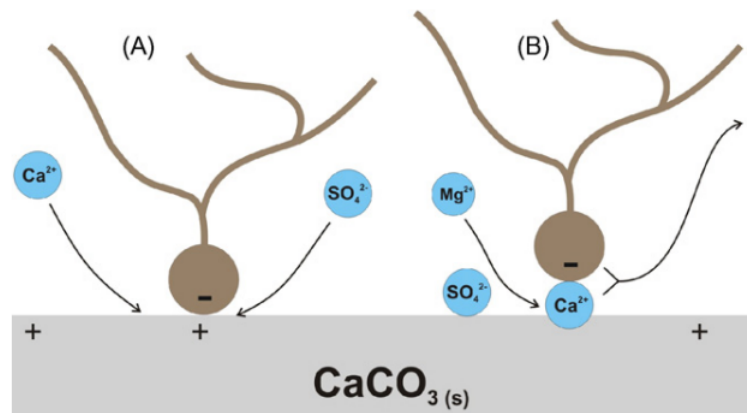


Figure 3.4: Suggested chemical reaction for the wettability modification by seawater injection. Illustration by Zhang et al. (2007).

In summary, seawater is an excellent wettability modifier in chalk, especially at higher temperatures, due to its ionic composition consisting of the important PDIs  $\text{Ca}^{2+}$ ,  $\text{Mg}^{2+}$  and  $\text{SO}_4^{2-}$ . Additionally, seawater can be optimized to improve wetting conditions and oil recovery even further by modifying the ionic composition. This is explored in the following section.

### 3.3 Smart Water

The definition of a "Smart Water" is a fluid with an optimized ionic composition, either natural or artificial, whose purpose is to disturb and modify the initial wetting state of a reservoir rock and ultimately improve the total oil recovery. Injection of Smart Water can be classified as an EOR technique as it is not in chemical equilibrium with the established system. This will in turn trigger chemical reactions that can improve the ultimate oil recovery. The main advantages of implementing smart water, rather than other EOR methods, is that its cheap and environmentally friendly, with no expensive or harmful chemicals added.

Seawater is, by the definition above, a natural Smart Water in chalk reservoirs. However, with the knowledge of the mechanisms for wettability alterations in chalk, the seawater can be modified to act even "smarter". This is achieved by optimizing the concentrations of active ions near the surface, most importantly the PDIs  $\text{Ca}^{2+}$ ,  $\text{Mg}^{2+}$  and  $\text{SO}_4^{2-}$ . Zhang et al. (2007) observed that increasing the  $\text{SO}_4^{2-}$  concentration beyond the normal concentration in seawater (24 mM) has a positive effect on the oil recovery. This effect was

more prominent at lower temperatures, as shown in Figure 3.5. At 100°C, the oil recovery by spontaneous imbibition almost doubled when the  $\text{SO}_4^{2-}$  concentration was increased 4 times the normal seawater concentration. Although, a high  $\text{SO}_4^{2-}$  concentration is not recommended due to the risk of precipitation of  $\text{CaSO}_4$ .

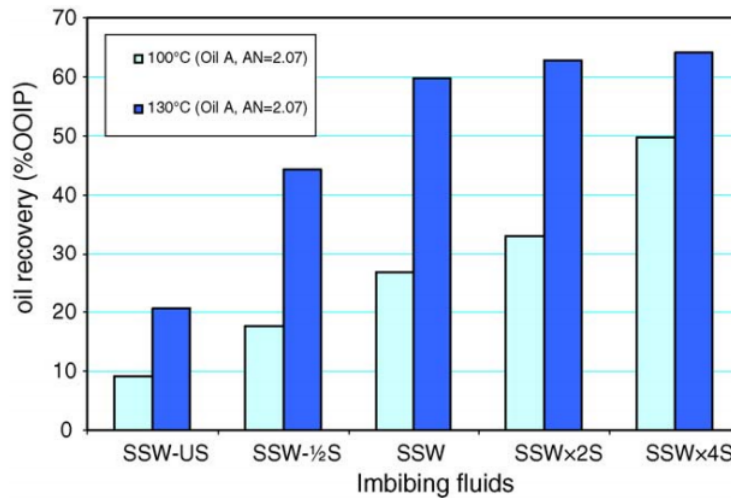


Figure 3.5: Total oil recovery from oil saturated chalk cores by spontaneous imbibition at 100 and 130°C. Different imbibing brines with varying  $\text{SO}_4^{2-}$  conc. were used. The oil had AN=2.07 mgKOH/g. Figure by Zhang and Austad (2006).

When a charged chalk surface interacts with a brine, a layer of ions is formed close to the surface called an electrical double layer. The previously mentioned PDIs are desired as they contribute to the wettability alteration. Other ions such as  $\text{Na}^+$  and  $\text{Cl}^-$  are non-active ions and do not participate in the process. The concentration of these ions is far greater compared to  $\text{Ca}^{2+}$ ,  $\text{Mg}^{2+}$  and  $\text{SO}_4^{2-}$  and prevents the active ions of fully having access to the chalk surface. From the understanding of the mechanism, depleting the seawater of NaCl should improve the effectiveness of the EOR process (Punternold et al., 2015).

Figure 3.6 shows that spontaneous imbibition by seawater depleted of NaCl, SW0Na, increased the oil recovery by 9% of OOIP compared to regular seawater. Increasing the amount of NaCl had an opposite effect and led to a poorer oil recovery (Fathi et al., 2011). The "smartest" water at 90°C is obviously SW0Na4S, which is seawater depleted of NaCl and spiked with 4 times its initial  $\text{SO}_4^{2-}$  concentration. Comparing this modified seawater to regular seawater, there is a drastic improvement in oil recovery from 37 to 62% of OOIP (Fathi et al., 2011). This shows that knowledge of the wettability alteration



mechanisms allows for optimized oil recovery by making a few adjustments to pre-existing injection fluids.

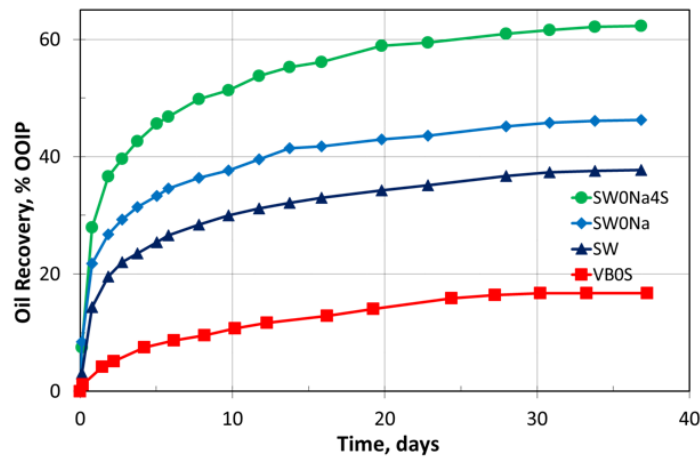


Figure 3.6: Spontaneous imbibition of chalk cores saturated with oil at 90°C. Four different imbibing brines were compared: formation water (VB0S), seawater (SW), and two smart waters SW0Na and SW0Na4S. Oil: AN=0.5 mgKOH/g. Figure by Fathi et al. (2011).

The same experiment was performed at 70°C to observe the effect of temperature on wettability alteration (Figure 3.7). Comparing the oil recovery by spontaneous imbibition of SW and SW0Na at both 70°C and 90°C, the results were very similar. However, imbibing SW0Na4S at 70°C showed only a small improvement in oil recovery compared to regular SW. Spontaneous imbibition with SW0Na4S yielded a total oil recovery of 48% of OOIP at 70°C, which was significantly lower compared to 62% of OOIP at 90°C. This confirmed the effect temperature has on the reactivity  $\text{SO}_4^{2-}$  ions and wettability alteration.

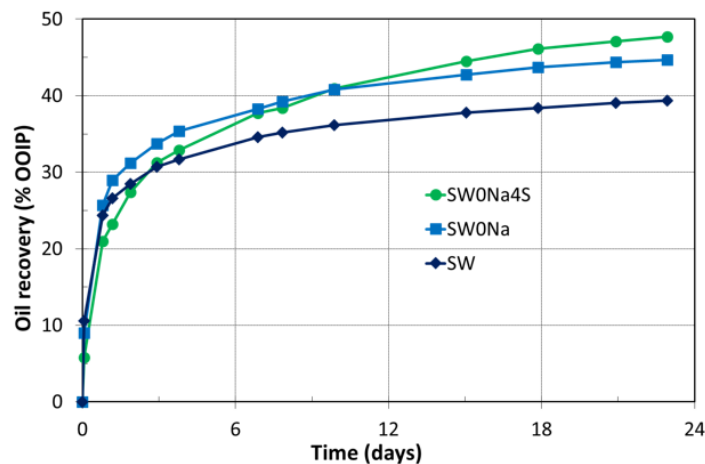


Figure 3.7: Spontaneous imbibition of chalk cores saturated with oil at 70°C. Three different imbibing brines were compared: seawater (SW) and two smart waters SW0Na and SW0Na4S. Oil: AN=0.5 mgKOH/g. Figure by Fathi et al. (2011).

### 3.3.1 Low-Salinity EOR

Low-salinity waterflooding (LSW) have for a long time been associated with water-based EOR in sandstone reservoirs. Based on previous experiments, spontaneous imbibition and forced imbibition tests using chalk cores had not shown a low-salinity EOR effect when exposed to diluted seawater. However, Austad et al. (2011) proved that if anhydrite is present in the rock, diluted seawater can improve oil recovery compared to high-salinity brines. The experiments were performed on limestone cores, where small amounts of anhydrite usually is present. By first flooding with high-salinity formation water, followed by a low-salinity brine, the increase in oil recovery varied between 1 and 5% of OOIP for the different tests. One of the forced imbibition tests are presented in Figure 3.8.

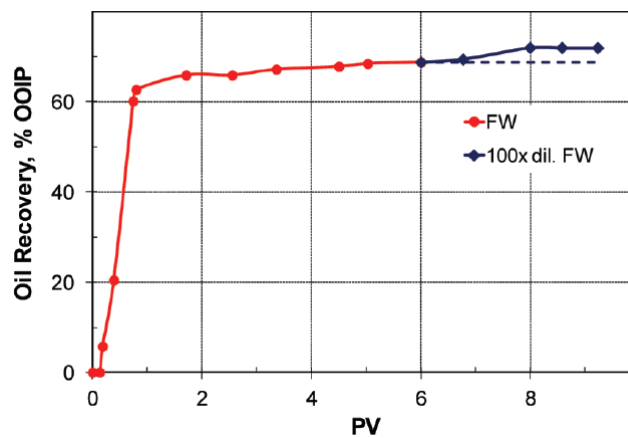


Figure 3.8: Successive flooding with FW and 100x diluted FW into reservoir limestone core at rate 1 PV/day and 90°C. Oil: AN=0.7 mgKOH/g.  $S_{wi}$ =10%. Figure by Austad et al. (2011).

The solubility of anhydrite in high-salinity waters is quite low due to the high concentration of  $Ca^{2+}$  and the common ion effect. By reducing the salinity of the injected brine, the solubility of anhydrite increases, allowing free  $Ca^{2+}$  and  $SO_4^{2-}$  to appear in-situ. The  $SO_4^{2-}$  can then adsorb onto the chalk surface and catalyze the wettability alteration process, as described in Section (3.2.2).

### 3.4 Production of Smart Water in Carbonates

#### 3.4.1 Nanofiltration Membranes

Smart Water production by nanofiltration (NF) membranes was proposed in a recent study (Nair, 2019). Membranes are defined as selective barriers, which allows certain elements to pass through while retaining others (Cheryan, 1998). The study proposed membrane desalination of seawater and produced water to produce injection water with relevant Smart Water composition. By feeding seawater through NF membranes, small monovalent ions ( $\text{Na}^+$ ,  $\text{Cl}^-$ ) would permeate through the membrane, while larger divalent ions ( $\text{Ca}^{2+}$ ,  $\text{SO}_4^{2-}$ ) would be rejected as retentate. The rejected feed would be enriched in surface active ions and depleted in non-active salt, which meet the criteria for a successful Smart Water in carbonates. Figure 3.9 is a schematic of the proposed Smart Water production from seawater using NF membranes.

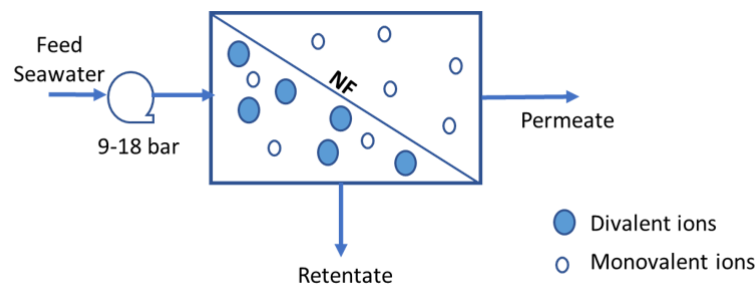


Figure 3.9: Principle of nanofiltration membrane. Figure by Nair 2019.

The NF membranes that were tested proved to be somewhat ineffective. They were able to reject most of the  $\text{SO}_4^{2-}$ , but only about 60% of  $\text{Ca}^{2+}$ . The ion rejection at different pressures for a certain NF membrane is shown in Figure 3.10. Pretreated seawater at  $1 \text{ m}^3/\text{h}$  and TDS of  $30\,000 \text{ mg/L}$  was used as feed and the NF retentate intended as Smart Water for carbonates came out at  $0.79 \text{ m}^3/\text{h}$  and with a TDS of  $31\,500 \text{ mg/L}$ . This shows that the NF membrane was not able to reduce the salinity of the final product. The membranes were not successful in removing monovalent ions from the retentate as the separation of divalent and monovalent ions created an unstable charge balance. This caused more  $\text{Na}^+$  and  $\text{Cl}^-$  to hang back in the retentate.

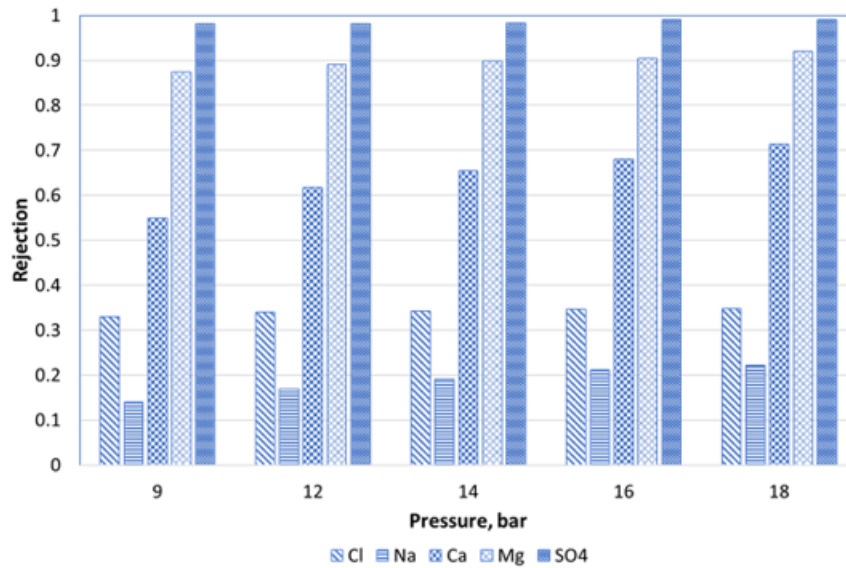


Figure 3.10: Ion rejection for NANO-SW NF membrane with increasing pressure. Figure by Nair 2019.

### H<sub>2</sub>SO<sub>4</sub>-injection

The proposed technique for producing a Smart Water in this thesis is by injection of H<sub>2</sub>SO<sub>4</sub> into chalk material. By injecting a diluted H<sub>2</sub>SO<sub>4</sub>-solution, SO<sub>4</sub><sup>2-</sup> is directly provided by the injectant, while Ca<sup>2+</sup> is produced in-situ by dissolving parts of the chalk material which mainly consist of CaCO<sub>3</sub>. The end result will be a simple brine consisting of a controlled amount of the main PDIs Ca<sup>2+</sup> and SO<sub>4</sub><sup>2-</sup>. The brine will also be free of non-active salts, improving the access of PDIs on the surface. The method is described more in-depth in the following chapters.

# Chapter 4

## Experimental Work

This chapter outlines the materials, instruments and methods used to carry out the experimental part of the thesis.

### 4.1 Materials

#### 4.1.1 Core Material

The experiments in this study were performed on Stevns Klint (SK) outcrop chalk material. All the cores were drilled parallel to each other from the same outcrop block. SK chalk was selected for the experiments due to its resemblance to North Sea reservoir chalk (Frykman, 2001). The chalk is of Upper Maastrichtian age, has a fairly high porosity (45-50%) and low matrix permeability (3-5 mD). This material consists of  $\sim 98\%$  pure chalk and has a low clay content resulting in an average specific surface area of approximately  $2 \text{ m}^2/\text{g}$  (Røgen and Fabricius, 2002). The cores used in this thesis are presented in Table 4.1 below.

Table 4.1: Stevns Klint outcrop chalk core properties.

Core name	Length (cm)	Diameter (cm)	Pore Volume (ml)	Porosity (%)	k (mD)	$S_{wi}$ (%)	OOIP (ml)
SK1	7.02	3.78	38.32	49	4.659	-	-
SK2	6.47	3.78	36.15	50	5.465	10	32.54
SK3	6.30	3.79	34.37	48	4.834	10	30.93
SK4	6.31	3.80	36.27	51	4.952	10	32.64
SK5	6.23	3.79	35.39	50	4.979	10	31.85
SK6	6.25	3.80	33.75	51	5.140	10	30.38
SKWW	7.07	3.79	39.17	49	4.637	20	31.54

Core SK1 was used as chalk material during H<sub>2</sub>SO<sub>4</sub>-flooding experiment and cores SK2, SK3 and SK4 were used during the oil recovery tests at 70°C. Cores SK5 and SK6 were used during parallel oil recovery tests at 90°C and the data were borrowed from Lindanger (2019). Core SKWW was used to represent oil recovery in a strongly water-wet core.

#### 4.1.2 Oils

Throughout the experiments, a model crude oil, Oil A, was used with AN and BN values of ~0.50 and ~0.23 mgKOH/g oil, respectively. A base oil, RES-40, was prepared by mixing Heidrun Oil with n-heptane in a volume ratio of 60:40, then centrifuged and filtrated through a 5 µm Milipore filter. Some of the base oil was treated with silica gel to remove any surface-active components, which resulted in AN and BN values close to zero. This oil was called RES-40-0. Oil A was made by mixing RES-40 and RES-40-0 in a calculated volume ratio dictated by the desired AN:

$$Target\ AN = AN_{RES-40} \cdot \frac{V_{RES-40}}{V_{RES-40+RES-40-0}} + AN_{RES-40-0} \cdot \frac{V_{RES-40-0}}{V_{RES-40+RES-40-0}} \quad (4.1)$$

Mineral oil was used in a spontaneous imbibition experiment on a strongly water-wet core, SKWW, demonstrating the significance of AN. Mineral oil does not contain any polar compounds, and therefore has AN=0. It was prepared by mixing Marcol 85 and n-heptane in a volume ratio of 58:42. The ratio was determined by measuring the viscosity of mineral oils with different volume ratios and trying to match the viscosity of the crude oils used in the experiments (Figure 4.1).

Table 4.2: Measured oil properties.

	Density (g/cm <sup>3</sup> )	AN (mgKOH/g oil)	BN (mgKOH/g oil)	Viscosity (cP)
RES-40	0.82	2.40	0.90	2.7
RES-40-0	0.81	0.06	0.01	2.4
Oil A	0.81	0.50	0.23	2.5
Mineral Oil	0.78	-	-	2.7

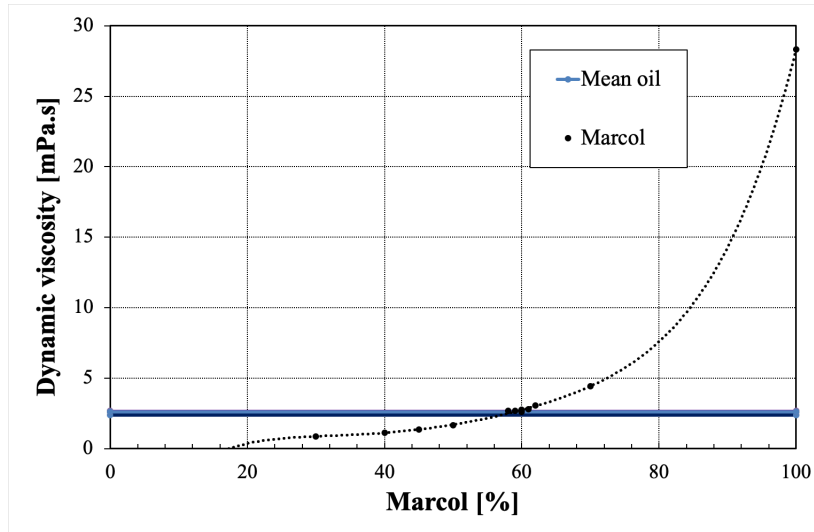


Figure 4.1: The viscosity of different mineral oils with increasing amounts of Marcol 85. The light blue line represents mean viscosity of the crude oils. Figure by Wathne (2019).

### 4.1.3 Brines

The brines were artificially prepared in the laboratory to be used in the core restoration process and the oil recovery experiments. By following a set of recipes, different predetermined brines were made by dissolving salts in de-ionized (DI) water. All brines were filtrated through membrane filters with 0.22  $\mu\text{m}$  pore size. The composition of the different brines can be found in Table 4.3.

Table 4.3: Compositions of the brines in mM used in the oil recovery experiments.

Ion	FW (VB0S) (mM)	SW (mM)	Smart Water (mM)
NaCl	987.0	400.0	0.0
Na <sub>2</sub> SO <sub>4</sub>	0.0	24.0	0.0
NaHCO <sub>3</sub>	9.0	2.0	0.0
KCl	5.0	10.0	0.0
MgCl <sub>2</sub> · 6 H <sub>2</sub> O	8.0	45.0	0.0
CaCl <sub>2</sub> · 2 H <sub>2</sub> O	29.0	13.0	0.0
CaSO <sub>4</sub> · 2 H <sub>2</sub> O	0.0	0.0	13.0
Density	1.040	1.024	0.995
TDS	62.83	33.39	1.770
Ionic strength	0.657	1.112	0.026

Artificial formation water (FW) was made to resemble the formation water located in the Valhall field. The brine was labeled VB0S, due to its exclusion of sulfate-ions (SO<sub>4</sub><sup>2-</sup>). It was then diluted 10 times and used to establish initial wetting in the cores and as imbibing fluid for the reference core during the oil recovery experiments. Two other brines were

used as imbibition fluids in this experiment: synthetic seawater (SW) and Smart Water. The Smart Water brine was made by dissolving gypsum ( $\text{CaSO}_4 \cdot 2\text{H}_2\text{O}$ ) in DI water and is supposed to represent the Smart Water achieved by flooding sulfuric acid through chalk. The composition of the Smart Water brine was determined from the acid flooding experiments which were conducted prior to starting the oil recovery processes.

The IFT values between selected oils and the various brines were measured at ambient temperature ( $23^\circ\text{C}$ ) and pressure (1 atm) (Table 4.4). The measured IFT was lowest for the brines with higher salinity, such as FW and SW. The salinity of the Smart Water is significantly lower compared to FW, which is reflected in the higher IFT value. The highest IFT was measured between the mineral oil and DI water.

Table 4.4: IFT values between interacting oils and brines. Measurements taken at ambient temperature ( $23^\circ\text{C}$ ) and pressure (1 atm).

	IFT (mN/m)
Oil A/DI water	18.17
Oil A/FW	10.67
Oil A/SW	10.17
Oil A/Smart Water	14.33
Mineral Oil/DI Water	41.00



## 4.2 Analyses

The different instruments, programs and techniques used in this study are presented in this section.

### 4.2.1 pH Measurements

The pH of prepared brines and effluents was measured using the Mettler Toledo SevenCompact™ pH meter. The electrode used was an InLab semi-micro electrode. The measurements were taken at room temperature and repeated a couple of times until the accuracy of the pH values were within a  $\pm 0.01$  range.

### 4.2.2 Density Measurements

The Anton Paar densimeter DMA 4500 was used to measure the density of oils, brines and effluents. Prior to each measurement, the equipment was cleaned with white spirit, acetone and distilled water. After injecting the sample, the system needed to be checked for any contamination like air bubbles to ensure that the apparatus correctly measured the sample.

### 4.2.3 Viscosity Determination

The Anton Paar rheometer Physica MCR 302 was used to determine the viscosity of the oil and brines. For each fluid sample, approx. 650  $\mu\text{l}$  was analyzed at a time. The viscosities were determined via shear rate/stress relations at room temperature ( $\sim 23^\circ\text{C}$ ). The measurements from the analysis of Oil A are included in Appendix B.2.

### 4.2.4 Acid and Base Number Determination

The amount of acidic and basic polar components (mg KOH/g) in the prepared oils was determined using potentiometric titration techniques. The techniques used were developed by Fan and Buckley (2006) and are altered versions of ASTM D664 and ASTM D2896 for AN and BN titration, respectively. A Mettler Toledo T50 automatic titrator was used.

To perform the AN and BN measurements, four solutions per measurement were prepared; an electrolyte, standard solution, titration solution and spiking solution. The contents of the different solutions are presented in Appendix A.

#### 4.2.5 Ion Chromatography (IC)

The amount of  $\text{Ca}^{2+}$ ,  $\text{SO}_4^{2-}$  and other ions in effluent samples were analyzed by a Dionex™ ICS-5000+ ion chromatograph. Before analyzing the samples, they were diluted 1000 times with DI water and filtrated through 0.2  $\mu\text{m}$  Supor (PES) Membrane. The results from the analyses were saved in the affiliated computer software. The software plots the conductivity against retention time, and the relative concentration of each ion is represented by the area under their respective peak on the graph. Then, a standard method is used to convert the output into an estimate of the concentrations of each separate anion and cation.

#### 4.2.6 Interfacial Tension (IFT) Measurements

The IFT between selected oils and brines was measured using a Krüss K6 Force Tensiometer at room temperature (23°C). The instrument uses the ring method, where a measuring ring is connected to a torsion wire and suspended in an oil/water sample. IFT measurements are made by slowly lowering the sample, causing the ring to withdraw and move from the water phase to the oil phase. The tension between the phase boundary pulls on the wire and its deflection is calibrated for the IFT (KRÜSS, 2019).

#### 4.2.7 Scanning Electron Microscopy (SEM) Analysis

The topography and mineral structure of the chalk cores were analyzed using a Zeiss Supra 35VP environmental scanning electron microscope (SEM). The apparatus generates a highly detailed image of the chalk surface by using a focused electron beam. The cores were cut into circular slices and broken into small rock fragments which were used as representative, uncontaminated samples of the chalk surface. The rock samples were coated with palladium (Pd) in a K550 Emitech Sputter Coater in order to enhance the electrical conductivity of the samples. This conductive film on the surface improves the imaging, inhibits charging and reduces thermal damage of the sample (Emitech, 1999).

The SEM was equipped with an energy-dispersive x-ray spectroscope (EDS) that was used to identify the elemental composition of the chalk samples. The elements on the surface are targeted by an electron beam and emits specific x-rays that are representative of their atomic structure (S. Ebnesajjad and C. Ebnesajjad, 2013). The x-ray emissions were analyzed by a Si(Li) detector.

### 4.3 Methods

The experimental methods and instruments used in the experimental parts of the thesis are summarized in this section.

#### 4.3.1 Porosity Calculation

Initially, the length ( $L$ ) and diameter ( $D$ ) of the cores were measured and used to determine the bulk volume ( $V_B$ ) assuming fully cylindrical cores:

$$V_B = \frac{\pi \cdot D^2 \cdot L}{4} \quad (4.2)$$

After the cores had been dried, the dry weight ( $W_{dry}$ ) was measured. The cores were then 100% saturated with DI water in a vacuum chamber and the saturated weight ( $W_{sat}$ ) was measured. The difference between  $W_{sat}$  and  $W_{dry}$  was used to determine the pore volume ( $V_P$ ):

$$V_P = \frac{W_{sat} - W_{dry}}{\rho_{DIW}} = W_{sat} - W_{dry} \quad (4.3)$$

The density of DI water ( $\rho_{DIW}$ ) is 1.0 g/cm<sup>3</sup>. Finally, the porosity ( $\phi$ ) could be calculated by the following relationship between  $V_P$  and  $V_B$ :

$$\phi = \frac{V_P}{V_B} \quad (4.4)$$

#### 4.3.2 Permeability Determination

The permeability of each core sample was calculated using data from core flooding tests with DI water. The cores were flooded at three different rates, 0.05, 0.10 and 0.15 ml/min, and the average pressure drop across the core during each rate was recorded. The relation between the flow rates and the pressure drops was noted and used in the Darcy equation, see Equation 2.3 in Section (2.2.2). By rearranging the equation and knowing the water viscosity and dimensions of the core, the permeability could be determined:

$$k = \frac{q}{\Delta P} \cdot \frac{\mu \cdot L}{A} \quad (4.5)$$

See Appendix B.1 for an example of permeability calculation for a core.

### 4.3.3 Core Flooding Setup

The general setup for a core flooding experiment was made up of a Gilson HPLC pump, stainless steel piston cells and a Hassler type core holder. Some experiments were performed at certain temperatures and for these tests the core holder was placed inside a heating oven. The confining pressure and back pressure in the system was consistent throughout all core floodings at 20 bar and 10 bar, respectively. A schematic diagram is shown in Figure 4.2. While flooding a core, the pump rate, pressure difference, system limitations, etc. were easily monitored and controlled using the computer program LabVIEW.

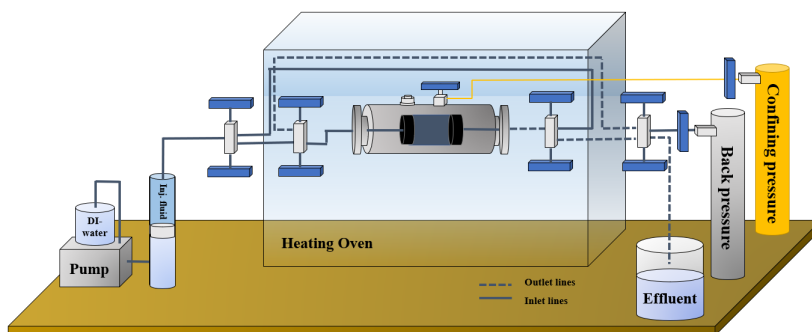
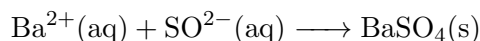


Figure 4.2: Illustration of a general core flooding setup. Redrawn after Jakobsen (2018).

### 4.3.4 Core Cleaning

The cores were initially cleaned in a flooding setup with DI water and a rate of 0.1 ml/min to remove any easily dissovlabl ions, specifically  $\text{SO}_4^{2-}$  which is known to affect the wetting state (Punternvold et al., 2007). Batch tests of the effluent using a  $\text{BaCl}_2$ -salt were taken regularly to check for remaining  $\text{SO}_4^{2-}$  in the core. If sulfate was present, it would react with  $\text{Ba}^{2+}$  and precipitate as  $\text{BaSO}_4$ , as shown in the chemical equation below.



All cores were cleaned at room temperature for approximately 2-3 days, before being completely dried again in an oven at 90°C.

### 4.3.5 Chalk Core Restoration

When performing experiments on outcrop chalk cores, it is ideal to resemble the reservoir conditions as closely as possible. The restoration process followed a procedure proposed by Puntervold et al. (2007).

#### 4.3.5.1 Establishing Initial Water Saturation

First, the cores were 100% saturated with the diluted FW. In order to establish a 10% initial water saturation ( $S_{wi}$ ) the cores were placed in a desiccator containing heated silica gel (Springer et al., 2003). Silica gel is a hygroscopic substance, meaning it attracts and stores water molecules from the surrounding environment. This caused a steady vaporization of the water molecules within the cores, resulting in a salinity close to VB0S. The weight of the cores was constantly monitored to know when they had reached their target  $S_{wi}$ . This target weight at  $S_{wi}=10\%$  was calculated by the following equation:

$$W_{target} = W_{dry} + S_{wi} \cdot V_P \cdot \rho_{FW} \quad (4.6)$$

where:

$W_{target}$	target weight of the core (g)
$W_{dry}$	dry weight of the core (g)
$S_{wi}$	initial water saturation
$V_P$	pore volume (ml)
$\rho_{FW}$	density of FW (1.04 g/cm <sup>3</sup> )

#### 4.3.5.2 Oil Saturation and Flooding

Once the cores had been drained to  $S_{wi}=10\%$ , the remaining 90% of the pore volume was to be saturated with crude oil. Oil saturation was done in a flooding setup at 50°C, without back pressure and confining pressure of 20 bar. Each core was flooded with crude

oil a total of 5 PV. First, the lines and cores were exposed to vacuum. Thereafter, the cores were saturated with crude oil by flooding 1 PV at 0.5 ml/min from both directions simultaneously. After this, the cores were flooded 2 PV at 0.165 ml/min in each direction, while collecting the effluent oil to be used in the ageing process.

#### 4.3.5.3 Ageing

For the cores to best resemble reservoir conditions, they were wrapped in Teflon tape, placed inside a stainless steel cell, immersed in effluent oil, and aged for two weeks at 70°C. The temperature was set to correspond with the temperature used in the following oil recovery experiments. The purpose of the Teflon tape was to protect the core from adsorbing any unrepresentative polar components onto its surface.

#### 4.3.6 Oil Recovery by Spontaneous Imbibition

Following the ageing process, spontaneous imbibition (SI) was performed on the newly restored cores. A SI setup consisted of a stainless steel cell inside an oven at 70°C, a piston cell providing back pressure of 10 bar to prevent the oil from boiling, and a burette to collect the produced oil (Figure 4.3).

First, the cores were cooled down and the teflon tape removed. They were then placed in the steel cells and immersed in their respective imbibing brines. The FW brine was used as imbibing fluid for SK2. This core was used as a reference core, as FW was already in equilibrium with the core and oil. FW should therefore not cause any new chemical interactions leading to a wettability change. Brines SW and Smart Water were used as imbibing fluids for SK3 and SK4, respectively. The oil production was continuously recorded and % of OOIP was measured against time until a plateau was reached. The % of OOIP was calculated by dividing the volume produced oil ( $V_{o,p}$ ) by the OOIP:

$$\% OOIP = \frac{V_{o,p}}{OOIP} \cdot 100\% \quad (4.7)$$

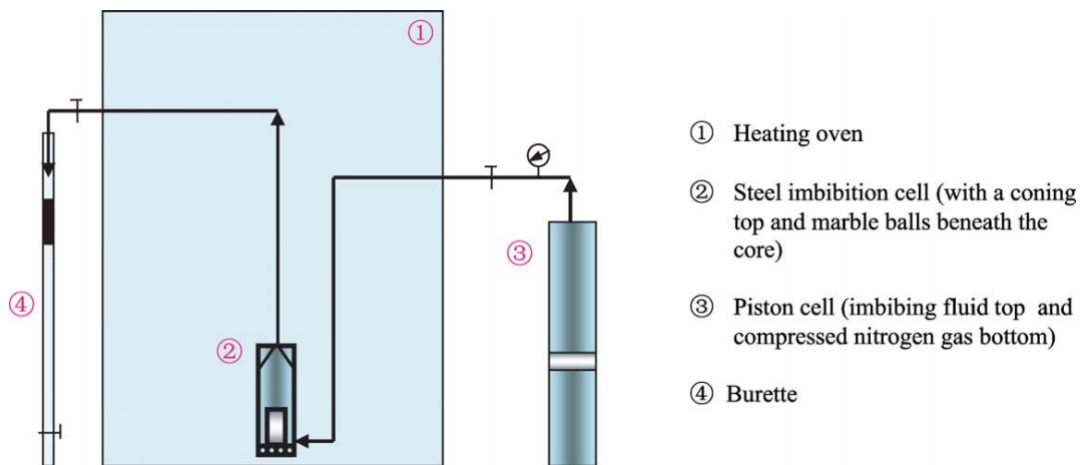


Figure 4.3: Illustration of spontaneous imbibition setup for high temperature tests. Figure by Zhang (2006).

#### 4.3.7 Additional Oil Recovery by Forced Imbibition

Forced imbibition (FI) experiments, also called viscous flooding (VF), were conducted following the spontaneous imbibition experiments. Both procedures involve displacement of oil, only instead of a spontaneous uptake of the brines by the cores, forced imbibition is achieved by injecting brine through the core at a set rate, forcing a displacement of the oil. The setup was similar to Figure 4.2, only addition being a burette for collecting and monitoring the cumulative oil production. The recovered oil was measured as % of OOIP and plotted against time. All FI experiments were conducted at 70°C.

The first part of the FI experiments was to inject the same brines that were used in the SI experiments for the respective cores. The flooding rate was initially set to 1 PV/day. After reaching a plateau, the brine was switched from SW and FW to Smart Water for the cores SK3 and SK4, respectively. After reaching a final plateau, the rate was increased to 4 PV/day to observe the effect of the viscous forces.



## 4.4 Production of Smart Water by Acid Flooding

### 4.4.1 Bulk Solution Tests of H<sub>2</sub>SO<sub>4</sub>-CaCO<sub>3</sub> Mixtures

Previous to writing this thesis, an unpublished experiment was conducted by the Smart Water EOR Group at the University of Stavanger (UiS) where different solutions of H<sub>2</sub>SO<sub>4</sub> and CaCO<sub>3</sub> in DI water were mixed together to observe when precipitation of CaSO<sub>4</sub> occurred (Nanidou and Mirkovic, 2019). More specifically, 10 g of CaCO<sub>3</sub> was dissolved in 10 ml of DI water and subsequently tested with H<sub>2</sub>SO<sub>4</sub> concentrations from 4 to 20 mM. The samples were then stirred for 24 hours at selected temperatures of 50, 70, 100 and 130°C. Following this, the samples were centrifuged and the equilibrated fluid was gathered and analyzed using an Ion Chromatograph. The results from the experiment are presented in Table 4.5. The results coincide with the theory that solubility of CaSO<sub>4</sub> decreases with higher temperatures. This is depicted by a general trend in the results as the concentration needed to avoid precipitation becomes lower for each increasing step in temperature. It is important to mention that the results from the IC are not entirely accurate as the apparatus is very sensitive. This is evident by some results displaying higher output of ions than the initial concentration.

The bulk solution tests were the basis of which the concentrations were considered for the following H<sub>2</sub>SO<sub>4</sub>-flooding tests. As they were only mixed in vials and not exposed to any carbonate rocks, the next step was to test if the results were comparable to similar concentrations of H<sub>2</sub>SO<sub>4</sub> being flooded through a chalk core.

Table 4.5: The results from the IC analysis of the equilibrated H<sub>2</sub>SO<sub>4</sub>-CaCO<sub>3</sub> solutions. The values in bold are samples where CaSO<sub>4</sub> precipitated. Table provided by Nanidou and Mirkovic (2019).

Brines	T=50°C		T=70°C		T=100°C		T=130°C	
H <sub>2</sub> SO <sub>4</sub> [mM]	SO <sub>4</sub> <sup>2-</sup> [mM]	Ca <sup>2+</sup> [mM]	SO <sub>4</sub> <sup>2-</sup> [mM]	Ca <sup>2+</sup> [mM]	SO <sub>4</sub> <sup>2-</sup> [mM]	Ca <sup>2+</sup> [mM]	SO <sub>4</sub> <sup>2-</sup> [mM]	Ca <sup>2+</sup> [mM]
4							4.2	4.9
6							7.0	9.6
8							<b>8.0</b>	<b>9.3</b>
10					9.4	6.3	<b>8.5</b>	<b>4.8</b>
12					12.1	11.5	<b>9.2</b>	<b>7.3</b>
16			15.7	18.2	<b>13.4</b>	<b>11.9</b>		
18	19.4	17.1	<b>14.9</b>	<b>11.8</b>	<b>13.6</b>	<b>10.0</b>		
20	20.2	20.5	<b>14.4</b>	<b>14.8</b>	<b>12.7</b>	<b>13.0</b>		

#### 4.4.2 Core Flooding with Sulfuric Acid

Based on the results from the bulk solution tests, it was decided to monitor dissolution of  $\text{CaCO}_3$  during  $\text{H}_2\text{SO}_4$  flooding at two temperatures, 70 and 130°C. The concentrations of the sulfuric acid solutions were chosen within range of  $\text{CaSO}_4$  precipitation for each temperature. A pre-prepared 1 molar  $\text{H}_2\text{SO}_4$  solution was diluted with DI water into five solutions of varying concentrations (Table 4.6). Each solution was prepared in a volumetric flask and stirred for 24 hours. For 70°C, three sulfuric acid solutions were made; 9.7, 13.3 and 16.7 mM  $\text{H}_2\text{SO}_4$ . For 130°C, only two solutions were made; 4.9 and 8.5 mM  $\text{H}_2\text{SO}_4$ . The pH of the prepared solutions were measured and are presented in Table 4.6.

Table 4.6: Prepared sulfuric acid solutions.

$\text{H}_2\text{SO}_4$ conc.	pH
4.9 mM	2.25
8.5 mM	2.19
9.7 mM	2.16
13.3 mM	2.09
16.7 mM	2.05

A single SK chalk core, SK1, was cleaned, following the procedure in Section (4.3.4), before being subjected to the five different  $\text{H}_2\text{SO}_4$  solutions. Each acid solution was flooded through the core at a rate of 12 PV/day and a total of 6 PV. A setup like Figure 4.2 was used and the effluent was automatically sampled by having a Gilson GX-271 Liquid Handler connected to the outlet. The pH and ionic composition of collected effluent samples were analyzed to check for precipitation of  $\text{CaSO}_4$  and dissolution of the chalk core. In-between each round of acid flooding, the core was cleaned with approximately 18 PV of DI water to remove any sulfate in the system. Two piston cells were utilized to easily alternate between DI water and  $\text{H}_2\text{SO}_4$  solution.

## Chapter 5

# Results and Discussion

The efficiency of a water-based EOR method is heavily reliant on the ionic composition of the injected brines. Seawater has proven through several studies to be an effective wettability modifier in chalk at high temperatures ( $<90^{\circ}\text{C}$ ) (Strand et al., 2006; Zhang and Austad, 2006). The interplay between the active PDIs  $\text{Ca}^{2+}$ ,  $\text{Mg}^{2+}$  and  $\text{SO}_4^{2-}$  at the chalk surface displaces the adsorbed carboxylic components from the oil and induces higher water-wetness.

Wettability alteration has further been optimized by the introduction of Smart Water EOR. Smart Water can be described as an EOR fluid with optimal ionic composition and concentration, which is able to improve the wettability in a system. Different approaches to producing a Smart Water have been explored, where main focus have been to optimize the amount of PDIs and reduce the amount of NaCl, e.g. nanofiltration membranes (Nair, 2019).

The purpose of this thesis is to investigate the potential of using a simple  $\text{H}_2\text{SO}_4$ -based Smart Water as wettability modifier in chalk at  $70^{\circ}\text{C}$ .  $\text{H}_2\text{SO}_4$  is a very cheap chemical, which in turn would make the Smart Water cheap to produce. As mentioned, temperature has been shown in previous studies to limit the Smart Water EOR effect below  $90^{\circ}\text{C}$ ; the surface reactivity of PDIs decreases as the temperature decreases. Parts of the experimental work in the thesis were performed in conjunction with another master's thesis investigating the Smart Water effects at  $90^{\circ}\text{C}$  (Lindanger, 2019). By testing the Smart Water at  $70^{\circ}\text{C}$ , the temperature effect can be studied by comparing the results with with the results obtained at  $90^{\circ}\text{C}$ . The efficiency of Smart Water on oil displacement in SK

outcrop chalk cores is experimentally investigated. The experimental work can be divided into two main parts; H<sub>2</sub>SO<sub>4</sub>-flooding tests through SK chalk to determine an optimal Smart Water composition, and successive oil recovery experiments using said Smart Water.

## 5.1 Sulfuric Acid Flooding - A Sensitivity Analysis

Several studies have proven the positive effect sulfate and calcium-ions have on wettability alteration in chalk. SO<sub>4</sub><sup>2-</sup> act as a catalyst for the process and Ca<sup>2+</sup> reacts with the adsorbed carboxylic groups on the chalk surface. Thus, when designing a Smart Water, the presence and concentration of both these ions are important factors. Too high concentration of either SO<sub>4</sub><sup>2-</sup> or Ca<sup>2+</sup> in the Smart Water can result in precipitation of CaSO<sub>4</sub> as solubility decreases due to the common-ion effect. The solubility of CaSO<sub>4</sub> is also sensitive to temperature and will decrease with increasing temperature.

By injecting a H<sub>2</sub>SO<sub>4</sub>-solution into chalk, it supplies the solution directly with SO<sub>4</sub><sup>2-</sup>, while also dissolving Ca<sup>2+</sup> from the rock. The amount of dissolved Ca<sup>2+</sup> will initially be determined by the solubility of CaCO<sub>3</sub> at the different temperatures. Therefore, the objective when designing this Smart Water was to decide on an optimal SO<sub>4</sub><sup>2-</sup> concentration to ensure sufficient dissolution of Ca<sup>2+</sup>, while also avoiding precipitation of CaSO<sub>4</sub>. The optimal amount of SO<sub>4</sub><sup>2-</sup> to be used in the Smart Water was determined by injecting DI water with different concentrations of H<sub>2</sub>SO<sub>4</sub> into the chalk core at different temperatures. The ionic composition and pH of the effluent collected during H<sub>2</sub>SO<sub>4</sub>-flooding were then analyzed to track the dissolution of Ca<sup>2+</sup> and the possible precipitation of CaSO<sub>4</sub>. Core SK1 was used as chalk material during these tests. The results from the effluent analyses are presented in the following sections.

### 5.1.1 Dissolution of $\text{CaCO}_3$ during $\text{H}_2\text{SO}_4$ Flooding at $70^\circ\text{C}$

The ionic composition and concentrations of the effluent samples were analyzed throughout the  $\text{H}_2\text{SO}_4$ -flooding by the means of ion chromatography. By comparing the IC results with the input concentrations of  $\text{H}_2\text{SO}_4$ , it gives an indication of the interactions between  $\text{SO}_4^{2-}$  and  $\text{Ca}^{2+}$  within the core. Figure 5.1 displays the concentrations of  $\text{Ca}^{2+}$  and  $\text{SO}_4^{2-}$  in the effluent plotted versus PV injected. The injected  $\text{H}_2\text{SO}_4$  concentrations were 9.7, 13.3 and 16.7 mM and are visualized by the black stapled lines.

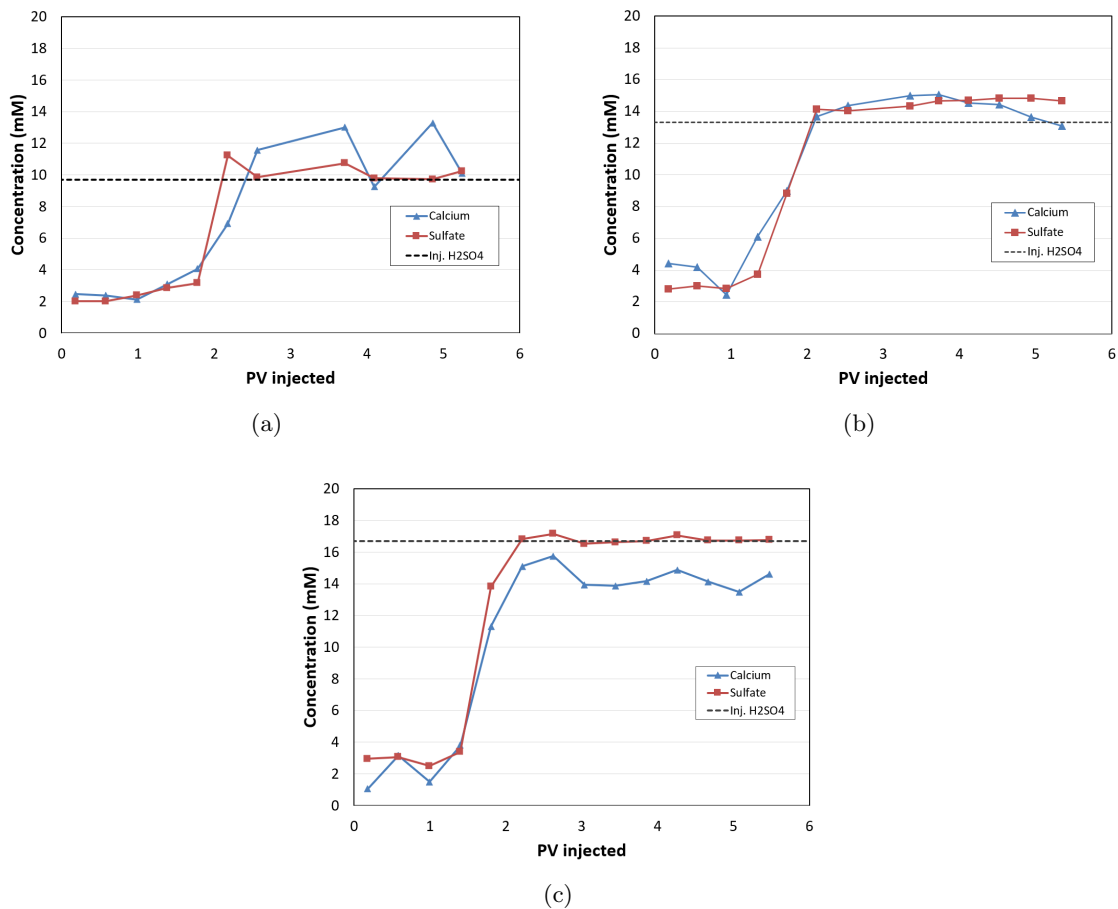


Figure 5.1: Dissolution of  $\text{CaCO}_3$  at  $70^\circ\text{C}$  during injection of different  $\text{H}_2\text{SO}_4$  solutions at 12 PV/day. In (a) 9.7 mM  $\text{H}_2\text{SO}_4$  was injected, in (b) 13.3 mM  $\text{H}_2\text{SO}_4$  and in (c) 16.7 mM  $\text{H}_2\text{SO}_4$ . The concentrations of  $\text{Ca}^{2+}$  and  $\text{SO}_4^{2-}$  in the effluent are estimated from IC analysis.

From the figures, no precipitation is detected within the core for any of the  $\text{H}_2\text{SO}_4$  solutions at  $70^\circ\text{C}$ . This is evident by the  $\text{SO}_4^{2-}$  concentrations which equilibrates very close the injected  $\text{H}_2\text{SO}_4$  concentrations. The  $\text{Ca}^{2+}$  concentrations also follows the  $\text{SO}_4^{2-}$  trends, which fits the prediction from Section (1.1). There is a small difference of  $\sim 2.5$  mM between  $\text{SO}_4^{2-}$  and  $\text{Ca}^{2+}$  at 16.7 mM (Figure 5.1c), although, this may be attributed to a couple of factors. Most likely, the sulfuric acid was not able to dissolve any more  $\text{Ca}^{2+}$  from the chalk due to the common ion effect, as described in Section (2.5). The amount of dissolved  $\text{Ca}^{2+}$  stabilized around 14 mM. Uncertainties can also be attributed to the instruments and equipment used. The IC samples are diluted 1000 times before being analyzed and are thus very sensitive to contaminants in the vials containing the samples. Small inaccuracies can also come from the IC software when it tries to calculate the area under the peaks. Depending on the shape of the peak, the estimation can sometimes be slightly off, resulting in inaccurate calculations of the ion concentrations. For each solution, the  $\text{SO}_4^{2-}$  and  $\text{Ca}^{2+}$  in the effluent arrive at approximately 1.5 PV, which signals adsorption of  $\text{SO}_4^{2-}$  in the core. If no adsorption had taken place,  $\text{SO}_4^{2-}$  would have arrived after 1 PV. The concentration profiles appear to stabilize after  $\sim 2$  PV as equilibrium is reached within the core.

In all three tests, the first effluent samples show an initial  $\text{SO}_4^{2-}$  concentration of  $\sim 2.5$  mM. This may indicate that the cleaning procedure was not sufficient in removing all adsorbed or precipitated  $\text{SO}_4^{2-}$  ions. Approximately 18 PV of DI water was injected in between each acid flooding. Towards the end of the cleaning, the effluent was collected and mixed with a  $\text{BaCl}_2$ -salt to check for remaining  $\text{SO}_4^{2-}$ , as explained in Section (4.3.4). Despite a supposedly clean  $\text{BaSO}_4$ -precipitation test, it seems there still were tiny amounts of  $\text{SO}_4^{2-}$  in the tests.

### 5.1.2 Dissolution of $\text{CaCO}_3$ during $\text{H}_2\text{SO}_4$ Flooding at $130^\circ\text{C}$

The results from the IC analyses of the tests at  $130^\circ\text{C}$  are presented in this section. Figure 5.2 shows the concentrations of  $\text{Ca}^{2+}$  and  $\text{SO}_4^{2-}$  from the effluent samples plotted against injected PV. The  $\text{H}_2\text{SO}_4$  concentration of the injected solutions were 4.9 and 8.5 mM.

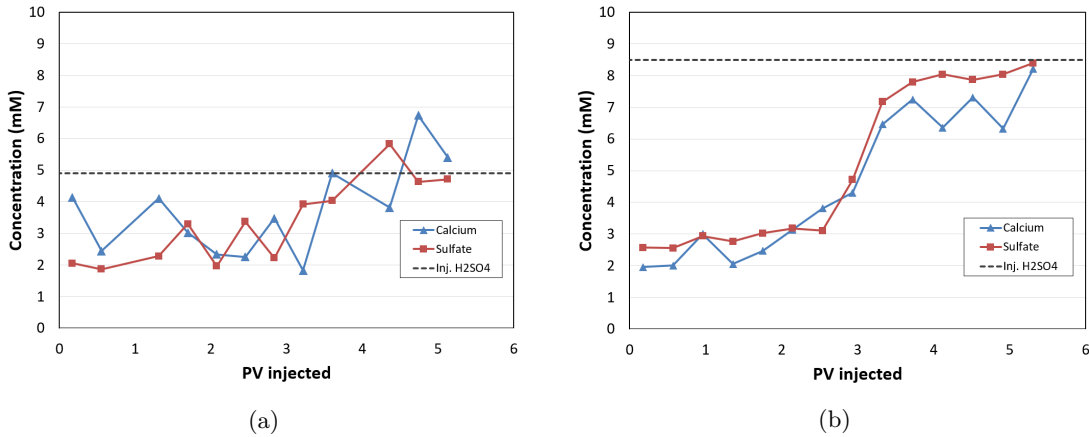


Figure 5.2: Dissolution of  $\text{CaCO}_3$  at  $130^\circ\text{C}$  during injection of different  $\text{H}_2\text{SO}_4$  solutions at 12 PV/day. In (a) 4.9 mM  $\text{H}_2\text{SO}_4$  was injected, and in (b) 8.5 mM  $\text{H}_2\text{SO}_4$ . The concentrations of  $\text{Ca}^{2+}$  and  $\text{SO}_4^{2-}$  in the effluent are estimated from IC analysis.

From the analyses, it appears that no precipitation took place for neither of the tests at  $130^\circ\text{C}$ . Similar to the tests at  $70^\circ\text{C}$ , the amount of dissolved  $\text{Ca}^{2+}$  follows the free  $\text{SO}_4^{2-}$  ions. For both 4.9 and 8.5 mM, the increase of  $\text{SO}_4^{2-}$  in the effluent is observed at approximately 3 PV. Compared to the tests at  $70^\circ\text{C}$ , the time of arrival is almost twice as long. This is in line with the theory in Section (3.2.2) regarding the effect of temperature on the reactivity of  $\text{SO}_4^{2-}$  ions towards chalk surfaces. At higher temperatures, larger amounts of  $\text{SO}_4^{2-}$  are adsorbed on the surface and, therefore, takes longer to reach the outlet. The concentration profiles look to stabilize after  $\sim 3.5$  PV as the systems reach equilibrium and effluent concentrations resemble the input  $\text{H}_2\text{SO}_4$  concentrations.

The same uncertainties mentioned in the previous section apply here as well with regards to sensitivity and the cleaning process. One can question the correlation between the concentration profiles in Figure 5.2a, however, larger inaccuracies are expected when working with lower concentrations.

### 5.1.3 pH Measurements during H<sub>2</sub>SO<sub>4</sub> Flooding

The pH of the effluent was measured throughout the acid flooding experiments and plotted against the injected PV (Figure 5.3). The trend is very similar for all the H<sub>2</sub>SO<sub>4</sub>-solutions. In all experiments, the first three pH measurements lie between 7-9 and are essentially the pH of the DI water used to clean the core. The water appears somewhat alkaline (pH>7), most likely due to being exposed to calcium carbonate. The pH measurements of the water are visibly lower at 130°C than at 70°C. The pH of water traditionally decreases with increasing temperature and CaCO<sub>3</sub> has the unusual characteristic that its solubility decreases as temperature increases.

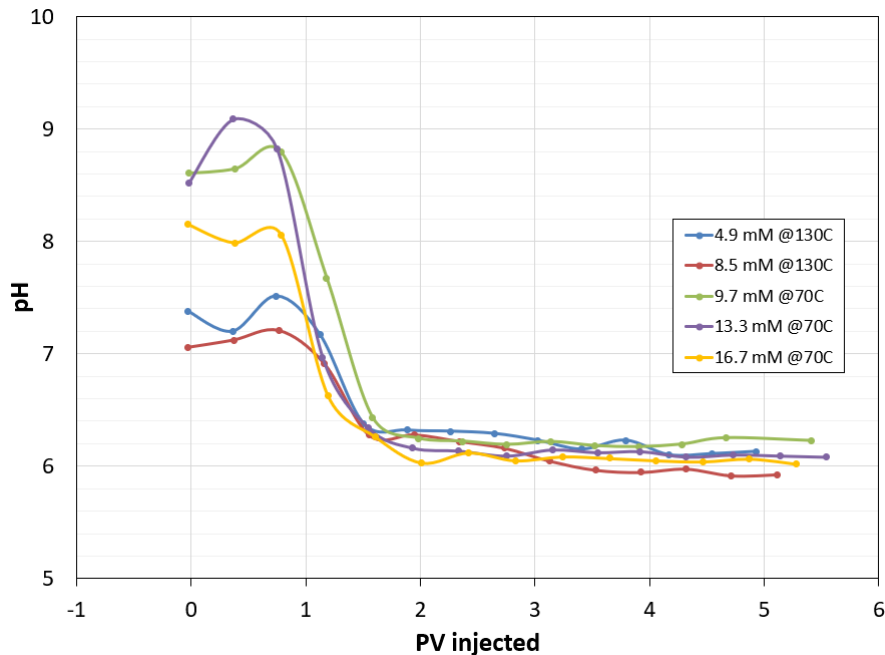


Figure 5.3: pH measurements of the effluent from the different H<sub>2</sub>SO<sub>4</sub> floodings at 70 and 130°C.

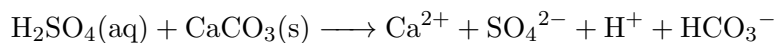
The sulfuric acid front reaches the outlet around 1-1.5 PV, which is illustrated by the drastic drop in pH. The pH falls and stabilizes around  $6.10 \pm 0.15$  after 2 PV for the solutions at 70°C and after 3.5 PV at 130°C. The average pH for the equilibrated solutions are presented in Table 5.1.

Table 5.1: Calculated pH averages of the H<sub>2</sub>SO<sub>4</sub> solutions after reaching equilibrium in the core.

H <sub>2</sub> SO <sub>4</sub> conc.	4.9 mM	8.5 mM	9.7 mM	13.3 mM	16.7 mM
pH at EQ	6.12	5.96	6.21	6.11	6.06



H<sub>2</sub>SO<sub>4</sub> is a strong acid and the initial pH of the solutions were measured close to 2, see Table 4.6. The H<sub>2</sub>SO<sub>4</sub>-solution reacts with the CaCO<sub>3</sub> in the core and produces the relevant PDIs Ca<sup>2+</sup> and SO<sub>4</sub><sup>2-</sup>, as well as HCO<sub>3</sub><sup>-</sup> and H<sup>+</sup>:



As mentioned, CaSO<sub>4</sub>(s) will only precipitate if the H<sub>2</sub>SO<sub>4</sub>(aq) concentration and/or temperature is sufficiently high. The bicarbonate, HCO<sub>3</sub><sup>-</sup>, reacts with the surrounding water molecules and forms H<sub>2</sub>CO<sub>3</sub>. HCO<sub>3</sub><sup>-</sup> also acts as a buffer and prevents the pH of the effluent from dropping too low. Using the Bjerrum plot (Figure 2.6) from Section (2.5.3), a solution at equilibrium around pH = 6 will be deficient in CO<sub>3</sub><sup>2-</sup> and contain approx. equal amounts of H<sub>2</sub>CO<sub>3</sub> and HCO<sub>3</sub><sup>-</sup>.

#### 5.1.4 Designing the Smart Water Brine

The sulfuric acid flooding experiment was a part of the thesis done in conjunction with another thesis looking into the effects the same Smart Water brine at 90°C (Lindanger, 2019). To be able to compare the results at 90°C to those at 70°C, a decision was made to use the same concentration of SO<sub>4</sub><sup>2-</sup> in the Smart Water. To avoid the risk of precipitation of CaSO<sub>4</sub> in both experiments, the Smart Water was designed for a 90°C setting. This would slightly reduce the effectiveness of the Smart Water at 70°C, as the amount of SO<sub>4</sub><sup>2-</sup> could have been higher without risking precipitation of CaSO<sub>4</sub>.

To decide the optimal SO<sub>4</sub><sup>2-</sup> concentration at 90°C, the results from the bulk solution test (Table 4.5) was used. The highest input concentration of H<sub>2</sub>SO<sub>4</sub> that didn't precipitate for each temperature was plotted against their respective temperature and a simple linear regression model was applied to determine the concentration at 90°C (Figure 5.4). The exact value was calculated to 13.34 mM H<sub>2</sub>SO<sub>4</sub>, however, the final concentration of SO<sub>4</sub><sup>2-</sup> in the Smart Water brine was decided to 13 mM to safely assure no precipitation of CaSO<sub>4</sub> when implemented at both 70 and 90°C.

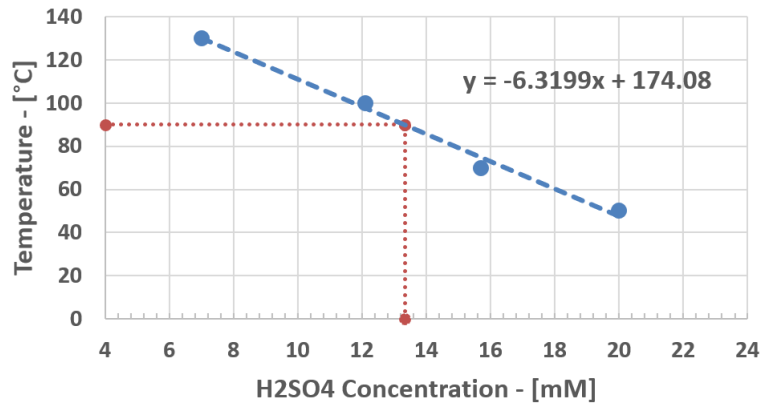


Figure 5.4: Linear regression used to find the optimal concentration of  $\text{SO}_4^{2-}$  at  $90^\circ\text{C}$ .

It was decided to dissolve gypsum ( $\text{CaSO}_4 + 2\text{H}_2\text{O}$ ) in DI water as the source of sulfate and calcium-ions to make the Smart Water brine. This was done to save time and ensure the correct amount of free  $\text{Ca}^{2+}$  ions were in the prepared brine when performing the oil recovery experiments. Oil displacement by spontaneous imbibition is a process where the initial reaction is very important. If a  $\text{H}_2\text{SO}_4$  solution was to be used, there would not be any  $\text{Ca}^{2+}$  present initially as the dissolution of chalk takes time. This would not be representative of the intended Smart Water brine. Gypsum was used instead of anhydrite, as gypsum is hydrated and therefore easier to dissolve. The solubility of gypsum in DI water is 2.531 g/l, or 14.7 mM at  $20^\circ\text{C}$  (Klimchouk, 1996).

A gypsum solution at 13 mM would not be at risk of precipitating at  $70^\circ\text{C}$  nor  $90^\circ\text{C}$ . However, if a similar Smart Water brine with a higher concentration of gypsum ever were considered, a way to avoid precipitation of  $\text{CaSO}_4$  would be to include  $\text{Mg}^{2+}$  in the brine, as it forms complexes with sulfate,  $\text{MgSO}_4$ . This reduces the reactivity of  $\text{SO}_4^{2-}$  and delays the formation of  $\text{CaSO}_4$ .

## 5.2 SEM and EDS Analysis of Reference Core SK1

The reference core SK1 was inspected after being flooded with sulfuric acid for several weeks at high temperatures. When the core was taken out, it looked somewhat deteriorated at the inlet (Figure 5.5). An increase in permeability was measured from 4.66 to 5.29 mD, which is an increase of 13.5% of its initial value. For a detailed calculation of the permeability, see Appdenix B.1. A combined SEM and EDS analysis was issued to check the effect of sulfuric acid on the mineralogy and eventual differences from the inlet of the core to the outlet.



Figure 5.5: Picture of the inlet of core SK1, still in the rubber sleeve, after being subjected several PV of sulfuric acid and high temperatures.

The core was cut and three samples were analyzed; one near the inlet, middle and outlet of the core. SEM images were captured at the magnifications 100x, 1 000x, 2 000x, 5 000x, 10 000x, 20 000x and 30 000x. Figure 5.6a and Figure 5.6b are images of the mineralogy at the inlet and outlet of SK1, respectively, both magnified 10 000 times.

The SEM images showed little to no signs of dissolution or degradation of the chalk. There were no visible textural differences from the inlet to the outlet of the core. The grains and coccolith structures seemed intact and fine, and were mostly unaffected by the sulfuric acid based on these SEM images. If the acid had any effect, the chalk fragments would most likely appear smaller and rounder. This implies that most of the dissolved chalk that provided the  $\text{Ca}^{2+}$  to the solution were dissolved at the inlet, as observed by the deterioration in Figure 5.5, and not inside the core.

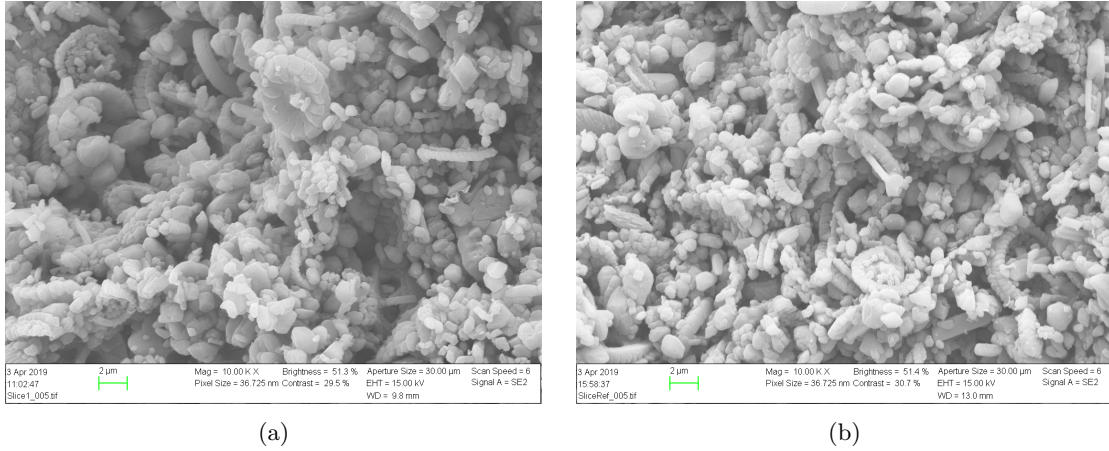


Figure 5.6: SEM images of SK1 at a) the inlet and b) the outlet.

### EDS Analysis

For each SEM image, composition analysis of the chalk samples was taken with the accompanying EDS apparatus. The elements looked at were calcium (Ca), magnesium (Mg), aluminum (Al), silicon (Si) and sulfur (S). The atomic weight (At%) of each element from the three samples is presented in Table 5.2. Ca was obviously dominant with  $\sim 97\text{--}98\%$ , which implies a really pure chalk. The other elements appears in smaller and almost negligible amounts, mostly below 1%. Mg may be linked to traces of dolomite, and Al and Si are most likely linked to small amounts of clay content. Small traces of S was also detected, which can mean the core was not properly cleaned. This supports the IC data from the acid floodings, where  $\text{SO}_4^{2-}$  concentration began at  $\sim 2$  mM after cleaning rather than zero, see Sections (5.1.1) and (5.1.2).

Table 5.2: Elemental composition of SK1 after acid flooding. The data is acquired from EDS analyses of three samples throughout the chalk core.

Element	Inlet, At%	Middle, At%	Outlet, At%	Average At%
Ca	97.6	98.9	97.1	97.9
Mg	0.10	0.05	0.40	0.18
Al	0.59	0.08	0.72	0.46
Si	1.01	0.55	1.29	0.95
S	0.68	0.42	0.47	0.52

### 5.3 Evaluation of Smart Water at 70°C

The use of a 13 mM gypsum Smart Water in oil recovery experiments have been compared with SW and FW at 70°C. Spontaneous imbibition tests were performed on outcrop SK chalk cores at 70°C to evaluate if the Smart Water was more efficient regarding wettability alteration. Three cores went through the same restoration process: the cores were cleaned, 10% initial FW saturation was established, the cores were saturated with and exposed to the same amount of crude oil before being aged for two weeks at 70°C. The initial wetting of the cores is assumed mixed-wet based on two main factors, the acid number of the oil and amount of crude oil exposure. The cores were exposed to 5 PV of Oil A, which has a moderate AN of 0.50 mgKOH/g oil. A lower AN would presumably ensure a higher degree of water wetness according to the theory in Section (3.2.2).

The imbibing fluids used for cores SK2, SK3 and SK4 were FW, SW and Smart Water, respectively. The Smart Water in this study is 13 mM gypsum dissolved in DI water, which is meant to represent the solution obtained by injecting 13 mM H<sub>2</sub>SO<sub>4</sub> through chalk. An advantage this Smart Water has over the other FW and SW is its absence of non-active salt, NaCl. This improves the access of active ions to the chalk surface. The reduced salinity is also responsible for a slightly higher IFT value between the oil and Smart Water, compared to the other two brines. The IFT was measured at 14.33 mN/m for the Smart Water, compared to 10.67 mN/m for FW and 10.17 mN/m for SW. The IFT is directly related to the capillary pressure in a system, as shown in Equation 2.8 in Section (2.2.5). Therefore, higher IFT leads to greater capillary pressure, which may contribute to a more effective SI process for the Smart Water.

SI was also performed on a strongly water-wet core, SKWW, which is used to evaluate the wetting condition of the other cores. All the results in this section are discussed in terms of recovery efficiency during spontaneous imbibition and wettability alteration. Results and data from the parallel experiments at 90°C are also included in this section and a brief comparison with the present work will be made.

### 5.3.1 Water-wet Reference Core for SI

A strongly water-wet core, SKWW, is used as reference for comparison of SI results. The core material is SK outcrop chalk, from the same block as the other cores in the experiment. After being cleaned, the core was established with  $S_{wi}=20\%$  DI water, and then saturated with mineral oil. The mineral oil does not contain any polar organic components and thus, will not adsorb onto the chalk surface. As a result, the core is expected to act very water-wet. The spontaneous imbibition was performed in an Amott cell at ambient temperature. DI water was used as imbibing fluid. The results from the SI experiment are presented in Figure 5.7, where the oil recovery is plotted as % of OOIP versus time.

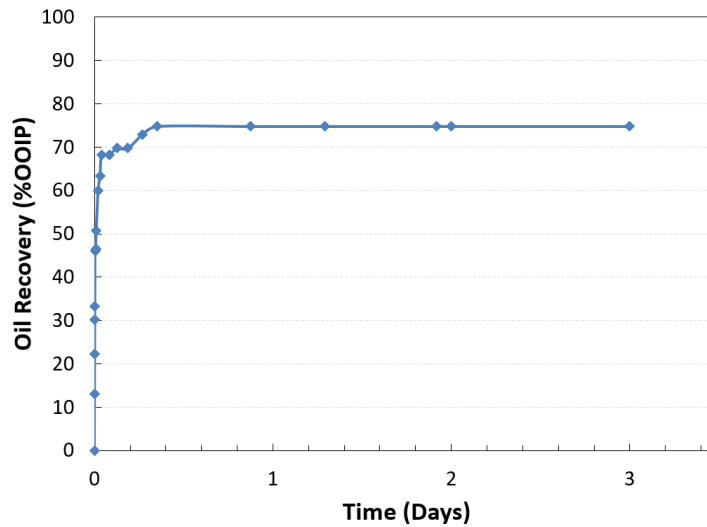


Figure 5.7: Spontaneous imbibition of DI water into a strongly water-wet core, SKWW, saturated with Mineral Oil. SI was performed at ambient temperature.

The reference core SKWW reached an oil recovery plateau after approximately 8.5 hours, with an total recovery of almost 75% of OOIP. The water-wet state of the core is confirmed by the very rapid rate of imbibition, where the majority of the total oil recovered are displaced within the first hour. The high ultimate oil recovery is also a good indicator of water-wet conditions. Following SI, the core was flooded with DI water, which yielded no additional recovery.

Table 5.3: SI data from SKWW by imbibition of DI water at 23°C.

Core	Imbibing Fluid	Oil	T (°C)	$S_{wi}$ (%)	Max. oil recovery (%OOIP)
SKWW	DI water	Mineral Oil	23	20	75

### 5.3.2 Spontaneous Imbibition at 70°C

The oil recovery by spontaneous imbibition of FW, SW and Smart Water was compared for SK cores restored with Oil A. The SI tests were performed at 70°C with a back pressure of 10 bars. The figures below show the SI curves for each core, presenting the oil production as % of OOIP versus time. The SI tests were considered finished when a stable plateau was reached. The result of the spontaneous imbibition of formation water into core SK2 is shown in Figure 5.8.

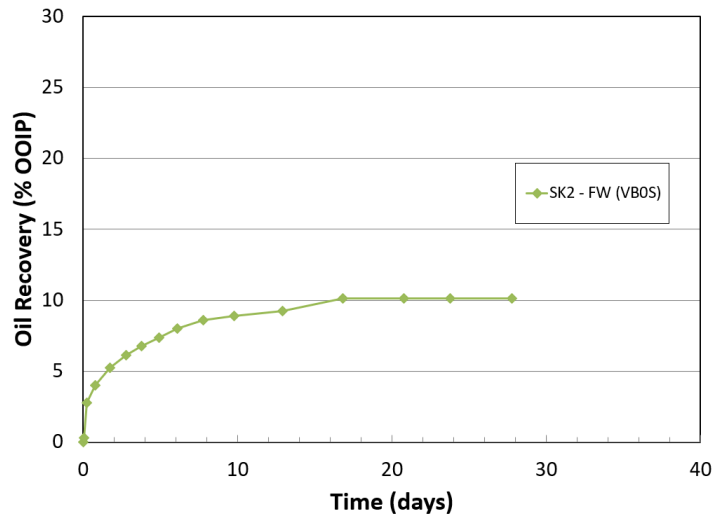


Figure 5.8: Spontaneous imbibition of formation water into oil saturated SK outcrop chalk core SK2 at 70°C. Oil A: AN=0.50 mgKOH/g.

The slope of the SI profile shows rapid imbibition rate the first day, followed by less and less production for each subsequent day. The production plateau was reached after 17 days. The process resulted in a total oil production of 10% of OOIP, which is in line with low water-wetness. Due to the lack of  $\text{SO}_4^{2-}$  in the imbibing FW, the brine is not able to induce wettability alteration during the process. The oil production is thus related to initial wetting state and capillary forces. The core was taken out of the heating oven after 28 days.

Figure 5.9 shows the spontaneous imbibition of SW into core SK3. The SI profile is very similar to the profile for FW, albeit the early imbibition rate is somewhat slower. The production plateau was reached after 20 days and the total oil production was about 9% of OOIP. The low recovery indicates that the imbibing seawater was not able to induce wettability alteration at 70°C. The core was taken out after 31 days.

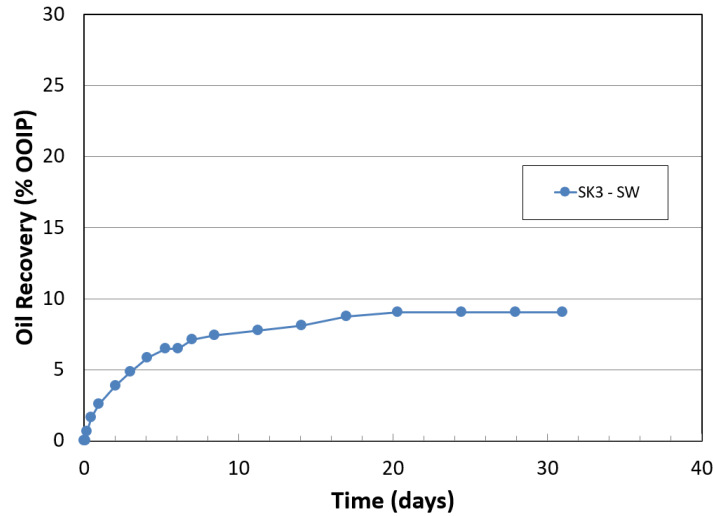


Figure 5.9: Spontaneous imbibition of seawater into oil saturated SK outcrop chalk core SK3 at 70°C. Oil A: AN=0.50 mgKOH/g.

The spontaneous imbibition of Smart Water into core SK4 is displayed in Figure 5.10. The early imbibition rate is the lowest of the three SI tests. However, due to a more stable slope, the oil recovery overtakes both FW and SW after only 2 days. The production plateau was reached after 19 days and the total oil production ends up at 11% of OOIP. The imbibing Smart Water produced the highest amount of oil, albeit only slightly and in the same range as the other SI tests. The core was taken out after 29 days.

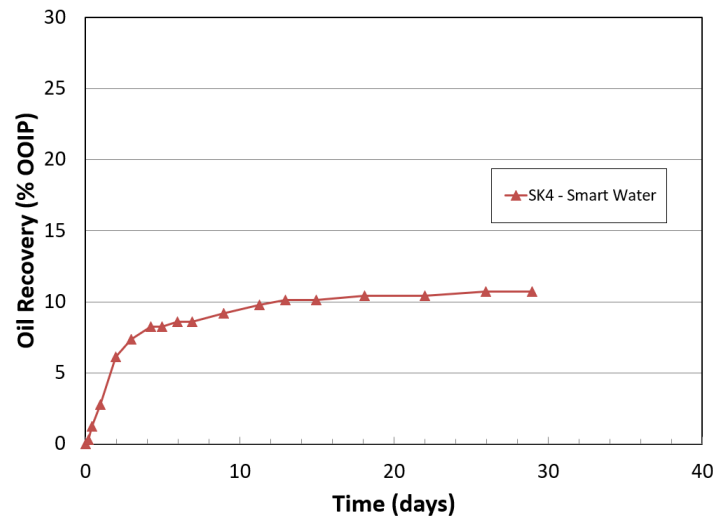


Figure 5.10: Spontaneous imbibition of Smart Water into oil saturated SK outcrop chalk core SK4 at 70°C. Oil A: AN=0.50 mgKOH/g.



### 5.3.3 Comparison of the Results from the Spontaneous Imbibition Tests

The results from the imbibition tests are summarized in Figure 5.11 and Table 5.4. At 70°C, the oil recovery by spontaneous imbibition of FW was about 10% of OOIP. The recovery by imbibing SW and Smart Water was about 9 and 11% of OOIP, respectively. There are several uncertainties related to these types of experiments, although a fair margin of error is about  $\pm 2\%$  of OOIP (Punternvold et al., 2007). Thus, the lower oil recovery with SW is justified, since it is within the margin of error. This also means the 1% increase in recovery from FW to Smart Water is negligible. Oil recovery was below 11% of OOIP for all spontaneous imbibition tests at 70°C, which implies cores of mixed-wet condition or at least very low water-wetness. Compared to the strongly water-wet core, the difference in ultimate oil recovery is close to 65% of OOIP. The oil production was significantly reduced for the cores that had been exposed to crude oil with AN=0.50 mgKOH/g.

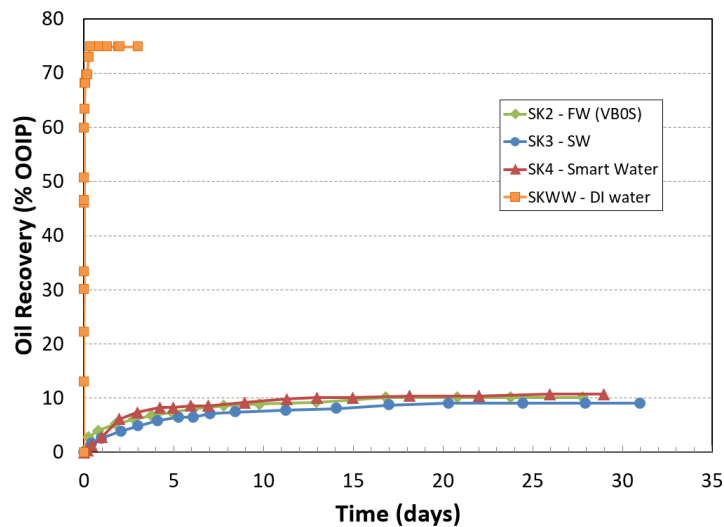


Figure 5.11: Comparison of SI test for SK2, SK3, SK4 and SKWW.

The similarity between the imbibition curves for FW, SW and Smart Water suggest that none of the imbibing fluids were able to induce any wettability alteration at 70°C. Therefore, the oil recovery by these fluids are directly related to the initial wetting condition, which derives from the adsorption of the organic polar components on the positively charged chalk surface.

The degree of water-wetness can be calculated using the modified Amott water index,  $I_{W-SI}^*$  (Torrijos et al., 2019). The strongly water-wet core, SKWW, is used as reference with  $SI_{WWC}=75\%$  of OOIP and  $I_{W-SI}^*=1.00$ . The modified Amott indices are calculated using Equation 2.12 from Section (2.4.3).

$$I_{W-SI-SK2}^* = \frac{10}{75} \approx 0.13 \quad (5.1)$$

$$I_{W-SI-SK3}^* = \frac{9}{75} = 0.12 \quad (5.2)$$

$$I_{W-SI-SK4}^* = \frac{11}{75} \approx 0.15 \quad (5.3)$$

The modified Amott water indices are presented in Table 5.4 and confirms a low degree of water-wetness in the chalk cores. The index for Smart Water in SK4 is slightly higher than FW which can indicate slight wettability alteration towards a more water-wet state. However, since the ultimate oil recovery used to calculate  $I_{W-SI-SK4}^*$  is within the margin of error, the possible wettability alteration is neglected.

The temperature was most likely too low for the PDIs to be sufficiently reactive, as observed in previous studies (Torrijos et al., 2019). At lower temperatures, the PDIs are more hydrated which hinders the adsorption of  $SO_4^{2-}$  and  $Ca^{2+}$  to the surface, as well as the desorption of acidic oil components.

Table 5.4: Results from spontaneous imbibition of different fluids into chalk cores. Cores SK2, SK3 and SK4 was saturated with Oil A with AN=0.50 mgKOH/g and SKWW with mineral oil.

Core	Imbibing Fluid	Oil	T (°C)	$S_{wi}$ (%)	Max. oil recovery (%OOIP)	$I_{W-SI}^*$
SK2	FW	Oil A	70	10	10	0.13
SK3	SW	Oil A	70	10	9	0.12
SK4	Smart Water	Oil A	70	10	11	0.15
SKWW	DI water	Mineral oil	23	20	75	1.00

### 5.3.4 Temperature Effects: A Brief Comparison with Smart Water at 90°C

The Smart Water brine was designed in conjunction with a parallel thesis that investigating its effects on SK outcrop chalk cores at 90°C (Lindanger, 2019). The experiments were performed on cores from the same outcrop block and the same crude oil, Oil A, was used. The core restoration process was also identical, with the exception of the ageing, which occurred at 90°C. Oil recovery experiments were performed at 90°C by spontaneous imbibition of SW and Smart Water. FW was not tested at 90°C, as it would not differ much from FW at 70°C. Since imbibing FW induces no wettability alteration, the only additional oil recovery at 90°C, compared to 70°C, would be a result of thermal expansion of the oil. The thermal expansion coefficient for crude oils is typically  $\sim 10^{-3}/^{\circ}\text{C}$  and would therefore only amount to an increase of  $\sim 2\%$  of OOIP from 70 to 90°C (Torrijos et al., 2019). The results from the experiments at 90°C are presented in Figure 5.12 together with the results from 70°C.

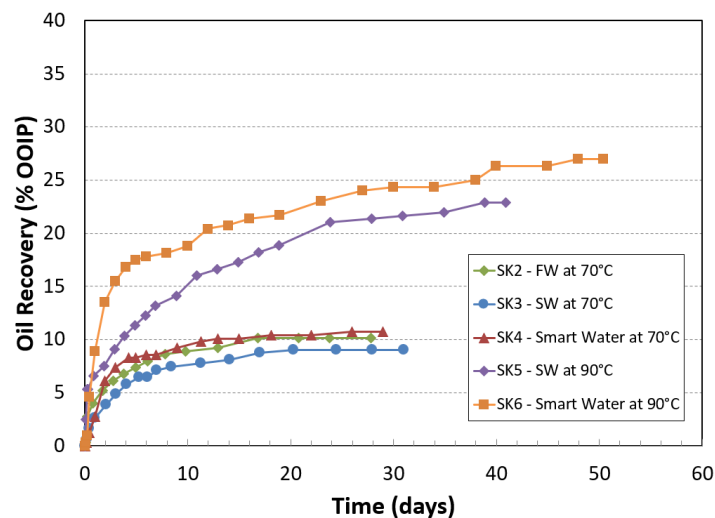


Figure 5.12: Spontaneous imbibition into oil saturated SK outcrop chalk cores at 70°C and 90°C. Different imbibing brines with different ionic compositions were used: FW, SW and Smart Water. Oil A: AN=0.50 mgKOH/g

At 90°C, the oil recovery by spontaneous imbibition of SW into chalk core SK5 was almost 23% of OOIP, which is an increase of 14% of OOIP compared to SW at 70°C. Furthermore, the oil recovery increased to 27% of OOIP when using Smart Water as the imbibing fluid in core SK6. Compared to Smart Water at 70°C, this is an increase of 16% of OOIP. The modified Amott water indices for SW and Smart Water at 90°C were calculated to 0.31 and 0.36. The improved oil recovery implies wettability alteration in the chalk cores towards more water-wet condition. This is in line with theory regarding temperature effects on wettability alteration, as mentioned in Section (3.2.2). The results from the experiments at 90°C confirms a slight improvement in oil recovery by 5% of OOIP by imbibing Smart Water over SW. The Smart Water only has a  $\text{SO}_4^{2-}$  concentration of 13 mM compared to SW which is 24 mM. The increase in oil recovery can therefore be attributed to the lack of NaCl in the Smart Water, which highlights the importance of optimizing the amount of adsorbed PDIs on the chalk surface. Given the shape of the curves, the oil recovery could possibly have been even higher over a longer SI period.

Table 5.5: Results from spontaneous imbibition of different fluids into chalk cores at 70°C and 90°C. All cores were saturated with Oil A with AN=0.5 mgKOH/g.  $S_{wi}=10\%$

Core	Imbibing Fluid	T (°C)	Max. oil recovery (%OOIP)	$I_{w-SI}^*$
SK2	FW	70	10	0.13
SK3	SW	70	9	0.12
SK4	Smart Water	70	11	0.15
SK5	SW	90	23	0.31
SK6	Smart Water	90	27	0.36

## 5.4 Additional Oil Recovery by Forced Imbibition at 70°C

Following the spontaneous imbibition, the cores were flooded by successive forced imbibition at 70°C, continuing with the same SI fluids at a rate of 1 PV/day. After the oil recovery reached a plateau, the injection fluids were switched to Smart Water for cores SK2 and SK3. Finally, the injection rate was changed to 4 PV/day to observe the effect of the viscous forces. The results from each core flooding at 70°C are presented in Figures 5.13, 5.14 and 5.15 below. The figures show the oil recovery (% of OOIP) and pressure drop (mbar) versus PV injected.

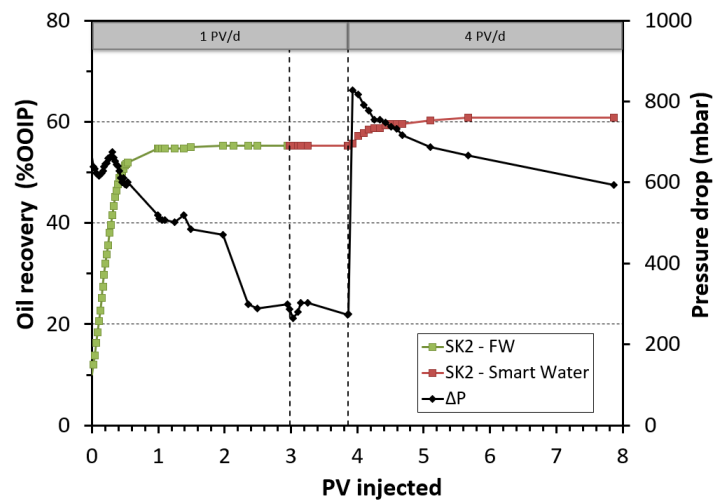


Figure 5.13: Forced imbibition with FW followed by Smart Water at 70°C

The result of flooding chalk core SK2 by successive injections of FW and Smart Water is shown in Figure 5.13. After SI, about 10% of OOIP had been produced. The oil displacement by FW flooding appears piston like as the majority of the oil was produced within the first PV injected. The recovery rate is initially stable, but decreases as the pressure drop across the core starts to decline. The initial pressure build up appears to be dampened by the presence of positive capillary forces within the core. The production plateau was reached at 53% of OOIP after less than 3 PV injected. Then, the core was flooded with Smart Water, which yielded no additional production. Lastly, the injection rate was increased to 4 PV/day which resulted in an increase in oil recovery by about 6% of OOIP. The corresponding pressure build up is rapid and significant compared to the initial pressure build up, due to extensive viscous forces and the absence of positive

capillary forces. The Amott wettability index to water,  $I_w$ , can be calculated from the amount of displaced oil after SI and FI at 1 PV/day:

$$I_{w-SK2} = \frac{10}{10 + 45} \approx 0.18 \quad (5.4)$$

The wetting index is in line with previous assumptions that initial water-wetness of the core was quite low.

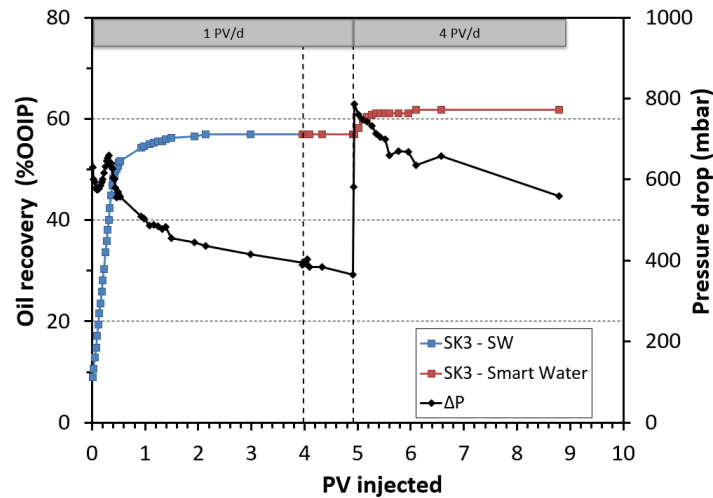


Figure 5.14: Forced imbibition with SW followed by Smart Water at 70°C

Figure 5.14 shows the results from successive injections of SW and Smart Water into core SK3. The oil recovery after SI was 9% of OOIP. The production and pressure profile is very similar to Figure 5.13. About 4 PV of SW was injected and resulted in a production plateau at 57% of OOIP. No extra oil was produced by switching to Smart Water. Changing the rate to 4 PV/day yielded a slight increase in oil recovery by 5% of OOIP. For core SK3,  $I_w$  was calculated by the following equation:

$$I_{w-SK3} = \frac{9}{9 + 48} \approx 0.16 \quad (5.5)$$

The low wetting index implies that SW was not able to induce wettability alteration and the value coincides with results of the modified Amott indices in Table 5.4, where SW is marginally lower.

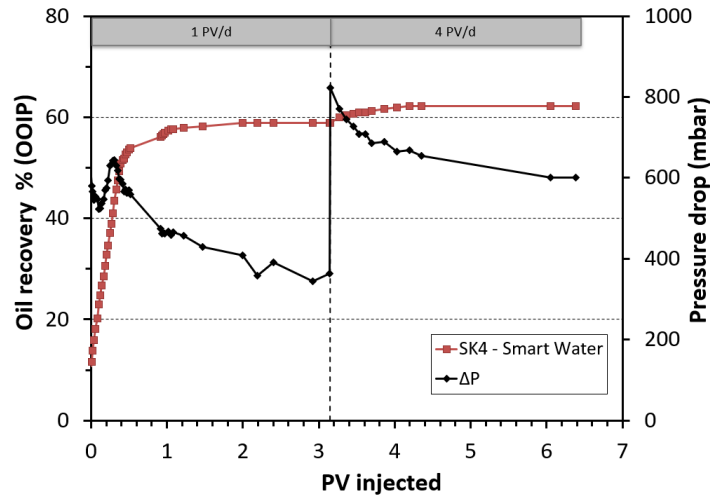


Figure 5.15: Forced imbibition with Smart Water at 70°C

The result of flooding core SK4 with Smart Water is shown in Figure 5.13. About 11% of OOIP was already displaced by SI. The rate and magnitude of the oil production and pressure drop is comparable with the previous two core floodings. Almost 59% of OOIP was produced after forced injection of Smart Water. The rate was increased after 3 PV, which marginally improved the oil recovery by 3% of OOIP. The degree of water-wetness in core SK4 is given by:

$$I_{w-SK4} = \frac{11}{11 + 48} \approx 0.19 \quad (5.6)$$

The incremental increase of the wetting index compared to FW indicates that Smart Water may have been able to induce slight, albeit negligible, wettability alteration in the core at 70°C. The increase also fits the modified Amott indices in Table 5.4, where Smart Water is largest.

### 5.4.1 Discussion of Results from Forced Imbibition

The forced imbibition experiments produced very similar results. Figure 5.16 shows the oil recovery with the initial injection fluids at 1 PV/day for all three cores. The initial production plateaus were 55, 57 and 59% of OOIP after and injecting FW, SW and Smart Water, respectively. Both the oil recovery and pressure drop profiles appeared very similar for the different injection fluids.

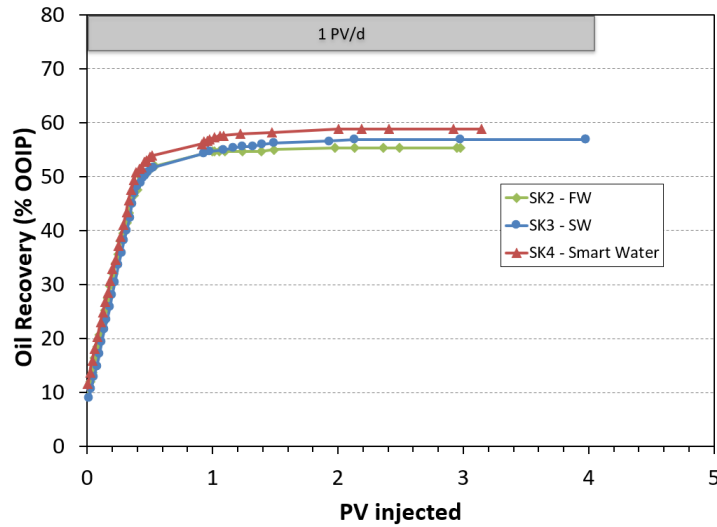


Figure 5.16: Forced imbibition at 1 PV/day at 70°C with three fluids: FW, SW and Smart Water.

The piston like displacement is observed for all core floodings and most of the oil was produced within 1 PV. No extra oil was produced by switching to Smart Water, neither from FW nor SW. The SI experiments showed that Smart Water could not improve wettability at 70°C, meaning no wettability alteration would occur during forced imbibition either. When the injection rate was increased from 1 to 4 PV/day, the additional oil recovery were almost negligible with an increase of only 3-6% of OOIP. This implies that most of the oil is able to be produced at low injection rates and that the oil recovery is less dependent on viscous forces. The ultimate oil recovery after core flooding were around 61-62% of OOIP for all cores. All the production plateaus are noted in Table 5.6.

Wettability analysis was conducted using the Amott wettability index to water,  $I_w$ , which used the results from both SI and FI. The wetting indices are presented in 5.6. The relative magnitude of the results were consistent with the results from the modified Amott method found in Section (5.3.3).



Table 5.6: Results from forced imbibition tests at 70°C. Oil A: AN=0.50 mgKOH/g.

Core	Injection Fluid	SI (%OOIP)	FI (1 PV/d) (%OOIP)	FI (4 PV/d) (%OOIP)	I <sub>w</sub>
SK2	FW	10	55	61	0.18
SK3	SW	9	57	62	0.16
SK4	Smart Water	11	59	62	0.19

# Chapter 6

## Conclusion

### 6.1 Concluding Remarks

The following concluding remarks are based on the experimental work in this thesis:

- The H<sub>2</sub>SO<sub>4</sub>-flooding experiment proved it was possible to create a Smart Water brine containing controlled amounts of active surface ions, SO<sub>4</sub><sup>2-</sup> and Ca<sup>2+</sup>, by dissolving CaCO<sub>3</sub> from the chalk core. SEM analysis of the core showed that the integrity and structure of the chalk minerals were mostly unaffected by the acid flooding.
- Spontaneous imbibition of FW, SW and Smart Water at 70°C resulted in oil recovery of 10, 9 and 11% of OOIP, respectively. The corresponding modified Amott wetting indices were 0.13, 0.12 and 0.15, which confirmed very low water-wetness in the cores. Regardless of the imbibing brine, the cores behaved similarly and the results lie within the margin of error. The temperature was most likely too low, which hindered high enough adsorption of SO<sub>4</sub><sup>2-</sup> and co-adsorption of Ca<sup>2+</sup> onto the chalk surface. The reduced reactivity of the PDIs would also prevent the desorption of acidic oil components. SO<sub>4</sub><sup>2-</sup> becomes dehydrated and more reactive towards the chalk surface at higher temperatures, as observed from the experiments at 90°C. Thus, on these slightly water-wet cores the Smart Water was not able to improve the wettability at 70°C.

- Wettability alteration was observed at 90°C as a result of increased reactivity of  $\text{SO}_4^{2-}$  ions towards the chalk surface. The oil recovery by spontaneous imbibition of SW and Smart Water was 23 and 27% of OOIP, respectively. The change toward a more water-wet state was confirmed by the corresponding modified Amott wetting indices, which were improved to 0.31 and 0.36. The increased recovery by imbibing Smart Water over SW can be attributed to the absence of non-active ions in the Smart Water.
- Subsequent oil recovery by forced imbibition displayed piston-like displacement of the oil for all cores. No significant amount of extra oil was produced by SW or Smart Water (over the production obtained by FW) by forced imbibition at 70°C. The initial pressure drop across the cores were subdued due to the presence of positive capillary forces within the core. Increasing the injection rate by 4 times its initial rate produced a small amount of extra oil, implying most of the oil can be produced at low injection rates.

## 6.2 Future Work

The following suggestions can be the focus in future studies:

- Reproduce the work done in this thesis to ensure its validity.
- Optimize the parameters within the oil recovery experiments in order to improve the efficiency of the Smart Water at 70°C. Some changes can be: a slightly more water-wet core system, lower AN of the oil and higher concentration of gypsum.
- Investigate the possibility of adding  $\text{Mg}^{2+}$  to the Smart Water brine. Focus should be on how it can increase the amount of dissolved  $\text{Ca}^{2+}$  from the chalk.
- Evaluate oil recovery experiments using a diluted  $\text{H}_2\text{SO}_4$ -solution compared to the prepared gypsum variant. The rate of  $\text{CaCO}_3$ -dissolution and oil displacement during spontaneous imbibition can be evaluated.
- Simulate the acid flooding experiment. A good correlation with the present work can be useful to optimize the composition of the Smart Water brine at different temperatures.

# Bibliography

- [1] Ahmed, T. *Reservoir engineering handbook*. Gulf Professional Publishing, 2018.
- [2] Ahr, W. M. *Geology of carbonate reservoirs: the identification, description and characterization of hydrocarbon reservoirs in carbonate rocks*. John Wiley & Sons, 2011.
- [3] Amott, E. “Observations relating to the wettability of porous rock”. In: *Petroleum Transactions, AIME* 216 (1959), pp. 156–162.
- [4] Anderson, W. G. “Wettability literature survey-part 1: rock/oil/brine interactions and the effects of core handling on wettability”. In: *Journal of petroleum technology* 38.10 (1986), pp. 1–125.
- [5] Austad, T. *Enhanced Oil Recovery Field Case Studies: Chapter 13. Water-Based EOR in Carbonates and Sandstones: New Chemical Understanding of the EOR Potential Using “Smart Water”*. Elsevier Inc. Chapters, 2013.
- [6] Austad, T., Shariatpanahi, S. F., Strand, S., Black, C. J. J., and Webb, K. J. “Conditions for a low-salinity enhanced oil recovery (EOR) effect in carbonate oil reservoirs”. In: *Energy & fuels* 26.1 (2011), pp. 569–575.
- [7] Austad, T., Strand, S., Madland, M. V., Puntervold, T., and Korsnes, R. I. “Seawater in chalk: An EOR and compaction fluid”. In: *International petroleum technology conference*. International Petroleum Technology Conference. 2007.
- [8] Bjørlykke, K. *Sedimentology and petroleum geology*. New York, NY (US); Springer-Verlag, 1989.
- [9] Boye, N. C. *Kjemi og miljølære*. Universitetsforl., 1995.

- [10] Castor, T. P., Somerton, W. H., and Kelly, J. F. "Recovery Mechanisms of Alkaline Flooding". In: *Surface Phenomena in Enhanced Oil Recovery*. Ed. by Dinesh O. Shah. Boston, MA: Springer US, 1981, pp. 249–291. ISBN: 978-1-4757-0337-5. DOI: 10.1007/978-1-4757-0337-5\_14. URL: [https://doi.org/10.1007/978-1-4757-0337-5\\_14](https://doi.org/10.1007/978-1-4757-0337-5_14).
- [11] Cheryan, M. *Ultrafiltration and microfiltration handbook*. CRC press, 1998.
- [12] Chilingar, G. V. and Yen, T. F. "Some notes on wettability and relative permeabilities of carbonate reservoir rocks, II". In: *Energy Sources* 7.1 (1983), pp. 67–75.
- [13] ConocoPhillips. *Research and Development*. Apr. 28, 2019. URL: <http://www.conocophillips.no/nn/vare-norske-operasjoner/forskning-og-utvikling/>.
- [14] COREC. *COREC Workshop*. Sola, Rogaland, Norway, 2005.
- [15] Craig, F. F. *The reservoir engineering aspects of waterflooding*. Vol. 3. HL Doherty Memorial Fund of AIME New York, 1971.
- [16] Cuiec, L. "Rock/crude-oil interactions and wettability: An attempt to understand their interrelation". In: *SPE Annual Technical Conference and Exhibition*. Society of Petroleum Engineers. 1984.
- [17] Cuiec, L., Bourbiaux, B., and Kalaydjian, F. "Oil recovery by imbibition in low-permeability chalk". In: *SPE Formation Evaluation (Society of Petroleum Engineers); (United States)* 9:3 (Sept. 1994). ISSN: 0885-923X. DOI: 10.2118/20259-PA.
- [18] Darcy, H. P. G. *Les Fontaines publiques de la ville de Dijon. Exposition et application des principes à suivre et des formules à employer dans les questions de distribution d'eau, etc.* V. Dalamont, 1856.
- [19] Donaldson, E. C. and Alam, W. *Wettability*. Elsevier Science, 2013. ISBN: 9780127999906. URL: <https://books.google.no/books?id=EQ1BAQAAQBAJ>.
- [20] Ebnesajjad, S. and Ebnesajjad, C. *Surface treatment of materials for adhesive bonding*. William Andrew, 2013.
- [21] Emitech. *SPUTTER COATING INCORPORATING EMITECH K500, K550, K575 and K675X*. Tech. rep. 1999. URL: [https://crn2.3it.usherbrooke.ca/guide\\_sb/appareils/Emitech/SputterCoating.pdf](https://crn2.3it.usherbrooke.ca/guide_sb/appareils/Emitech/SputterCoating.pdf).

- [22] Fan, T. and Buckley, J. S. “Acid number measurements revisited, SPE”. In: *DOE Symposium on Improved Oil Recovery, Tulsa, Oklahoma*. 2006, pp. 22–26.
- [23] Fathi, S. J., Austad, T., and Strand, S. “Water-based enhanced oil recovery (EOR) by “smart water”: Optimal ionic composition for EOR in carbonates”. In: *Energy & fuels* 25.11 (2011), pp. 5173–5179.
- [24] Frykman, P. “Spatial variability in petrophysical properties in Upper Maastrichtian chalk outcrops at Stevns Klint, Denmark”. In: *Marine and Petroleum Geology* 18.10 (2001), pp. 1041–1062.
- [25] Green, D. W. and Willhite, G. P. *Enhanced Oil Recovery*. SPE textbook series. Henry L. Doherty Memorial Fund of AIME, Society of Petroleum Engineers, 1998. ISBN: 9781555630775. URL: <https://books.google.no/books?id=0cUWAAAACAAJ>.
- [26] Grotzinger, J. and Jordan, T. H. *Understanding Earth*. W. H. Freeman, 2014. ISBN: 9781319129859.
- [27] INA. *Terms for entire coccoliths*. Ed. by J. R. Young. Apr. 26, 2019. URL: <http://ina.tmsoc.org/terminology/3coccoliths.htm>.
- [28] Jakobsen, A. B. “Adsorption of basic crude oil components onto carbonate chalk surfaces – effect on initial wettability”. MA thesis. University of Stavanger, 2018.
- [29] Klimchouk, A. “The dissolution and conversion of gypsum and anhydrite”. In: *International Journal of Speleology* 25.3 (1996), p. 2.
- [30] KRÜSS. *Force Tensiometer – K6*. June 14, 2019. URL: <https://www.kruss-scientific.com/products/tensiometers/force-tensiometer-k6/>.
- [31] Lake, L. W. *Enhanced Oil Recovery*. Society of Petroleum Engineers, 2010. ISBN: 9781555633059. URL: <https://books.google.no/books?id=RHb8ewEACAAJ>.
- [32] Lindanger, M. “Production of Smart Water by Acid Flooding in Chalk Cores: Oil Recovery Effects at Intermediate Temperature”. MA thesis. University of Stavanger, 2019.
- [33] Lodish, H. F. *Molecular Cell Biology 6 Ed*. W. H. Freeman and Company, 2008. ISBN: 9781429203142. URL: <https://books.google.no/books?id=WYcMQgAACAAJ>.
- [34] Lowry, T. M. “The uniqueness of hydrogen”. In: *Journal of the Society of Chemical Industry* 42.3 (1923), pp. 43–47.

- [35] Morrow, N. R. “Interplay of capillary, viscous and buoyancy forces in the mobilization of residual oil”. In: *Journal of Canadian Petroleum Technology* 18.03 (1979).
- [36] Morrow, N. R. “Wettability and its effect on oil recovery”. In: *Journal of Petroleum Technology* 42.12 (1990), pp. 1–476.
- [37] Nair, R. R. “Smart Water for Enhanced Oil Recovery from Seawater and Produced Water by Membranes”. PhD thesis. University of Stavanger, 2019.
- [38] Nanidou, K. and Mirkovic, A. “Bulk Solution Tests of H<sub>2</sub>SO<sub>4</sub>-CaCO<sub>3</sub> Mixtures”. 2019.
- [39] Pedersen, O., Colmer, T. D., and Sand-Jensen, K. “Underwater photosynthesis of submerged plants—recent advances and methods”. In: *Frontiers in Plant Science* 4 (2013), p. 140.
- [40] Puntervold, T., Strand, S., and Austad, T. “New Method To Prepare Outcrop Chalk Cores for Wettability and Oil Recovery Studies at Low Initial Water Saturation”. In: *Energy & Fuels - ENERGFUEL* 21 (Sept. 2007). DOI: 10.1021/ef700323c.
- [41] Puntervold, T., Strand, S., Ellouz, R., and Austad, T. “Modified seawater as a smart EOR fluid in chalk”. In: *Journal of Petroleum Science and Engineering* 133 (2015), pp. 440–443.
- [42] Røgen, B. and Fabricius, I. L. “Influence of clay and silica on permeability and capillary entry pressure of chalk reservoirs in the North Sea”. In: *Petroleum Geoscience* 8.3 (2002), pp. 287–293.
- [43] Salathiel, R. A. “Oil recovery by surface film drainage in mixed-wettability rocks”. In: *Journal of Petroleum Technology* 25.10 (1973), pp. 1–216.
- [44] Schlumberger. *Primary Recovery*. Mar. 10, 2019. URL: [https://www.glossary.oilfield.slb.com/en/Terms/p/primary\\_recovery.aspx](https://www.glossary.oilfield.slb.com/en/Terms/p/primary_recovery.aspx).
- [45] Shapley, P. *Carbon Dioxide-Bicarbonate-Carbonate Equilibrium*. 2011. URL: <http://butane.chem.uiuc.edu/pshapley/GenChem1/L26/3.html>.
- [46] Springer, N., Korsbech, U. C. C., and Aage, H. K. “Resistivity Index Measurement without the Porous Plate”. In: *Proceedings International Symposium of the Society of Core Analysts*. 2003.

- [47] Standnes, D. C. and Austad, T. “Wettability alteration in chalk: 2. Mechanism for wettability alteration from oil-wet to water-wet using surfactants”. In: *Journal of Petroleum Science and Engineering* 28.3 (2000), pp. 123–143.
- [48] Strand, S., Standnes, D. C., and Austad, T. “New wettability test for chalk based on chromatographic separation of SCN- and SO<sub>4</sub><sup>2-</sup>”. In: *Journal of Petroleum Science and Engineering* 52.1-4 (2006), pp. 187–197.
- [49] Taber, J. J., Martin, F. D., and Seright, R. S. “EOR screening criteria revisited-Part 1: Introduction to screening criteria and enhanced recovery field projects”. In: *SPE Reservoir Engineering* 12.03 (1997), pp. 189–198.
- [50] Thomas, S. “Enhanced oil recovery-an overview”. In: *Oil & Gas Science and Technology-Revue de l'IFP* 63.1 (2008), pp. 9–19.
- [51] Torrijos, I. D. Pinerez, Sæby, K. G., Strand, S., and Puntervold, T. “Impact of Temperature on Wettability Alteration by Smart Water in Chalk”. In: *IOR 2019 - 20th European Symposium on Improved Oil Recovery*. 2019.
- [52] Wathne, Agnes K. “Effect of Wettability on Waterflooding and Relative Permeability at Slightly Water-Wet Conditions”. MA thesis. University of Stavanger, 2019.
- [53] Young, T. *Miscellaneous works of the late Thomas Young...* Vol. 2. J. Murray, 1855.
- [54] Zhang, P. “Water-based EOR in Fractured Chalk – Wettability and Chemical Additives”. PhD thesis. University of Stavanger, 2006.
- [55] Zhang, P. and Austad, T. “Wettability and oil recovery from carbonates: Effects of temperature and potential determining ions”. In: *Colloids and Surfaces A: Physicochemical and Engineering Aspects* 279.1-3 (2006), pp. 179–187.
- [56] Zhang, P., Tweheyo, M. T., and Austad, T. “Wettability alteration and improved oil recovery by spontaneous imbibition of seawater into chalk: Impact of the potential determining ions Ca<sup>2+</sup>, Mg<sup>2+</sup>, and SO<sub>4</sub><sup>2-</sup>”. In: *Colloids and Surfaces A: Physicochemical and Engineering Aspects* 301.1-3 (2007), pp. 199–208.



# Appendix A

## Chemicals

### A.1 Acid Number Solutions

Table A.1: Chemicals used for acid number measurements

<b>Solution</b>	<b>Chemicals</b>	<b>Formula</b>	<b>Description</b>
<b>Titrant</b>	KOH (> 85%) 2-propanol	KOH CH <sub>3</sub> CHOHCH <sub>3</sub>	2.8 g KOH (> 85%) dilute to 1000 ml with 2-propanol (CH <sub>3</sub> CHOHCH <sub>3</sub> )
<b>Spiking solution</b>	Stearic acid Acid titration solvent	CH <sub>3</sub> (CH <sub>2</sub> ) <sub>16</sub> COOH	0.5g Stearic Acid - (CH <sub>3</sub> (CH <sub>2</sub> ) <sub>16</sub> COOH) dilute to 100 ml with Acid titration solvent
<b>Standard solution</b>	Potassium Hydrogen Phtalate, KHP DI water	HOCC <sub>6</sub> H <sub>4</sub> COOK	0.2 g Potassium Hydrogen Phtalate, KHP diluted to 500 ml with DI water
<b>Titration solvent</b>	DI water 2-propanol Toluene	CH <sub>3</sub> CHOHCH <sub>3</sub> C <sub>6</sub> H <sub>5</sub> CH <sub>3</sub>	6 ml DI water dilute with 494 ml 2-propanol and with 500 ml Toluene
<b>Electrode/ Electrolyte</b>	Potassium chloride DI water	KCl	Mettler DG-114 Electrode 3 M KCl in DI water

## A.2 Base Number Solutions

Table A.2: Chemicals used for base number measurements

Solution	Chemicals	Formula	Description
<b>Titrant</b>	Perchloric Acid (70%) Acetic Anhydride Acetic Acid	$\text{HClO}_4$ (70%) $(\text{CH}_3\text{CO})_2\text{O}$ $\text{CH}_3\text{COOH}$	5 ml 70% Perchloric Acid ( $\text{HClO}_4$ ) 15 ml Acetic Anhydride ( $(\text{CH}_3\text{CO})_2\text{O}$ ) dilute to 1000 ml with Acetic Acid ( $\text{CH}_3\text{COOH}$ )
<b>Spiking solution</b>	Quinoline Decane	$\text{C}_9\text{H}_7\text{N}$ $\text{CH}_3(\text{CH}_2)_8\text{CH}_3$	0.5 g Quinoline ( $\text{C}_9\text{H}_7\text{N}$ ) dilute to 100 ml with Decane ( $\text{CH}_3(\text{CH}_2)_8\text{CH}_3$ )
<b>Standard solution</b>	Potassium Hydrogen Phtalate, KHP Acetic Acid	$\text{HOOC}_6\text{H}_4\text{COOK}$  $\text{CH}_3\text{COOH}$	0.2 g Potassium Hydrogen Phtalate, KHP diluted to 250 ml with Acetic Acid ( $\text{CH}_3\text{COOH}$ )
<b>Titration solvent</b>	Methyl Isobutyl Ketone, MIKB	$(\text{CH}_3)_2\text{CHCH}_2\text{COCH}_3$	Methyl Isobutyl Ketone ( $(\text{CH}_3)_2\text{CHCH}_2\text{COCH}_3$ )
<b>Electrode/ Electrolyte</b>	Sodium Perchlorate, (solid) 2-propanol	$\text{NaClO}_4(\text{s})$  $\text{CH}_3\text{CHOHCH}_3$	Mettler DG-113 Electrode Electrolyte: Saturated Sodium Perchloride, ( $\text{NaClO}_4(\text{s})$ ), in 2-propanol

# Appendix B

## Experimental Data

### B.1 Permeability Calculation Example

SK1 - BEFORE H2SO4		SK1 - AFTER H2SO4											
Rate [ml/min]	Avg dP [mbar]	Rate [ml/min]	Avg dP [mbar]										
0.15	340.502	0.15	299.004										
0.1	228.404	0.1	202.232										
0.05	113.793	0.05	99.379										
1 mbar = 0.000987 atm		1 mbar = 0.000987 atm											
Rate [cm3/s]	Avg dP [atm]	Rate [cm3/s]	Avg dP [atm]										
0.00250	0.336	0.00250	0.295										
0.00167	0.225	0.00167	0.200										
0.00083	0.112	0.00083	0.098										
Use Darcy's law: $q = \frac{kA}{\mu L} \frac{dP}{A}$ to find perm. $k = \frac{q \mu L}{dP A}$		Use Darcy's law: $q = \frac{kA}{\mu L} \frac{dP}{A}$ to find perm. $k = \frac{q \mu L}{dP A}$											
A [cm2]	11.22208312	A [cm2]	11.22208312										
L [cm]	7.02	L [cm]	7.02										
$\mu$ [cP]	1	$\mu$ [cP]	1										
q/dP	0.007448092	q/dP	0.008456313										
k [Darcy]	0.004659171	k [Darcy]	0.005289866										
k [mD]	4.659	k [mD]	5.290										
		<table border="1"> <thead> <tr> <th colspan="2">Difference in permeability</th> </tr> </thead> <tbody> <tr> <td>k before [md]</td> <td>4.659</td> </tr> <tr> <td>k after [md]</td> <td>5.290</td> </tr> <tr> <td>Difference [md]</td> <td>0.631</td> </tr> <tr> <td><b>Increase [%]</b></td> <td><b>13.5</b></td> </tr> </tbody> </table>		Difference in permeability		k before [md]	4.659	k after [md]	5.290	Difference [md]	0.631	<b>Increase [%]</b>	<b>13.5</b>
Difference in permeability													
k before [md]	4.659												
k after [md]	5.290												
Difference [md]	0.631												
<b>Increase [%]</b>	<b>13.5</b>												

Figure B.1: Example of permeability calculation for one core. This example displays the permeability of SK1 before and after H<sub>2</sub>SO<sub>4</sub>-flooding.

## B.2 Viscosity of Oil A

Data Series Information			
Name: Oil A 1			
Meas. Pts.	Shear Rate	Shear Stress	Viscosity
	[1/s]	[Pa]	[Pa·s]
1	500	1.2	0.0024
2	281	0.693	0.00247
3	158	0.398	0.00252
4	88.9	0.228	0.00257
5	50	0.131	0.00263

Data Series Information			
Name: Oil A 2			
Meas. Pts.	Shear Rate	Shear Stress	Viscosity
	[1/s]	[Pa]	[Pa·s]
1	500	1.2	0.00239
2	281	0.686	0.00244
3	158	0.392	0.00248
4	88.9	0.224	0.00252
5	50	0.128	0.00255

Data Series Information			
Name: Oil A 3			
Meas. Pts.	Shear Rate	Shear Stress	Viscosity
	[1/s]	[Pa]	[Pa·s]
1	500	1.19	0.00239
2	281	0.688	0.00245
3	158	0.394	0.00249
4	88.9	0.225	0.00254
5	50	0.129	0.00258

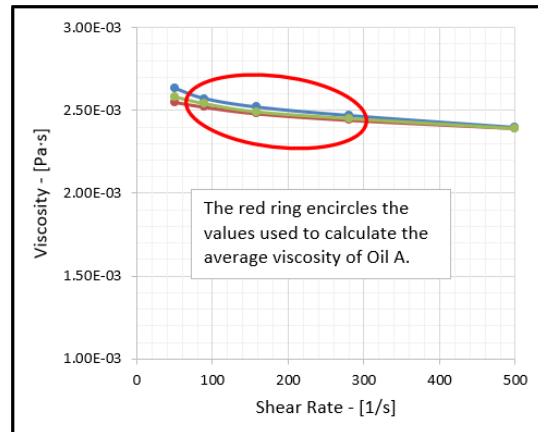


Figure B.2: The measurements used to determine the viscosity of Oil A.

# Appendix C

## H<sub>2</sub>SO<sub>4</sub> Flooding Data

### C.1 IC Results from H<sub>2</sub>SO<sub>4</sub> Flooding

Table C.1: IC results from flooding 9.7 mM H<sub>2</sub>SO<sub>4</sub> through chalk at 70°C

<b>PV corr.</b>	<b>Na (mM)</b>	<b>K (mM)</b>	<b>Mg (mM)</b>	<b>Ca (mM)</b>	<b>Cl (mM)</b>	<b>SO<sub>4</sub> (mM)</b>
0.18	3.33	0.70	0.21	2.46	0.98	2.01
0.58	16.12	1.81	0.19	2.38	5.03	2.02
0.98	10.87	0.38	0.16	2.13	1.81	2.37
1.38	13.02	0.15	0.18	3.08	2.06	2.87
1.78	6.98	1.47	0.55	4.07	2.53	3.16
2.18	48.34	0.11	0.36	6.91	0.69	11.23
2.56	23.72	0.27	0.52	11.56	3.26	9.85
2.95	92.11	0.25	0.27	5.76	0.74	12.44
3.33	45.16	n.a	0.32	7.52	0.70	11.40
3.71	24.84	0.19	0.41	12.99	2.83	10.74
4.10	8.54	0.16	0.18	9.25	0.74	9.80
4.47	107.59	0.16	0.19	6.39	0.91	14.26
4.86	18.52	4.12	0.48	13.28	6.37	9.73
5.24	11.14	0.35	0.23	10.09	0.91	10.23

Table C.2: IC results from flooding 13.3 mM H<sub>2</sub>SO<sub>4</sub> through chalk at 70°C

<b>PV corr.</b>	<b>Na (mM)</b>	<b>K (mM)</b>	<b>Mg (mM)</b>	<b>Ca (mM)</b>	<b>Cl (mM)</b>	<b>SO4 (mM)</b>
0.18	6.75	0.19	0.41	4.41	4.72	2.81
0.56	8.12	0.19	0.33	4.20	5.08	3.01
0.94	4.68	0.18	0.21	2.45	3.14	2.82
1.35	10.44	#VALUE!	0.37	6.11	6.62	3.72
1.73	6.37	0.15	0.46	8.99	3.59	8.84
2.13	3.85	0.13	0.38	13.68	2.36	14.15
2.54	2.29	#VALUE!	0.45	14.37	1.34	14.04
2.96	6.77	0.18	0.48	16.88	4.05	14.31
3.35	5.85	0.15	0.37	14.99	3.61	14.33
3.73	4.61	#VALUE!	0.38	15.04	2.92	14.66
4.12	4.61	#VALUE!	0.40	14.53	2.85	14.69
4.52	3.41	#VALUE!	0.42	14.43	2.18	14.82
4.94	2.36	#VALUE!	0.33	13.64	1.35	14.84
5.34	3.22	#VALUE!	0.51	13.06	2.10	14.67

Table C.3: IC results from flooding 16.7 mM H<sub>2</sub>SO<sub>4</sub> through chalk at 70°C

<b>PV corr.</b>	<b>Na (mM)</b>	<b>K (mM)</b>	<b>Mg (mM)</b>	<b>Ca (mM)</b>	<b>Cl (mM)</b>	<b>SO4 (mM)</b>
0.18	28.52	0.28	0.16	1.05	2.38	2.97
0.58	6.36	0.20	0.28	3.16	3.92	3.05
0.99	2.49	0.14	0.16	1.50	2.03	2.50
1.40	3.51	0.11	0.22	3.78	2.27	3.39
1.81	2.09	#VALUE!	0.41	11.31	1.52	13.80
2.22	7.28	0.09	0.44	15.10	4.63	16.81
2.63	3.74	#VALUE!	0.46	15.76	3.08	17.16
3.04	2.61	#VALUE!	0.36	13.93	2.29	16.53
3.44	5.68	0.89	0.35	13.86	3.82	16.61
3.85	4.97	0.50	0.36	14.15	3.97	16.69
4.26	6.06	1.09	0.39	14.87	3.40	17.06
4.67	2.27	0.13	0.34	14.13	1.97	16.73
5.07	2.24	0.15	0.31	13.47	1.92	16.71
5.47	3.58	0.11	0.37	14.61	3.04	16.75

Table C.4: IC results from flooding 4.9 mM H<sub>2</sub>SO<sub>4</sub> through chalk at 130°C

<b>PV corr.</b>	<b>Na (mM)</b>	<b>K (mM)</b>	<b>Mg (mM)</b>	<b>Ca (mM)</b>	<b>Cl (mM)</b>	<b>SO4 (mM)</b>
0.17	3.36	0.14	0.43	4.14	2.29	2.05
0.55	2.52	1.12	0.24	2.44	1.83	1.86
0.93	15.16	1.24	0.63	5.76	6.61	5.46
1.31	4.15	0.33	0.35	4.11	3.16	2.28
1.70	73.59	3.31	0.20	3.03	6.36	3.30
2.08	5.24	0.42	0.21	2.34	3.03	1.96
2.45	56.32	0.13	0.12	2.25	1.14	3.37
2.84	4.75	0.36	0.34	3.47	3.11	2.22
3.22	55.96	0.13	0.15	1.83	2.50	3.92
3.60	27.40	0.11	0.48	4.91	3.14	4.03
3.98	5.67	0.95	0.58	7.39	4.44	4.52
4.36	87.61	1.01	0.21	3.82	6.39	5.83
4.74	7.33	0.38	0.31	6.74	1.56	4.63
5.13	1.49	0.39	0.23	5.40	0.91	4.72

Table C.5: IC results from flooding 8.5 mM H<sub>2</sub>SO<sub>4</sub> through chalk at 130°C

<b>PV corr.</b>	<b>Na (mM)</b>	<b>K (mM)</b>	<b>Mg (mM)</b>	<b>Ca (mM)</b>	<b>Cl (mM)</b>	<b>SO4 (mM)</b>
0.17	0.11	0.28	0.21	1.95	0.42	2.57
0.57	0.14	0.40	0.16	2.01	0.40	2.55
0.96	1.53	#VALUE!	0.28	3.00	2.37	2.93
1.36	0.09	0.22	0.14	2.06	0.55	2.77
1.75	0.91	0.18	0.17	2.47	1.20	3.03
2.15	3.86	0.68	0.28	3.14	3.36	3.18
2.54	3.19	0.11	0.35	3.81	2.82	3.10
2.93	3.20	0.25	0.39	4.30	2.74	4.72
3.33	2.96	#VALUE!	0.48	6.46	2.55	7.17
3.72	3.28	#VALUE!	0.47	7.25	2.79	7.80
4.12	1.03	#VALUE!	0.24	6.35	0.74	8.03
4.51	3.83	0.13	0.50	7.31	3.42	7.87
4.91	1.43	#VALUE!	0.26	6.33	1.19	8.04
5.31	2.24	0.20	0.35	8.21	1.46	8.40

## C.2 pH Measurements from $H_2SO_4$ Flooding

Table C.6: pH measurements of the effluent during the different  $H_2SO_4$  floodings at 70 and 130°C.

T=70°C						T=130°C			
9.7 mM		13.3 mM		16.7 mM		4.9 mM		8.5 mM	
PV corr.	pH	PV corr.	pH	PV corr.	pH	PV corr.	pH	PV corr.	pH
-0.02	8.61	-0.02	8.52	-0.02	8.15	-0.03	7.38	-0.03	7.06
0.38	8.65	0.37	9.09	0.38	7.99	0.36	7.20	0.37	7.12
0.78	8.79	0.75	8.82	0.79	8.06	0.75	7.52	0.77	7.21
1.18	7.67	1.15	6.97	1.20	6.63	1.12	7.18	1.16	6.91
1.58	6.43	1.54	6.34	1.60	6.27	1.51	6.38	1.55	6.28
1.98	6.25	1.93	6.16	2.01	6.03	1.89	6.32	1.95	6.28
2.37	6.22	2.33	6.14	2.42	6.12	2.26	6.31	2.34	6.22
2.75	6.19	2.75	6.09	2.83	6.05	2.65	6.29	2.74	6.16
3.14	6.22	3.15	6.15	3.24	6.09	3.02	6.23	3.13	6.05
3.52	6.18	3.54	6.12	3.65	6.07	3.41	6.15	3.53	5.97
3.90	6.17	3.92	6.13	4.06	6.05	3.79	6.23	3.92	5.95
4.28	6.19	4.32	6.08	4.46	6.04	4.17	6.10	4.31	5.98
4.67	6.25	4.73	6.10	4.87	6.07	4.55	6.11	4.71	5.92
5.05	#N/A	5.14	6.09	5.28	6.02	4.93	6.13	5.11	5.93
5.41	6.23	5.54	6.08						



# Appendix D

## Imbibition Data

### D.1 Results from Spontaneous Imbibition Tests

Table D.1: Spontaneous imbibition of FW into SK2 at 70°C. Oil A: AN=0.50 mgKOH/g.

<b>Time (days)</b>	<b>Cum. Oil (ml)</b>	<b>% OOIP</b>
0.00	0.00	0.00
0.07	0.10	0.31
0.25	0.90	2.77
0.78	1.30	4.00
1.76	1.70	5.23
2.78	2.00	6.15
3.77	2.20	6.76
4.92	2.40	7.38
6.11	2.60	7.99
7.78	2.80	8.61
9.79	2.90	8.91
12.94	3.00	9.22
16.82	3.30	10.14
20.79	3.30	10.14
23.78	3.30	10.14
27.80	3.30	10.14

Table D.2: Spontaneous imbibition of SW into SK3 at 70°C. Oil A: AN=0.50 mgKOH/g.

<b>Time (days)</b>	<b>Cum. Oil (ml)</b>	<b>% OOIP</b>
0.00	0.00	0.00
0.10	0.00	0.00
0.21	0.20	0.65
0.44	0.50	1.62
0.96	0.80	2.59
2.06	1.20	3.88
3.00	1.50	4.85
4.09	1.80	5.82
5.27	2.00	6.47
6.11	2.00	6.47
7.02	2.20	7.11
8.44	2.30	7.44
11.27	2.40	7.76
14.09	2.50	8.08
16.99	2.70	8.73
20.32	2.80	9.05
24.45	2.80	9.05
27.96	2.80	9.05
31.00	2.80	9.05

Table D.3: Spontaneous imbibition of Smart Water into SK4 at 70°C. Oil A: AN=0.50 mgKOH/g.

<b>Time (days)</b>	<b>Cum. Oil (ml)</b>	<b>% OOIP</b>
0.00	0.00	0.00
0.19	0.10	0.31
0.44	0.40	1.23
0.97	0.90	2.76
1.97	2.00	6.13
2.97	2.40	7.35
4.24	2.70	8.27
4.95	2.70	8.27
5.96	2.80	8.58
6.94	2.80	8.58
8.95	3.00	9.19
11.29	3.20	9.80
12.96	3.30	10.11
14.97	3.30	10.11
18.12	3.40	10.42
22.00	3.40	10.42
25.97	3.50	10.72
28.96	3.50	10.72

Table D.4: Spontaneous imbibition of DI water into SKWW at 23°C.

Time (min)	Time (days)	Cum. Oil (ml)	% OOIP
0	0.0000	0.00	0.00
1	0.0007	4.10	13.00
2	0.0014	7.00	22.19
3	0.0021	9.50	30.12
4	0.0028	10.50	33.29
5	0.0035	14.50	45.97
10	0.0069	14.70	46.60
15	0.0104	16.00	50.72
30	0.0208	18.90	59.92
45	0.0313	20.00	63.40
60	0.0417	21.50	68.16
120	0.0833	21.50	68.16
180	0.1250	22.00	69.74
268	0.1861	22.00	69.74
388	0.2694	23.00	72.91
508	0.3528	23.60	74.82
1258	0.8736	23.60	74.82
1858	1.2903	23.60	74.82
2760	1.9167	23.60	74.82
2880	2.0000	23.60	74.82
4320	3.0000	23.60	74.82

## D.2 Results from Forced Imbibition Tests

Table D.5: Forced imbibition with FW followed by Smart Water at 70°C.

Inj. Fluid	Inj. Rate (ml/min)	PV corr.	Cum. Oil (ml)	% OOIP	$\Delta P$ (mbar)
VB0S	0.025	-0.09	3.3	10.14	100
VB0S	0.025	-0.06	3.3	10.14	737
VB0S	0.025	-0.01	3.3	10.14	673
VB0S	0.025	0.00	3.3	10.14	662
VB0S	0.025	0.02	3.9	11.99	638
VB0S	0.025	0.04	4.5	13.83	633
VB0S	0.025	0.06	5.3	16.29	623
VB0S	0.025	0.08	6.0	18.44	619
VB0S	0.025	0.10	6.7	20.59	616
VB0S	0.025	0.12	7.4	22.74	619
VB0S	0.025	0.14	8.2	25.20	624
VB0S	0.025	0.16	8.9	27.36	628
VB0S	0.025	0.19	9.7	29.81	639
VB0S	0.025	0.21	10.4	31.97	646
VB0S	0.025	0.23	11.0	33.81	648
VB0S	0.025	0.25	11.6	35.65	659
VB0S	0.025	0.27	12.4	38.11	659
VB0S	0.025	0.29	12.9	39.65	664
VB0S	0.025	0.31	13.5	41.49	676
VB0S	0.025	0.33	14.1	43.34	661
VB0S	0.025	0.35	14.7	45.18	652
VB0S	0.025	0.37	15.1	46.41	644
VB0S	0.025	0.39	15.5	47.64	640
VB0S	0.025	0.41	15.9	48.87	629
VB0S	0.025	0.43	16.2	49.79	612
VB0S	0.025	0.46	16.3	50.10	601
VB0S	0.025	0.48	16.5	50.71	611
VB0S	0.025	0.50	16.7	51.33	596
VB0S	0.025	0.52	16.8	51.64	594
VB0S	0.025	0.54	16.9	51.94	600
VB0S	0.025	0.99	17.8	54.71	520
VB0S	0.025	1.01	17.8	54.71	510
VB0S	0.025	1.06	17.8	54.71	507

Table D.5: (continued)

Inj. Fluid	Inj. Rate (ml/min)	PV corr.	Cum. Oil (ml)	% OOIP	$\Delta P$ (mbar)
VB0S	0.025	1.10	17.8	54.71	508
VB0S	0.025	1.24	17.8	54.71	502
VB0S	0.025	1.38	17.8	54.71	519
VB0S	0.025	1.49	17.9	55.02	485
VB0S	0.025	1.97	18.0	55.33	470
VB0S	0.025	2.13	18.0	55.33	283
VB0S	0.025	2.36	18.0	55.33	300
VB0S	0.025	2.49	18.0	55.33	289
VB0S	0.025	2.95	18.0	55.33	300
VB0S	0.025	2.98	18.0	55.33	125
Smart Water	0.025	2.98	18.0	55.33	288
Smart Water	0.025	3.03	18.0	55.33	264
Smart Water	0.025	3.10	18.0	55.33	280
Smart Water	0.025	3.15	18.0	55.33	303
Smart Water	0.025	3.25	18.0	55.33	302
Smart Water	0.025	3.85	18.0	55.33	273
Smart Water	0.025	3.86	18.0	55.33	275
Smart Water	0.100	3.93	18.1	55.63	827
Smart Water	0.100	4.01	18.6	57.17	818
Smart Water	0.100	4.09	18.8	57.78	792
Smart Water	0.100	4.18	19.0	58.40	777
Smart Water	0.100	4.26	19.1	58.71	755
Smart Water	0.100	4.34	19.1	58.71	755
Smart Water	0.100	4.43	19.3	59.32	748
Smart Water	0.100	4.51	19.4	59.63	737
Smart Water	0.100	4.59	19.4	59.63	733
Smart Water	0.100	4.67	19.4	59.63	717
Smart Water	0.100	5.10	19.6	60.24	688
Smart Water	0.100	5.67	19.8	60.86	666
Smart Water	0.100	7.87	19.8	60.86	593

Table D.6: Forced imbibition with SW followed by Smart Water at 70°C.

Inj. Fluid	Inj. Rate (ml/min)	PV corr.	Cum. Oil (ml)	% OOIP	$\Delta P$ (mbar)
SW	0.024	-0.09	2.8	9.05	100
SW	0.024	-0.07	2.8	9.05	672
SW	0.024	-0.02	2.8	9.05	670
SW	0.024	0.01	2.8	9.05	630
SW	0.024	0.03	3.3	10.67	600
SW	0.024	0.05	4	12.93	593
SW	0.024	0.08	4.6	14.87	580
SW	0.024	0.10	5.3	17.13	575
SW	0.024	0.12	6	19.40	577
SW	0.024	0.14	6.7	21.66	579
SW	0.024	0.16	7.3	23.60	586
SW	0.024	0.18	8	25.86	594
SW	0.024	0.20	8.7	28.13	600
SW	0.024	0.22	9.4	30.39	617
SW	0.024	0.25	10.4	33.62	632
SW	0.024	0.27	11.1	35.88	645
SW	0.024	0.30	11.8	38.15	652
SW	0.024	0.32	12.4	40.09	660
SW	0.024	0.34	13.1	42.35	637
SW	0.024	0.36	13.9	44.94	640
SW	0.024	0.38	14.5	46.88	627
SW	0.024	0.40	14.9	48.17	605
SW	0.024	0.42	15.1	48.82	600
SW	0.024	0.44	15.4	49.79	580
SW	0.024	0.46	15.5	50.11	556
SW	0.024	0.48	15.7	50.75	569
SW	0.024	0.51	15.9	51.40	563
SW	0.024	0.53	16	51.72	558
SW	0.024	0.93	16.8	54.31	509
SW	0.024	0.98	16.9	54.63	504
SW	0.024	1.09	17	54.96	487
SW	0.024	1.17	17.1	55.28	489
SW	0.024	1.24	17.2	55.60	484

Table D.6: (continued)

Inj. Fluid	Inj. Rate (ml/min)	PV corr.	Cum. Oil (ml)	% OOIP	$\Delta P$ (mbar)
SW	0.024	1.32	17.2	55.60	478
SW	0.024	1.39	17.3	55.93	483
SW	0.024	1.49	17.4	56.25	455
SW	0.024	1.93	17.5	56.57	444
SW	0.024	2.14	17.6	56.90	436
SW	0.024	2.98	17.6	56.90	415
SW	0.024	3.97	17.6	56.90	395
SW	0.024	3.97	17.6	56.90	397
Smart Water	0.024	3.97	17.6	56.90	389
Smart Water	0.024	4.01	17.6	56.90	393
Smart Water	0.024	4.05	17.6	56.90	404
Smart Water	0.024	4.09	17.6	56.90	385
Smart Water	0.024	4.33	17.6	56.90	384
Smart Water	0.024	4.91	17.6	56.90	365
Smart Water	0.096	4.92	17.6	56.90	581
Smart Water	0.096	4.94	17.6	56.90	786
Smart Water	0.096	5.01	18	58.19	760
Smart Water	0.096	5.10	18.5	59.81	748
Smart Water	0.096	5.18	18.7	60.45	743
Smart Water	0.096	5.26	18.8	60.78	733
Smart Water	0.096	5.35	18.9	61.10	714
Smart Water	0.096	5.43	18.9	61.10	705
Smart Water	0.096	5.52	18.9	61.10	700
Smart Water	0.096	5.60	18.9	61.10	660
Smart Water	0.096	5.77	18.9	61.10	670
Smart Water	0.096	5.95	18.9	61.10	669
Smart Water	0.096	6.10	19.1	61.75	636
Smart Water	0.096	6.58	19.1	61.75	658
Smart Water	0.096	8.79	19.1	61.75	560

Table D.7: Forced imbibition with Smart Water at 70°C.

Inj. Fluid	Inj. Rate (ml/min)	PV corr.	Cum. Oil (ml)	% OOIP	$\Delta P$ (mbar)
Smart Water	0.025	-0.09	3.5	10.72	105
Smart Water	0.025	-0.06	3.5	10.72	685
Smart Water	0.025	-0.01	3.5	10.72	650
Smart Water	0.025	0.00	3.5	10.72	603
Smart Water	0.025	0.01	3.8	11.64	580
Smart Water	0.025	0.02	4.5	13.79	566
Smart Water	0.025	0.04	5.2	15.93	546
Smart Water	0.025	0.06	5.9	18.07	554
Smart Water	0.025	0.08	6.6	20.22	547
Smart Water	0.025	0.10	7.5	22.98	523
Smart Water	0.025	0.12	8.1	24.81	525
Smart Water	0.025	0.14	8.7	26.65	536
Smart Water	0.025	0.16	9.3	28.49	547
Smart Water	0.025	0.18	10.0	30.63	570
Smart Water	0.025	0.21	10.7	32.78	574
Smart Water	0.025	0.23	11.3	34.62	594
Smart Water	0.025	0.25	12.1	37.07	631
Smart Water	0.025	0.27	12.7	38.91	633
Smart Water	0.025	0.29	13.4	41.05	643
Smart Water	0.025	0.31	14.2	43.50	644
Smart Water	0.025	0.33	14.9	45.65	631
Smart Water	0.025	0.35	15.5	47.48	618
Smart Water	0.025	0.37	16.1	49.32	598
Smart Water	0.025	0.39	16.6	50.85	595
Smart Water	0.025	0.41	16.8	51.47	586
Smart Water	0.025	0.43	16.9	51.77	566
Smart Water	0.025	0.45	17.2	52.69	572
Smart Water	0.025	0.47	17.3	53.00	563
Smart Water	0.025	0.50	17.5	53.61	570
Smart Water	0.025	0.52	17.6	53.92	560
Smart Water	0.025	0.91	18.3	56.06	474
Smart Water	0.025	0.93	18.4	56.37	463
Smart Water	0.025	0.95	18.5	56.67	464



Table D.7: (continued)

Inj. Fluid	Inj. Rate (ml/min)	PV corr.	Cum. Oil (ml)	% OOIP	$\Delta P$ (mbar)
Smart Water	0.025	0.97	18.6	56.98	463
Smart Water	0.025	1.02	18.7	57.29	467
Smart Water	0.025	1.06	18.8	57.59	459
Smart Water	0.025	1.09	18.8	57.59	465
Smart Water	0.025	1.22	18.9	57.90	457
Smart Water	0.025	1.47	19.0	58.21	429
Smart Water	0.025	2.00	19.2	58.82	408
Smart Water	0.025	2.19	19.2	58.82	358
Smart Water	0.025	2.41	19.2	58.82	391
Smart Water	0.025	2.92	19.2	58.82	345
Smart Water	0.025	3.15	19.2	58.82	363
Smart Water	0.100	3.15	19.2	58.82	823
Smart Water	0.100	3.28	19.6	60.04	770
Smart Water	0.100	3.36	19.7	60.35	744
Smart Water	0.100	3.46	19.8	60.66	728
Smart Water	0.100	3.53	19.9	60.96	709
Smart Water	0.100	3.61	19.9	60.96	709
Smart Water	0.100	3.69	20.0	61.27	686
Smart Water	0.100	3.86	20.1	61.58	689
Smart Water	0.100	4.03	20.2	61.88	665
Smart Water	0.100	4.19	20.3	62.19	669
Smart Water	0.100	4.35	20.3	62.19	655
Smart Water	0.100	6.05	20.3	62.19	600
Smart Water	0.100	6.38	20.3	62.19	600